BNL 37376

PHYSICO-CHEMICAL FACTORS AFFECTING HYDROTHERMAL RESISTANCE AND BONDING OF POLYMERIC COMPOSITES TO STEEL SURFACES

FINAL REPORT

T. Sugama, L. E. Kukacka, N. R. Carciello, and J. B. Warren

November 1985

Prepared for the
U.S. Army Research Office
P.O. Box 12211
Research Triangle Park, NC 27709

DEPARTMENT OF APPLIED SCIENCE
PROCESS SCIENCES DIVISION
BROOKHAVEN NATIONAL LABORATORY
UPTON, LONG ISLAND, NEW YORK 11973

PHYSICO-CHEMICAL FACTORS AFFECTING HYDROTHERMAL RESISTANCE AND BONDING OF POLYMERIC COMPOSITES TO STEEL SURFACES

FINAL REPORT

T. Sugama, L. E. Kukacka, N. R. Carciello, and J. B. Warren

November 1985

Prepared for the
U.S. Army Research Office
P.O. Box 12211
Research Triangle Park, NC 27709

Meyer Steinberg
PROCESS SCIENCES DIVISION
DEPARTMENT OF APPLIED SCIENCE
BROOKHAVEN NATIONAL LABORATORY
UPTON, NY 11973

This work was performed under the auspices of the
U.S. Department of Energy, under contract No. DE-AC02-76CH00016,
and supported by the U.S. Army Research Office Program MIPR-ARO-62-82,
ARO-155-83 and ARO-139-84

MASTER COPY FOR REPRODUCTION PURPOSES

UNCLASSIFIED
SECURITY CLASSIFICATION OF THIS PAGE (When Data Entered)

REPORT DOCUMENTATION PAGE

READ INSTRUCTIONS BEFORE COMPLETING FORM

1. REPORT NUMBER: ARO 19708.7-MS	2. GOVT ACCESSION NO.: N/A
3. RECIPIENT'S CATALOG NUMBER: N/A	
4. TITLE (and Subtitle): PHYSICO-CHEMICAL FACTORS AFFECTING HYDROTHERMAL RESISTANCE AND BONDING OF POLYMERIC COMPOSITES TO STEEL SURFACES	5. TYPE OF REPORT & PERIOD COVERED: Final, August 82 - July 85
	6. PERFORMING ORG. REPORT NUMBER: BNL 37376
7. AUTHOR(s): T. Sugama, L. E. Kukacka, N. R. Carciello, and J. B. Warren	8. CONTRACT OR GRANT NUMBER(s): MIPR-ARO-62-82, ARO 155-83, and ARO-139-84
9. PERFORMING ORGANIZATION NAME AND ADDRESS: Associated Universities, Inc., Brookhaven National Laboratory, Upton, NY 11973	10. PROGRAM ELEMENT, PROJECT, TASK AREA & WORK UNIT NUMBERS
11. CONTROLLING OFFICE NAME AND ADDRESS: U. S. Army Research Office, Post Office Box 12211, Research Triangle Park, NC 27709	12. REPORT DATE: November 1985
	13. NUMBER OF PAGES: 151
14. MONITORING AGENCY NAME & ADDRESS (if different from Controlling Office)	15. SECURITY CLASS. (of this report): Unclassified
	15a. DECLASSIFICATION/DOWNGRADING SCHEDULE

16. DISTRIBUTION STATEMENT (of this Report)

Approved for public release; distribution unlimited.

17. DISTRIBUTION STATEMENT (of the abstract entered in Block 20, if different from Report)

NA

18. SUPPLEMENTARY NOTES

The view, opinions, and/or findings contained in this report are those of the author(s) and should not be construed as an official Department of the Army position, policy, or decision, unless so designated by other documentation.

19. KEY WORDS (Continue on reverse side if necessary and identify by block number)

Ca-complexed methylmethacrylate ionomer	Interfacial interaction
Hydrothermal stability	Functional polymers
Hydrated calcium-silicate macromolecules	Zinc phosphate conversion precoat
Stiffness	Cold-rolled carbon steel
Adhesion	Polyelectrolyte macromolecule

20. ABSTRACT (Continue on reverse side if necessary and identify by block number)

A CaO-SiO_2-H_2O macromolecular-ionomer complex was found to be formed in the superficial layers of MMA-TMPTMA copolymer composite films made with filler containing hydraulic cement during exposure in an autoclave at temperatures up to 200°C. This superficially formed complex in terms of self-healing protective layers, acted to prevent the hydrothermal deterioration of the original composite films, which is important if the films are used as protective layers on metals.

DD FORM 1 JAN 73 1473 EDITION OF 1 NOV 65 IS OBSOLETE

UNCLASSIFIED

20. ABSTRACT (continued)

In studies of the interfacial interactions between functional polymers containing carboxylate and carboxylic acid groups and crystalline zinc phosphate conversion precoats deposited on cold-rolled carbon steel surfaces, it was found that the surface topography of crystal precoats, which are characterized by the presence of a dendritic microstructure array of interlocking triclinic crystals, is a major factor affecting the mechanical interlocking forces associated with the anchoring of the polymers yielded by penetration of liquid resins into the open surface microstructure and macrofissures of the precoats. The magnitude of the mechanical bond was primarily responsible for the development of the interfacial adhesion forces, whereas, the formation of weak chemical bonds such as a hydrogen bond or acid/base interactions occuring between the functional groups in the polymers and the crystallized H_2O molecules or polar OH groups on the precoat surface sites had little effect on the adhesion strength.

When high-strength cold rolled steels having carbon concentrations ranging from 0.05 to 0.2%, were immersed into zinc orthophosphate dihydrate-based phosphating solutions, a high quality zinc phosphate (Zn·Ph) conversion precoating was produced. The precoat, which consists of a uniform array of large and thick crystals, can be deposited on the substrate surfaces. The magnitude of improvement in the corrosion-inhibiting ability and mechanical properties of these Zn·Ph coatings appears to depend primarily on the thickness, fineness and density of the coating layers. The introduction of polyelectrolyte macromolecules into the phosphating liquids was found to be a very effective method for improving these characteristics. Adsorption of polyelectrolyte segments with molecular weights ranging from 90,000 to 250,000 on the Zn·Ph crystals plays a key role in increasing the stiffness and flexibility of the layers and in advancing the crystalline reorganization. The addition of materials with molecular weight >250,000 completely prevented the crystal growth of Zn·Ph. This was due to the segmental adsorption of more randomly coiled-up chains. In addition, the organic composites at the outermost surface sites on the crystal act to promote the adhesion with polymeric topcoat systems by the formation of organic-organic chemical bonds, thereby enhancing the bond durability of the Zn·Ph precoat-to-polymer topcoat adhesive joints.

TABLE OF CONTENTS

TABLE OF CONTENTS cont.

LIST OF TABLES

LIST OF FIGURES

LIST OF FIGURES

LIST OF FIGURES

LIST OF FIGURES

LIST OF FIGURES

SUMMARY

The failure upon exposure to hydrothermal conditions of most conventional polymers containing functional groups in which any two atoms selected from N, O, and S are joined to the same carbon atom, is generally due to 1) high segmental mobility of molecular chains, 2) low thermal relaxation of the polymers, 3) an increase in hydrophilic groups, and 4) low dynamic mechanical properties. Each of these factors must be considered in attempting to provide the total protection needed for long service life in hydrothermal environments. Therefore, the physico-chemical factors that determine the hydrothermal stability and the bonding characteristics of inorganic macromolecule-ionomer composite films have been investigated.

A CaO-SiO_2-H_2O macromolecular-ionomer complex was found to be formed in the superficial layers of MMA-TMPTMA copolymer composite films made with fillers containing hydraulic-type calcium silicate admixtures during exposure in an autoclave at temperatures up to 200°C. This complex acted in terms of a self-healing protective layer to prevent the hydrothermal deterioration of the original composite films, which is important if the films are used as protective layers on metals. This complex also contributed significantly to hydrophobicity, a low energy surface, and less surface roughness, thereby lowering the intrinsic water permeability of the films. The glass transition temperature, T_g, and the tensile strength of the complexed films increased with increasing concentration of the cement additive used as a source of Ca^{2+} metallic ions, but they decreased when the hydraulic admixture concentration became excessive because of the chain enlargement caused by the growth of a large quantity of hydrated macromolecules.

Since one of the main factors affecting the durability of protective coatings is the adhesion force to the substrate, it is very important to clearly understand the nature and role of the adhesion mechanisms and how they affect the interactions and interplay at the functional polymer-to-metal interface regions. Also, the surface preparation of the substrate

appears to play a keying role in enhancing the interfacial adhesion force at polymer/metal joints. Hence, this study emphasized the elucidation of adhesive mechanisms for two functional polymers, polyacrylic acid and levulinic acid-modified furan, when applied to cold-rolled carbon steel surfaces pre-treated with phosphating solutions. The work entailed studies of the mechanical and chemical interactions occurring between the functional polymers and crystalline iron (III) orthophosphate dihydrate or zinc phosphate hydrate (hopeite) conversion precoats that were deposited on the steel surfaces.

The typical surface topography of the highly crystallized zinc phosphate films was found to be characterized by the presence of a dendritic microstructure array of interlocking triclinic crystals. This structure acts significantly to develop mechanical interlocking bonds with the functional polymer, which penetrates into the open surface structure of the films.

Studies of the interfacial chemical reactions indicated that the conformation changes in the polyacrylic acid macromolecules relate directly to the frequency of the magnitude of acid/base and change transfer interactions between the proton-donating pendent COOH groups in polyacrylic acid molecules and the polar OH groups at hydrated precoat surface sites. The presence of numerous free nucleophilic ions existing on the deposited precoat film leads to a substrantial increase in the coil-up and entanglement macromolecule density. These entangled complex macromolecules at the interfaces resulted in a decrease in the degree of chemisorption at the precoat surfaces, whereas regularly oriented COOH groups produce strong interfacial chemisorption with the polar groups. When the polarized furan polymers spread on the zinc phosphate surfaces, the carboxylate groups derived from the levulinic ester and acid molecules react to form hydrogen bonds with the crystallized H_2O molecules on the hopeite film. This formation of hydrogen bonding was shown to be a major factor affecting the chemical intermolecular attractions.

From the studies of the interfacial bond mechanisms at functional polymer-to-crystalline conversion precoat joints, it was confirmed that the mechanical interlocking bond is primarily responsible for the development of interfacial adhesion forces. The formation of hydrogen bonds and acid/base interactions, which are categorized as weak chemical bonding systems, is likely to have little effect on the advanced adhesion forces. This information suggested that successful bonding can be attributed to the following four elements: (1) mechanical interlocking associated with the surface topography of metals, (2) surface wettability of metal by the polymers, (3) strong chemisorption, and (4) type and degree of polymer-metal interfacial interaction.

When water-soluble polyacrylic acid (PAA) macromolecules are introduced into zinc phosphating liquids, significant improvements in the yield of conventional zinc phosphate conversion films deposited on carbon steel surfaces are obtained. The improvements include controllability of crystal dimensions, degree of crystallinity, and coating weight. The conversion layer formed is a composite microstructure consisting of a bulk PAA polymer and complexed PAA continuously overlaying a uniform array of fine dense zinc phosphate crystals. Interfacial studies of the composite layer using infrared spectroscopy, energy-dispersive x-ray spectrometry associated with scanning electron microscopy, and x-ray photoelectron spectroscopy indicated that the functional carboxylic acid groups in the PAA molecules were strongly chemisorbed by the Zn atoms at the outermost surface sites of the crystal layers. The intermolecular bridging action of the surface Zn atoms which connect the PAA and the zinc phosphate crystal layers results in good adhesion at the PAA-crystal interfaces. The presence of the organic composites at the outermost surface sites on the crystal acted to promote the adhesion with polymeric topcoat systems by the formation of organic-organic chemical bonds, thereby enhancing the bond durability of the Zn·Ph precoat-to-polymer topcoat adhesive joints. Adsorption of polyelectrolyte segments with molecular weights ranging from 90,000 to 250,000 on the Zn·Ph crystals plays a key role in increasing the stiffness and flexibility of the layers and in advancing the crystalline reorganization. The addition of material with molecular weight

>250,000 completely prevented the crystal growth of Zn·Ph. This was due to the segmental adsorption of more randomly coiled-up chains. In addition, the protective polymer topcoat overlaied on the complex precoat surfaces increases the flexibility of the crystalline precoat itself. The most important factors controlling the flexibility of the precoat were low elastic modulus, high tensile strength, and elongation of the topcoat systems. These characteristics are more important than the magnitude of interfacial adhesive bonds at topcoat/precoat joints.

I. INTRODUCTION

Ca^{2+} ion-complexed polymethylmethacrylate (Ca-PMMA) ionomer composites have been studied earlier[1]. The composites contain hydrated calcium-silica ($CaO-SiO_2$) compounds and are formed by ionic reactions between divalent Ca ions released from $CaO-SiO_2$ grains and carboxylate anions (COO^-) yielded during the hydrolysis of functional pendent carboxyl groups in MMA upon exposure to hydrothermally aggressive environments. In the presence of hot water, the hydraulic inorganic $CaO·SiO_2$ grains are progressively converted into highly crystallized macromolecules[2]. These macromolecules are produced in the vicinity of amorphous ionomer chains, and thereby restrict the segmental mobility of the molecular chains. This leads to a molecular configuration having a low segmental jumping frequency, which results in minimum permeability, good adhesion to metallic surfaces, and excellent hydrothermal stability. A more recent study indicated that the enhancement of the hydrothermal stability of the composite depends strongly on three characteristics of the $CaO-SiO_2-H_2O$ system macromolecules formed within the polymer matrices[3]: 1) the morphological features and orientation of microcrystalline formations which act to reinforce the polymer matrices, 2) the mechanical strength of the crystallized compounds, and 3) the space-filling properties of the macromolecules, which form a dense agglomeration of filled matrix. From these observations, it was concluded that the hydrothermal stability of $CaO-SiO_2-H_2O$ systems formed during hydrothermal exposures at >100°C is due not only to the degree of crystallization and the shape of the

microcrystal structure, but also to the relatively high quantity of SiO_2 molecules exisitng in the hybrid hydration macromolecules. The results suggested that, when an anhydrous $CaO-SiO_2$ compound powder is to be used as a reactive filler with polymer blends, a hydraulic cement having a low mole ratio of CaO/SiO_2 should be employed.

The above findings indicate that the composite system can be utilized as a protective coating for metal surfaces exposed to hydrothermal environments. The coating protects the metal substrate from corroding primarily by two mechanisms: (1) serving as a barrier for the reactants, water, oxygen, and ions, and (2) serving as a reservoir for corrosion inhibitors that assist the surface in resisting attack. Failures of most conventional polymer films during exposure to aggressive hot water environments are likely to be due to 1) high segmental mobility of molecular chains, 2) low thermal relaxation of the polymers, 3) increase in hydrophilic groups, and 4) low dynamic mechanical properties. Each of these factors must be considered in attempting to provide the total protection needed for long service life in hydrothermal environments. Therefore, the first objective in this study was to investigate the physico-chemical factors that determine the hydrothermal stability and the bonding characteristics of inorganic macromolecule-ionomer composite films. These factors include the degree of polymer-filler interactions, thermodynamic properties, water transport properties, mechanical behavior, morphological features of the film surfaces, surface free energy, interfacial adhesive strength, wetting behavior, and spreading kinetics.

Since adhesion is one of the main factors affecting the durability of protective coatings on metal substrate surfaces, the second objective was to study these processes. It is very important to understand the nature of the adhesion mechanisms and how they effect interactions between functional polymers and metal surfaces. The effects of functional carboxylic acid (COOH) groups located in the pendent of polyacrylic acid (PAA), on ionic reactions and adsorption are of primary interest in understanding the fundamental adhesion mechanisms between polar oxide metal surfaces and functional polyacid macromolecules. The PAA molecule which is generally

expressed as a polyelectrolyte macromolecule is characterized by a simple chemical structure consisting of a stabilized hydrophobic main chain $(-CH_2-CH-)_n$ and the hydrophilic pendent (COOH) groups. Several studies of the reactions between ions and polyelectrolyte macromolecules have been made, using spectroscopic and polarographic techniques and with pH titration curves.[4-8] Other reports dealing with polymer adsorption in which the adsorbed segments interact in the surface layers have emphasized theoretical studies.[9-13]

Recently, the ability of polyacid to function as an adhesive at an ionic interface was investigated by using Fourier Transform IR Spectroscopy techniques.[14] This study emphasized that the degree of neutralized polyelectrolyte macromolecule conformation results in a fraction of bound segments on the adsorbed molecules. Hence, in the present work we have made a systematic assessment of how the adhesive and adsorption mechanisms at the polyelectrolyte macromolecule-treated oxide metal interfaces affect the interfacial bond strength and the role of the interface in adhesion processes. This elucidation of the interfacial interaction mechanisms will provide the ability to utilize polyelectrolyte macromolecules as an adhesive and a coating.

To assist in the elucidation of the adhesion mechanisms at the polymer-metal interfacial joints, the nature of the interaction between levulinic acid-modified furan polymer and oxidized metal surfaces was also explored. When the furan resin is applied as a protective coating to metal surfaces, it is presumed that the reactivity of the functional levulinic ester will result in great improvements in the bonding forces at the furan-metal interfaces. Since the number of levulinic ester configurations in the furan macromolecules can be controlled,[15-17] the chemical affinity of COOH groups for the oxide films offers the potential for producing furan coatings which possess strong chemical activity.

The ideal modification of the furan polymers to obtain a high interfacial bond at the polymer-oxidized metal boundary would be to incorporate an adequate amount of levulinic acid reagent to interact with the methylol groups in alpha positions on neighboring furan rings to form a methylene

bridged polycondensate. Accordingly, an aim in the present work was to understand the fundamental physico-chemical factors needed do design levulinic acid-modified furan coatings which will have strong bonding forces with crystalline zinc phosphate hydrate films deposited on metal substrate surfaces.

On the other hand, crystalline zinc phosphate (Zn·Ph) conversion precoats deposited on carbon steel surfaces play an important industrial role in upgrading the corrosion resistance and coating adherence properties of substrate materials, and phosphating processes have been used for this purpose for decades.

Conventional Zn·Ph conversion crystals are formed by dipping steel plates in a phosphating solution which is composed of zinc oxide (ZnO) and phosphoric acid (H_3PO_4) as the major chemical constituents, and distilled water. The surface roughness of the crystalline Zn·Ph precoating acts to enhance the magnitude of wettability and spreadability of the liquid resins, thereby increasing the degree of the mechanical interlocking bonds at the polymer-Zn·Ph interfaces. In addition, the formation of highly dense Zn·Ph crystals contributes significantly to the corrosion resistance of the steel substrates. For maximum effectiveness, the Zn·Ph precoating should be impermeable since it could provide corrosion protection in the event that the polymeric topcoat is damaged or delaminates. It has been determined that the chemical constituents of the steel substrate upon which the conventional zinc phosphating formulation is placed, play a key role in forming high quality Zn·Ph coatings. In particular, a surface having a high carbon concentration impedes the formation of the Zn·Ph coating. Low zinc and phosphorous levels at high carbon areas result in a porous structure and poor bonding to the substrate. These characteristics lead to a higher oxygen and moisture availability at the substrate surface and promote a cathodic delamination reaction as follows:

$$H_2O + 1/2\ O_2 + 2e^- \longrightarrow 2\ OH^-.$$

The generated hydroxyl ions (OH^-) induce an alkaline condition which causes delamination at the precoat/substrate interfaces. The solution to this problem is to apply the ZnO-based phosphate solution onto steel

surfaces containing a low carbon content. The microstructure and thickness of the conversion layers play major roles in restraining physical deformation failures of the Zn·Ph layers. Increased thickness results in increased brittleness, thereby, enhancing the potential for failure during flexure or other deformation. A thin uniform array of fine dense crystals, which is flexible, is needed to yield the optimum precoating system.

The incorporation of organic materials in the zinc phosphating liquid as a method for improving the stiffness, the flexibility, and the moisture impermeability of crystalline films appears possible. The proton-donating COOH groups in polyacrylic acid (PAA) which can be expressed in terms of polyelectrolyte macromolecules undergo an ion-exchange reaction with the free metallic ions in an aqueous medium. The active high-valency metallic ions contribute to the formation of inter- and intramolecular cross-linking of the polyelectrolyte macromolecules due to the salt bridge structure which replaces two hydrogens in the COOH groups located in the pendent of PAA. The nature of the ion-polyanion reaction mechanism suggests that the addition of a high molecular weight PAA may be very effective in controlling the deposited crystal size.[18-20] When the polyelectrolyte macromolecules are added to the zinc phosphating liquids, it is assumed that acid-base and charge transfer interactions will occur between the COOH groups and the divalent Zn ions which are a major chemical component of the crystallized Zn·Ph hydrate films. This chemisorbing function of the COOH groups resulting from this complex formation may serve to restrict crystal growth.

Therefore, the final objective in this study was to determine how the polyelectrolyte macromolecule-containing zinc phosphate conversion crystal film, formed by treating the metal surface with the PAA-modified zinc phosphating liquid, contributes to the improvement in the controllability of crystal thickness, the wettability by liquid resin, and the adherent properties to polymeric topcoat systems. The presence of organic polymers in the conversion films is expected to result in a film which will act in a manner similar to a primer for conventional polymer topcoatings. Expected primer formations may display an ability to promote the bonding forces at the composite film - polymeric topcoat interfaces.

In an attempt to accomplish the three objectives described above, fundamental studies of the physico-chemical factors affecting the hydrothermal resistance and bonding of polymeric composites to steel surfaces were initiated in August 1982 by Brookhaven National Laboratory (BNL) under contract with the U.S. Army Research Office and completed at the end of July 1985. The work emphasized the fundamental understanding of the principles governing the formation and mechanisms of stable adherent protective coatings on steel substrates. The technical feasibility for the surface modification and tailoring of a given substrate to achieve certain desired characteristics was also appraised.

In order to achieve the program goals within the 3-yr contract period, a detailed outline and schedule for the study was prepared. This is shown in Figure 1. The Phase I study was performed within the first 12-mo and focused on the self-healing protective mechanisms of composite coating systems consisting of polymethylmethacrylate (MMA) and hydraulic-type calcium silicate compound fillers, under hydrothermal conditions up to 200°C, and their physico-chemical characteristics. Surface oxide treatments for the cold-rolled carbon steel substrates needed to achieve successful bonding were also explored in this phase of the program. Based upon the fundamental work conducted in FY 1983, the physico-chemical factors governing the nature and role of the interfacial interactions between the functional polymers and the chemically oxidized metal surfaces were studied in Phase II which was performed in FY 1984 and FY 1985. In Phase III, which was conducted during FY 1985, emphasis was given to the modification of the crystalline Zn·Ph conversion precoatings deposited on the metal surfaces, in order to significantly improve the mechanical properties of the precoat layers, adhesion forces to the polymeric topcoat, and corrosion-inhibiting ability.

II. SELF-HEALING TYPE METHYLMETHACRYLATE COMPOSITE COATINGS

In protective systems in which a topcoat is overlaid on a substrate, the most important factors for suppressing corrosion include, not only the formation of high quality interfaces and strong interfacial attractions, but

PHYSICO CHEMICAL FACTORS AFFECTING HYDROTHERMAL
RESISTANCE AND BONDING OF POLYMER COMPOSITES TO STEEL SURFACES

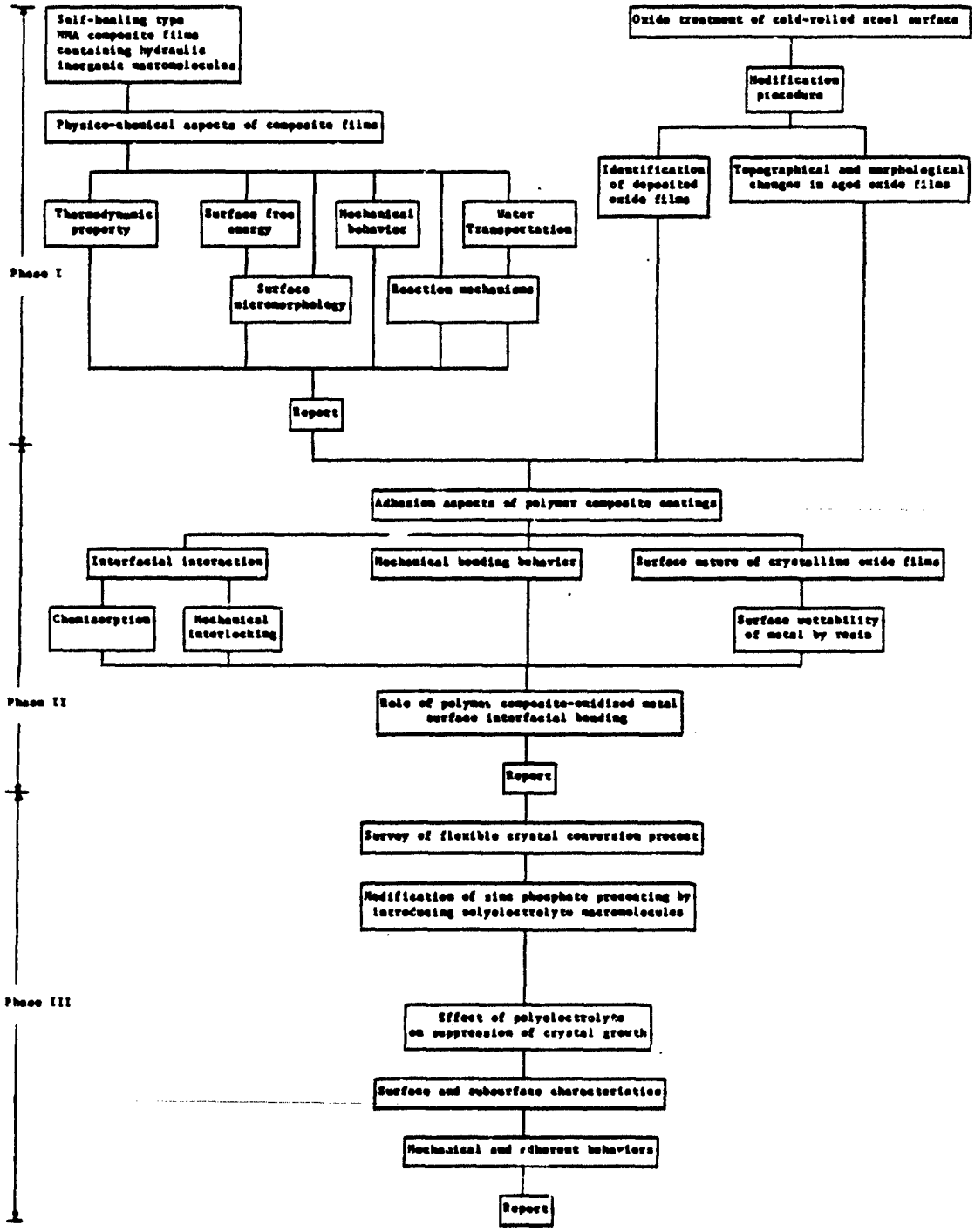

Figure 1. Program outline.

also the hydrophobicity and mechanical properties of the polymer topcoat itself. It is well-known that the organic polymers containing functional groups, such as amines (—— C(=O) —— NH ——), esters (—— C(=O) —— O ——), and acetals (—— O —— CH_2O ——), in which any two atoms selected from N, O, and S are joined to the same carbon atom, are very sensitive to hydrolysis, particularly in hydrothermal environments. The polymer degradation can be suppressed by increased coating thickness and by the presence of calcined reactive fillers. The latter, in particular, offers the interesting possibility of forming self-healing protective films. This reactive filler is characterized by the production of crystallized inorganic macromolecules and dissociation of the divalent metallic ions from the filler surfaces in an aqueous medium.

A. Materials

The methylmethacrylate (MMA)-based polymer system used as a film-forming material consisted of a mixture of 57 wt% MMA monomer (duPont Type EP-4160), 38 wt% bead polyMMA (duPont Elvacite 2008) with a molecular weight of ~$3x10^4$, and 5 wt% trimethylolpropane trimethacrylate (TMPTMA) cross-linking agent (Satamar Co., Ltd.). This resin blend had a viscosity of 217 cP and a surface tension ($\gamma_{L,V}$) of 32.10 dynes/cm at 24°C. Since MMA-TMPTMA copolymers are glassy and brittle, the flexibility of the resin over the temperature range of interest was enhanced by incorporating a 10 wt% dibutoxyethyl phthalate (DBEP) plasticizer (C.P. Hall Company). Polymerization of the plasticized MMA-TMPTMA resin was initiated by adding 3 wt% benzoyl peroxide (BPO) of 98% purity and 1 wt% N,N-dimethyl-ρ-toluidine (DMT) at an ambient temperature of 24°C. After mixing of all the ingredients, the gel time of the resin was ~10 min.

A commercial class J cement (Lehigh Portland Cement Company) was used as a hydraulic-type reactive additive and a source of divalent metallic cations. This type of cement is frequently used in the completion of oil wells operating at temperatures >110°C. Its chemical constituents were

as follows: CaO 40.68%, SiO_2 50.97%, Al_2O_3 0.86%, MgO 1.01%, Fe_2O_3 0.70%, and SO_3 0.29%; loss on ignition was 4.75%. Class J cement is characterized by its high silica content, which is needed to prevent strength retrogression at temperatures >110°C.

Silica flour filler, which is generally used as a pigment in organic coatings, was used as a reinforcement in the films. The particle size of both the cement and the silica flour additives was <200 mesh (0.074 mm). To prepare the composite films, 50 parts of the initiated MMA-TMPTMA resin were added to 50 parts of the silica flour-class J cement filler. Six different ratios of silica flour to cement (100/0, 90/10, 80/20, 70/30, 50/50, and 30/70) were tested. After the two components were thoroughly hand-mixed for ~30 sec, filled composite films with a thickness of 25 to 33 mils were cast on polyethylene sheets with a casting knife and then cured at room temperature for ~2 hr.

B. Measurements

Measurements of the physico-chemical factors were done on film and coated samples before and after exposure in an autoclave for up to 10 days at temperatures of 100°, 150°, and 200°C.

The glass transition temperature, T_g, of the polymer composites was measured with a duPont 910 differential scanning calorimeter (DSC) equipped with a DSC cell at a heating rate of 10°C/min under nitrogen gas flowing at a rate of 50 ml/min. The samples weighed 10 to 12 mg.

Tensile strength tests were done on dumbbell-like rigid composite film samples 70 mm long and 5 mm wide at the narrowest section. Stress-strain diagrams were obtained with a tensile tester having a crosshead speed of 0.5 mm/min. All strength values reported are for an average of three specimens. The changes in weight of the films after exposure were also measured as a function of time at the prescribed temperatures.

A Perkin-Elmer Model 257 spectrometer was used for infrared analysis. The tests were performed by preparing KBr discs made by mixing 200 mg KBr and 3 to 5 mg of the powdered samples that had been crushed to a size of <0.053 mm. The spectra were run at an 8 min scanning rate over the range of 4000 to 600 cm^{-1}.

Contact angle measurements on the film and metal surfaces were made with a Contact Angle Analyzer. All measurements were made at 60% R.H. and 24°C within 30 sec of drop application. Surface tension measurements were made with a Cenco-Du Nouy Tensiometer Model 70535.

Electrode potential measurements on metal plates (5.0 x 5.0 cm) coated with cement and silica-filled copolymer paints were made after exposure for up to 25 days in an autoclave at 150°C in order to estimate the water permeability through the coatings. Coatings of 10 and 25 mil thickness were tested. The coated and the base anode test plates were then immersed in a 4% NaCl solution at 24°C. The distance between the plates was 10.16 cm. A one volt potential was established across the plates and the resulting current flow measured.

Microstructure deformation of the film surfaces caused by hot water attack was observed by scanning electron microscopy (SEM) and JEOL transmission electron microscopy (TEM). The SEM samples were prepared by depositing a gold film on the surface of composite films. SEM and TEM examinations were also employed to identify the morphological features of the hydration compounds formed on the amorphous polymer layers.

C. Results and Discussion

1. Glass Transition Temperature

High molecular mobility and segmental jumping frequency of the main chains of an amorphous polymer, during exposure to hot water, is one of the physico-chemical factors affecting the hydrothermal disintegration of polymer films, caused by the chain scissions. It is therefore important to investigate the magnitude of the segmental immobilization in terms of the chain stiffness and the rigidity of the polymer molecules. Since the glass transition temperature, T_g, is a second-order temperature which can be regarded as the relaxation and motion of the major segments in the backbone molecular chains of an amorphous polymer,[21,22] the T_g of the polymer composites was determined as a means of estimating the degree of segmental mobility of the polymer molecules.

The influence of the hydrated inorganic macromolecules on the stiffness of the polymer chains was analyzed by comparing T_g values for the plasticized MMA-TMPTMA copolymer films containing mixed fillers with various ratios of silica flour (S) to hydralic cement (C). Differential scanning calorimetry (DSC) at a heating rate of 10°C/min was used to determine the T_g of the samples. Typical DSC thermograms showing the essential features for film samples containing S/C ratios of 100/0, 90/10, 70/30, and 30/70, after exposure in an autoclave to water at 150°C for 24 hr (Figure 2) all have endothermic peaks between 57° and 69°C. The T_g values were obtained from the endothermal peaks by finding the intersection point of the two linear extrapolations. The data indicate that use of an optimum amount of cement in the mixed filler consisting of silica and cement raises the T_g of the composite film after exposure to hot water. Samples containing filler with a S/C ratio of 70/30 had a T_g of 63°C, ~6°C higher than that at S/C = 100/0. Since the segmental immobilization of chains is directly related to an increase in T_g,[23] this apparently verifies that the macromolecules formed by hydraulic reactions of the cement in contact with hot water serve to restrict the segmental mobility of the main chains. The slight reduction in T_g at a S/C ratio of 30/70 indicates that the optimum concentration of cement in the filler is between 30 and 70%.

Tensile strength and T_g data, as a function of S/C ratio for the composite films after exposure to water at 150°C for 24 hr, are given in Figure 3. The T_g rises with increasing cement content until it reaches a maximum of 63.5°C at a S/C ratio of 50/50.

The curve for the tensile strength of the film as a function of the S/C ratio is similar to that for T_g. The data indicate that the strength increases with S/C ratio between 100/0 and 70/30, and then decreases. The ultimate strength, 1150 psi, for copolymer films with a mixed filler having an S/C ratio of 70/30 was ~70% higher than that of films with a silica flour filler lacking cement.

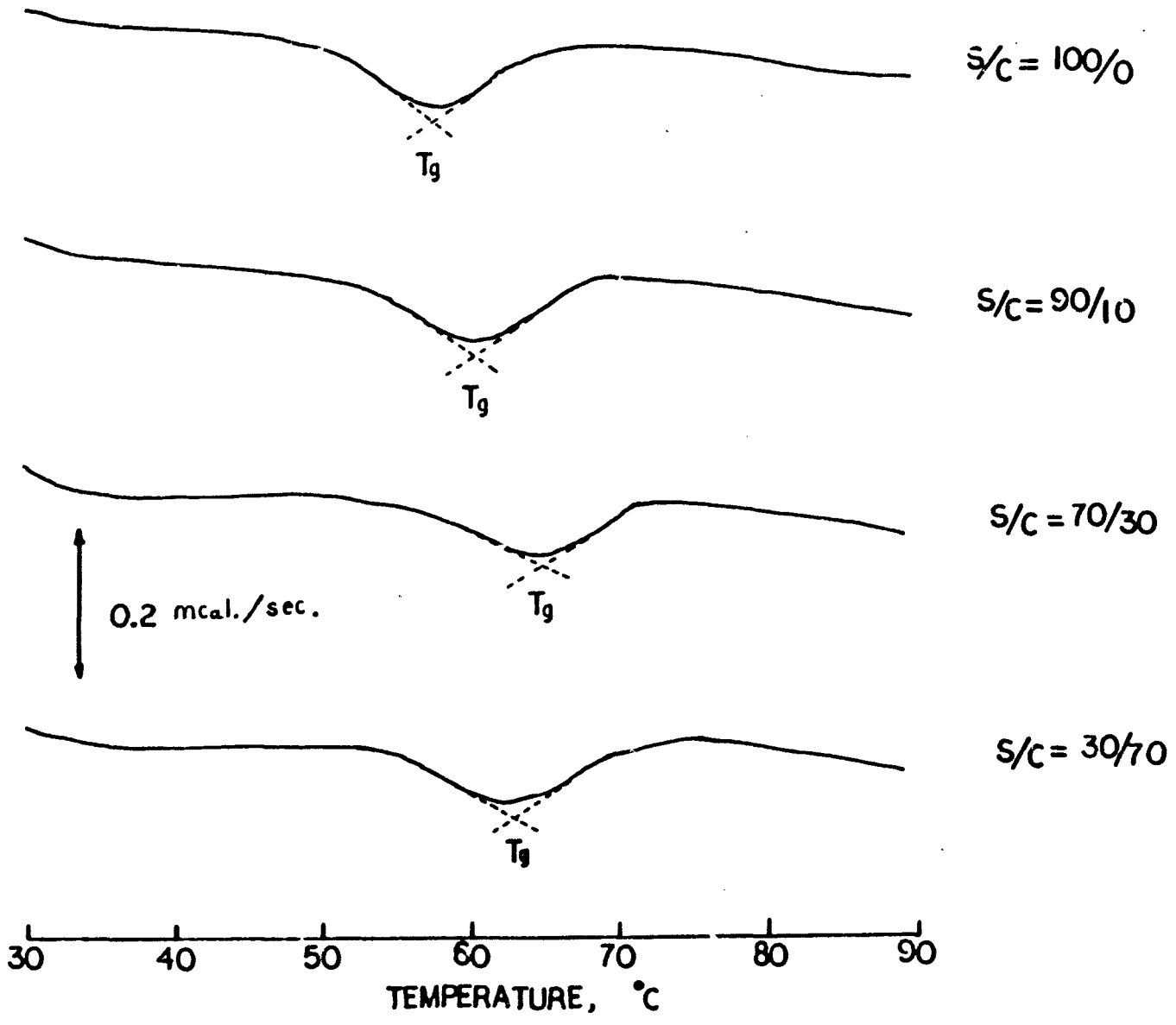

Figure 2. DSC thermograms of MMA-TMPTMA copolymers having fillers with various S/C ratios, after

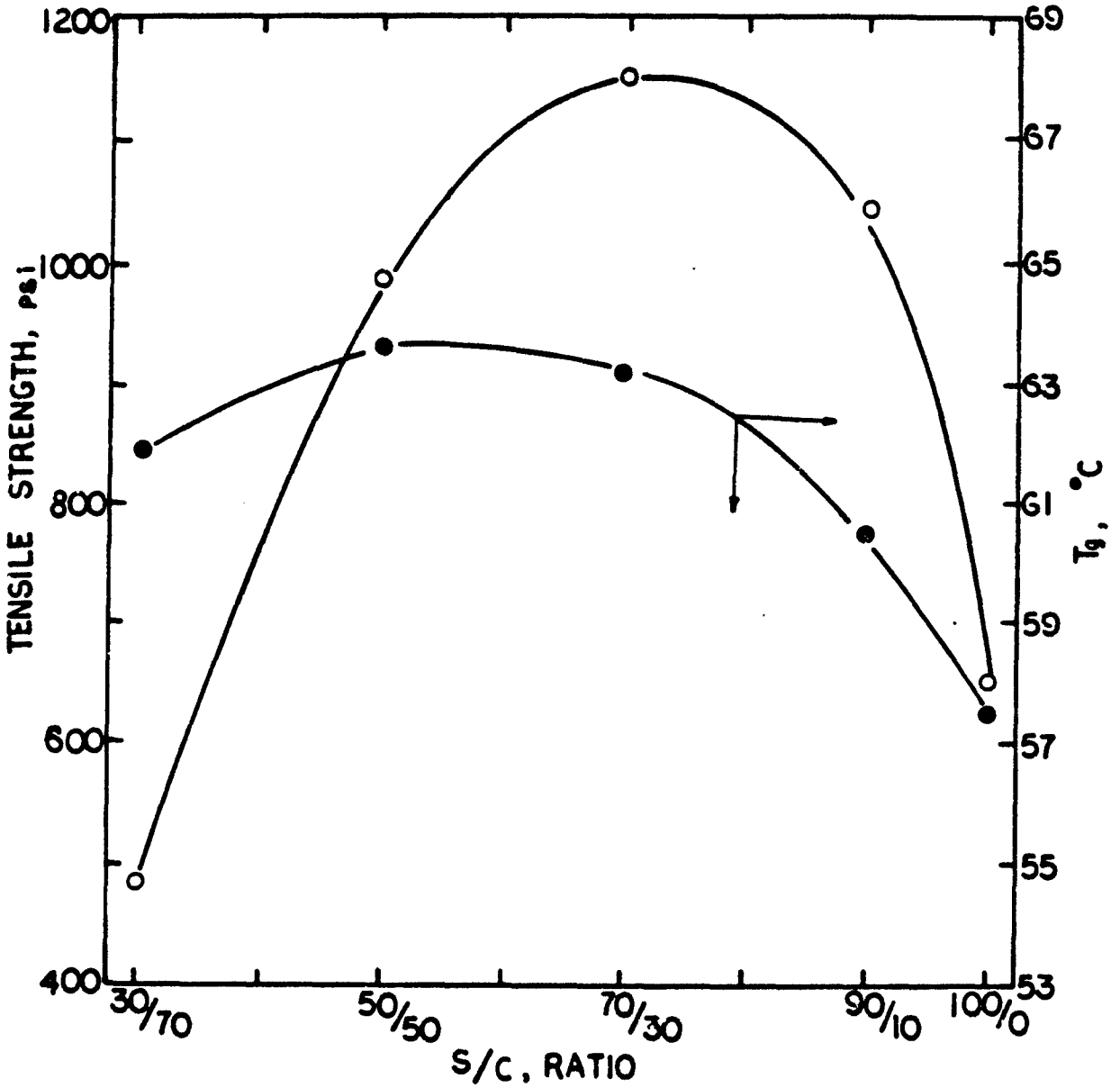

Figure 3. Tensile strength and T_g of films as a function of S/C ratio after exposure to water at 150°C for 24 hr.

Many recent investigations[24-26] have shown that the influence of T_g behavior on filled polymers depends mainly on the segmental adsorption and orientation of the main chains in the immediate vicinity of the filler surface. These can result in strong filler-polymer interactions and agglomeration forces. Strong filler-polymer interfacial forces also contribute to the enhancement of the mechanical strength of composite materials. However, the newly produced formations at the interface between the configurated macromolecules and the polymer chains not only yield strong agglomerations and chain entanglements but also are likely to produce increased interfacial stresses which result in chain enlargement occurring along with the growth of the macromolecules. Therefore, the reductions in film strength as the S/C ratio is decreased can be interpreted as being due to extraordinary chain enlargement which exerts a "squeezing" force on the larger macromolecules formed on the polymer layers. These high interfacial stresses can be reduced by the formation of microcracks between the polymer matrices and the macromolecules. In fact, for copolymer films containing a filler with a S/C of 30/70, and having a decreased T_g of 61.5°C, the tensile strength was down to 480 psi, which resulted in deformation and microcracking of the films. These results suggested that the optimum amount of reactive cement must be used with the silica flour in the filler to prevent film strength reduction due to squeezing deformations.

The changes in weight of the composite films after immersion in water at 150°C for periods of up to 10 days were also measured (Figure 4). The control samples (S/C = 100/0) showed weight loss throughout the exposure, up to ~15% after 10 days; they also showed many blisters on their surfaces. In contrast, the films with mixed fillers containing cement and silica flour increased in weight. Samples with S/C = 70/30 filler increased in weight rapidly over the first 24 hr, and then more gradually for the duration of the 10-day exposure. This was due to conversion of the cement grains in the copolymer matrix into hydrated cement compounds based on the $CaO-SiO_2-H_2O$ system during exposure to hot water. The film surfaces showed little or no blistering.

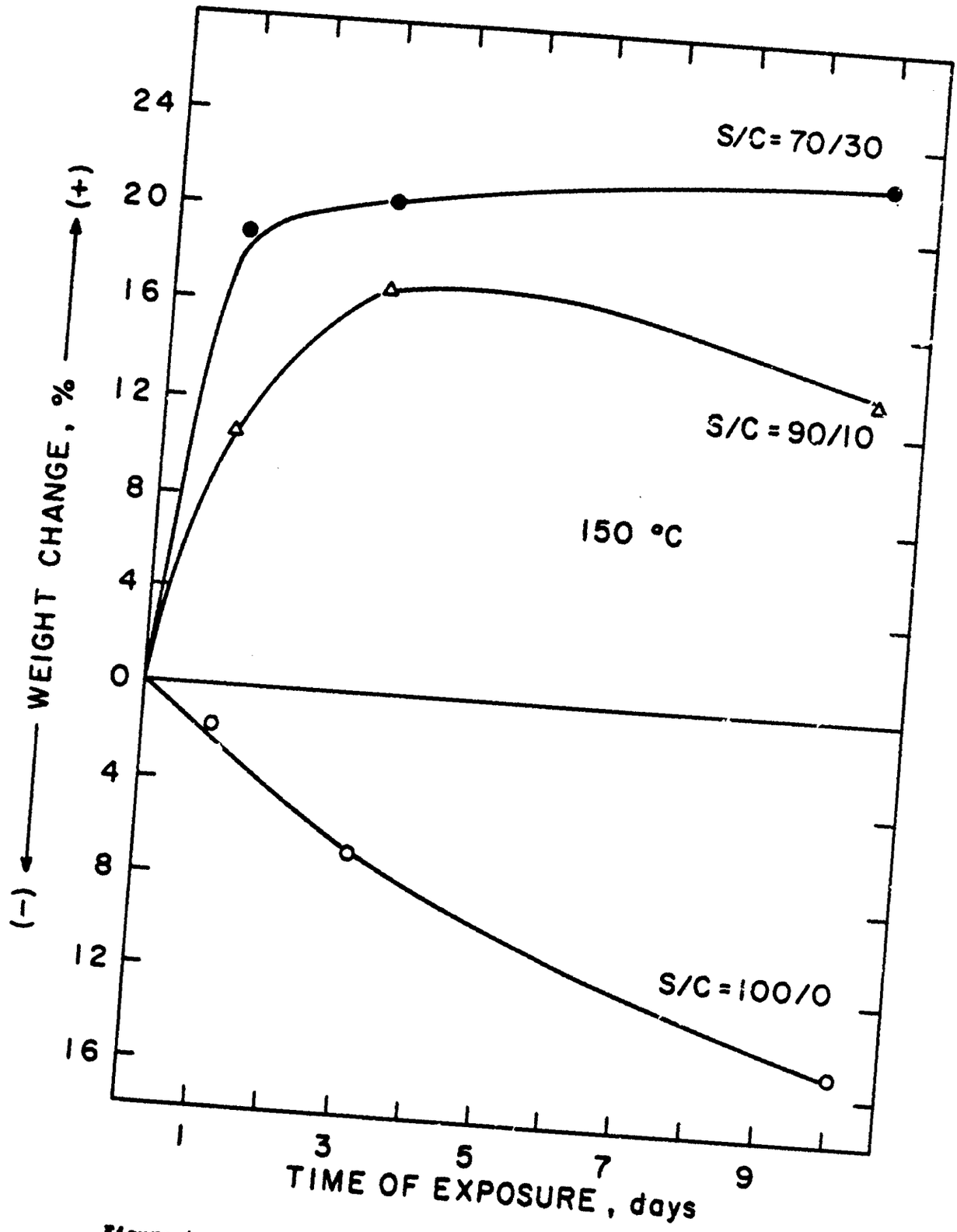

Figure 4. Film weight changes after exposure to water at 150°C.

Samples with S/C = 90/10 filler, when exposed for 10 days to the hydrothermal environment, increased in weight for ~3 days and then gradually decreased, but they showed no evidence of deterioration or corrosion.

2. Complex Mechanisms

Infrared (IR) absorption spectroscopy was used to elucidate the role of cement additives as a means for improving the hydrothermal stability of MMA-TMPTMA copolymer containing carboxyl groups (O=C-O-R) in the side chains. To prepare the samples, films exposed to 200°C hydrothermal conditions for 10 days were first dried in an oven at 100°C for 24 hr and then ground to a particle size <0.0074 mm.

Earlier work[1], had shown that hydrothermal deterioration of polymers, caused by the hydrolysis of a pendent carboxyl group, can be restrained by ionic cross-linking initiated by the strongly nucleophilic Ca^{2+} ions released from cement during contact with hot water. A salt bridge consisting of $-COO^{-}---Ca^{2+}---^{-}OOC$ complexed formulations, resulting from ionic bonding between the Ca^{2+} ions and the carboxylate anions (COO^{-}) from the hydrolysis of carboxyl groups, has been confirmed by asymmetrical and symmetrical stretching vibrations at 1540 and 1398 cm^{-1} in the IR spectrum. In addition, a correlation between the reduction in absorbance of the carbonyl groups at 1710 cm^{-1} and the increasing intensity of $COO^{-}(Ca^{2+})$ complex groups at 1540 and 1398 cm^{-1} suggested the possibility of measuring the rates of conversion to carboxylate anions. Accordingly, the degree to which ionic Ca^{2+} complex salt formations affected the restoration of hydrothermal degradation was assessed on the basis of the shifts in IR frequency and the changes in band intensity at 1710, 1540, and 1398 cm^{-1}.

The test results from these samples (Figure 5) show that the intensity of the $COO^{-}(Ca^{2+})$ frequency at 1540 and 1398 cm^{-1} increases as the cement content of the filler increases. Conversely, the band of carbonyl groups at 1710 cm^{-1} tends to shorten with growth of the $COO^{-}(Ca^{2+})$ bands. These results verify that the carboxylate anions, produced by hydrolysis of the pendent carboxyl groups in the copolymer molecules, are converted into $COO^{-}(Ca^{2+})$ groups by the nucleophilic Ca^{2+} ions released from cement

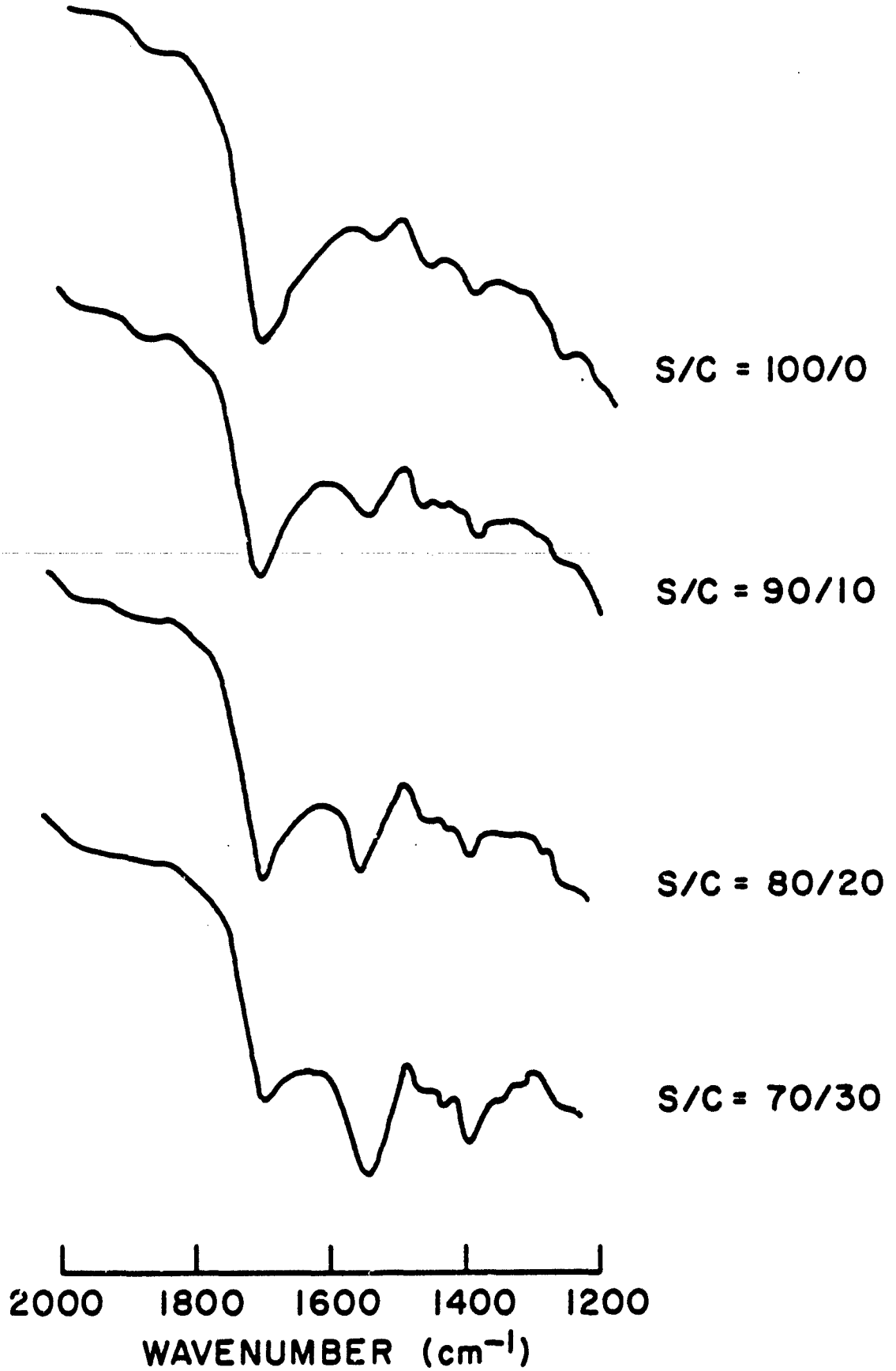

Figure 5. Shift in IR frequency as a function of S/C ratio at 200°C.

grains during exposure to hot water. Since an increment of salt bridge formations per molecule results in an abundant supply of Ca^{2+} ions, the optimum amount of cement additive should be used to provide a source of Ca^{2+} ions for inhibiting polymer chain scission caused by the hydrolytic decomposition of the pendent groups.

The rate of reaction between the Ca^{2+} ions and the COO^- anions as a function of hydrothermal temperature, from 50° to 200°C, was quantitatively estimated by comparing the absorbance ratios of the $-COO^-(Ca^{2+})$ groups at 1540 cm^{-1} and the C=O groups at 1710 cm^{-1}. Samples containing a filler with a S/C ratio of 70/30 were used in the IR spectrophotometry analysis. Prior to testing, the films were exposed for 10 days to water at temperatures of 50°, 100°, 150°, and 200°C.

In IR quantitative analysis, the peak height or the area of the band is taken as the criterion of band intensity. Therefore, an accurate measurement of band intensity is very important. The absorbances of two peaks were determined as the distance from the absorption maximum to a baseline connecting the two wings of the band.

A plot of the absorbance ratio as a function of temperature (Figure 6) shows a direct linear relationship. This implies that the intensity of the band characteristic of $COO^-(Ca^{2+})$ formation becomes stronger as the C=O group band intensity decreases. Accordingly, it appears that a large number of pendent carboxyl groups are converted into carboxylate anions by the hot water. These anions simultaneously produce Ca^{2+} salt bridge structures (formed by ionic reactions with the Ca^{2+} ions) which play an essential role in binding the COO^- ions. The data also suggest that the rate of ionic bonding through salt formation is directly related to the temperature up to 200°C and to the quantity of cement mixed with the silica flour filler. The absorbance ratio of 0.55 at 200°C seems to indicate that >50% of the carboxyl groups were changed in the Ca salt formations. This is ~18 times as large as the percentage for samples at 50°C.

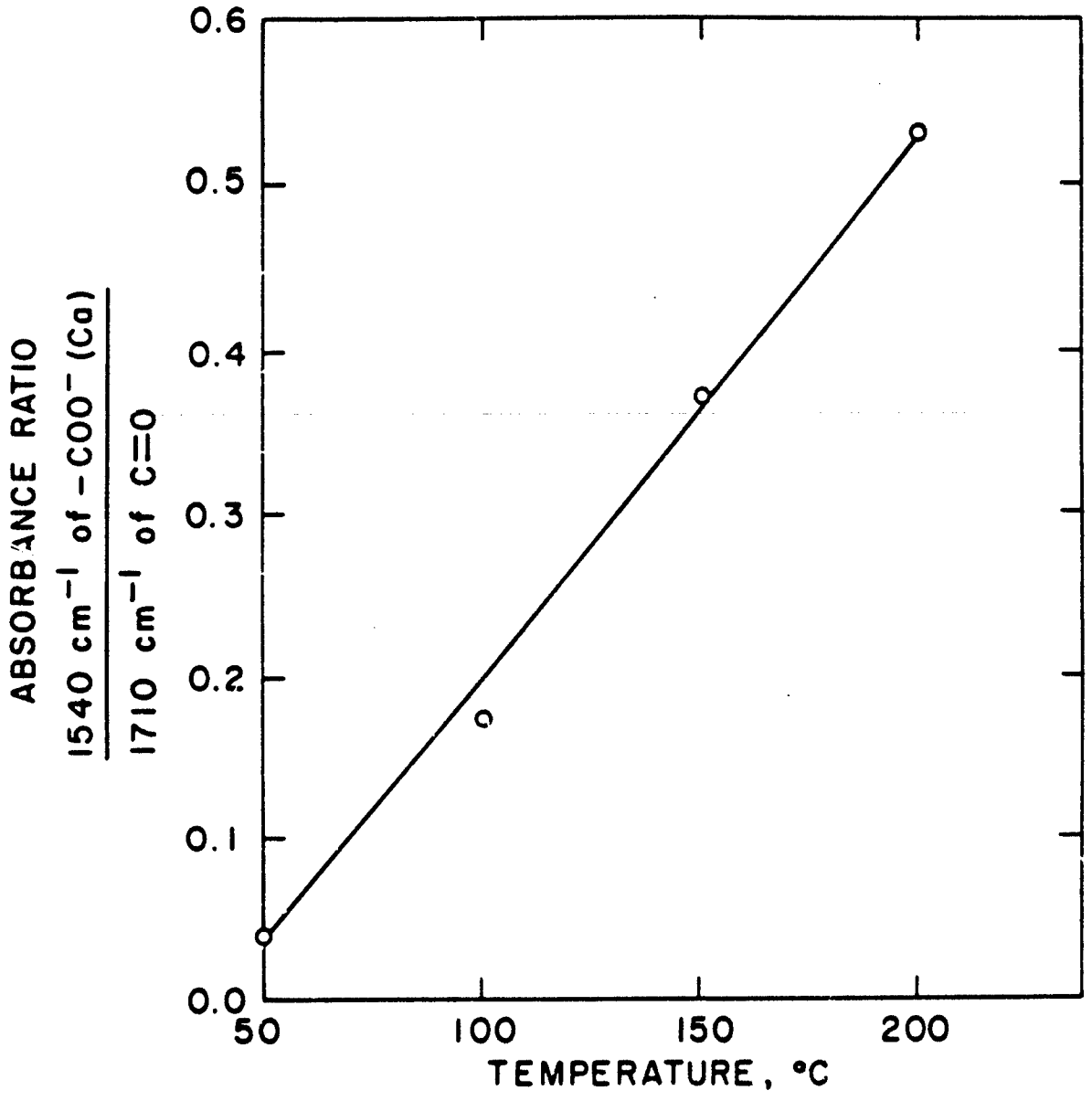

Figure 6. Relationship between absorbance ratio and hydrothermal temperature for film containing filler with a S/C ratio of 70/30 after exposure to hot water for 10 days.

Three possible molecular structures for the calcium carboxylate complexes can be deduced. These are shown below.

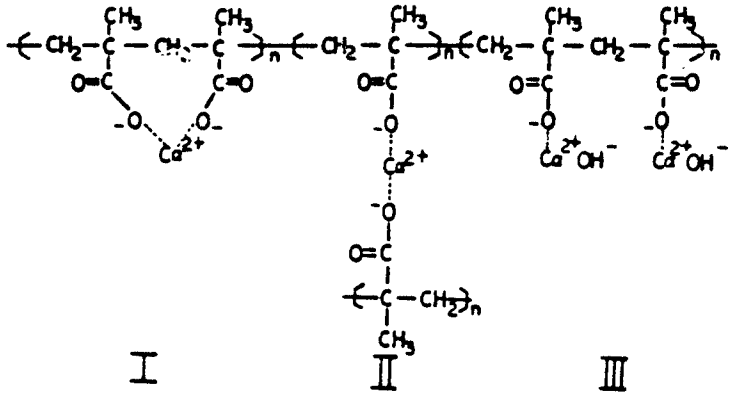

I II III

Complexed structure (I) is characterized as an intramolecule hydrated salt-type formed within the single chain, and (II) refers to an intermolecule hydrated salt-type through the cross-linking structure which connects two adjacent carboxylates between the chains. The calcium cation in a salt bridge will be stabilized by six water molecules to give an octahedral structure[27]. The neutral H_2O molecules coordinated to the Ca^{2+} ions will be stable enough to remove water vapor from ordinary air at ambient temperature[28]. An alternative formation, (III), may be interpreted as a pendent half-salt.

Assuming that the Ca-complexed ionomer matrix consists of the above three species, formations (I) and (II) contribute significantly to enhancement of the chain stiffness, lower the degree of free rotation of the chains, and increase the chain entanglements, thereby increasing T_g levels and the mechanical strength of the films[29]. On the other hand, the half-salt located in the pendent groups may be presumed to have little if any

effect on restraining chain rotation. With regard to half-salt molecular structures, $-COO^{-}--Ca^{2+}OH^{-}$ groups containing an interchangeable hydroxyl group are more likely to be hydrophilic than hydrophobic.

3. Thermal Behavior Analysis

The enhanced thermal stability of Ca-complexed compound films was assumed to be due mainly to the presence of a larger number of salt bridge formations and to the hydrated inorganic macromolecules formed during exposure to the hydrothermal environment. Thermal measurements intended to clarify this assumption were made by using thermogravimetric and differential thermal analysis (TGA and DTA). Since the numbers of salt formations and of hybrid macromolecules increase with increasing hydrothermal temperature, copolymer films with S/C 30/70 filler were exposed for 3 days to water at temperatures of 24°, 150°, and 200°C. After exposure, the thermal behavior analyses were performed at a heating rate of 10°C/min in nitrogen gas.

The TGA thermograms are shown in conjunction with the DTA curves in Figure 7. The TGA curve for the samples exposed at 24°C (the controls) indicates that weight loss began at ~225°C. It reached 13% at ~275° and 40% at ~400°C. These temperatures correspond to weak and strong endothermic peaks on the DTA curve. The former peak may be due to the rotational energy of the molecular chains and the latter to the integrated heat of fusion.

In contrast to the controls, which lost no weight up to ~225°C, the samples that had been exposed to water at 150° lost ~0.13 g over the temperature range 80° to 200°C. This appears to be directly related to the two weak DTA endothermal peaks at 80° and 175°C. The peak at ~80°C is attributed to vaporization of free water. The total amount of free water was calculated from the TGA data to be ~0.03 g. This corresponds to ~0.26% by weight of the total composite mass.

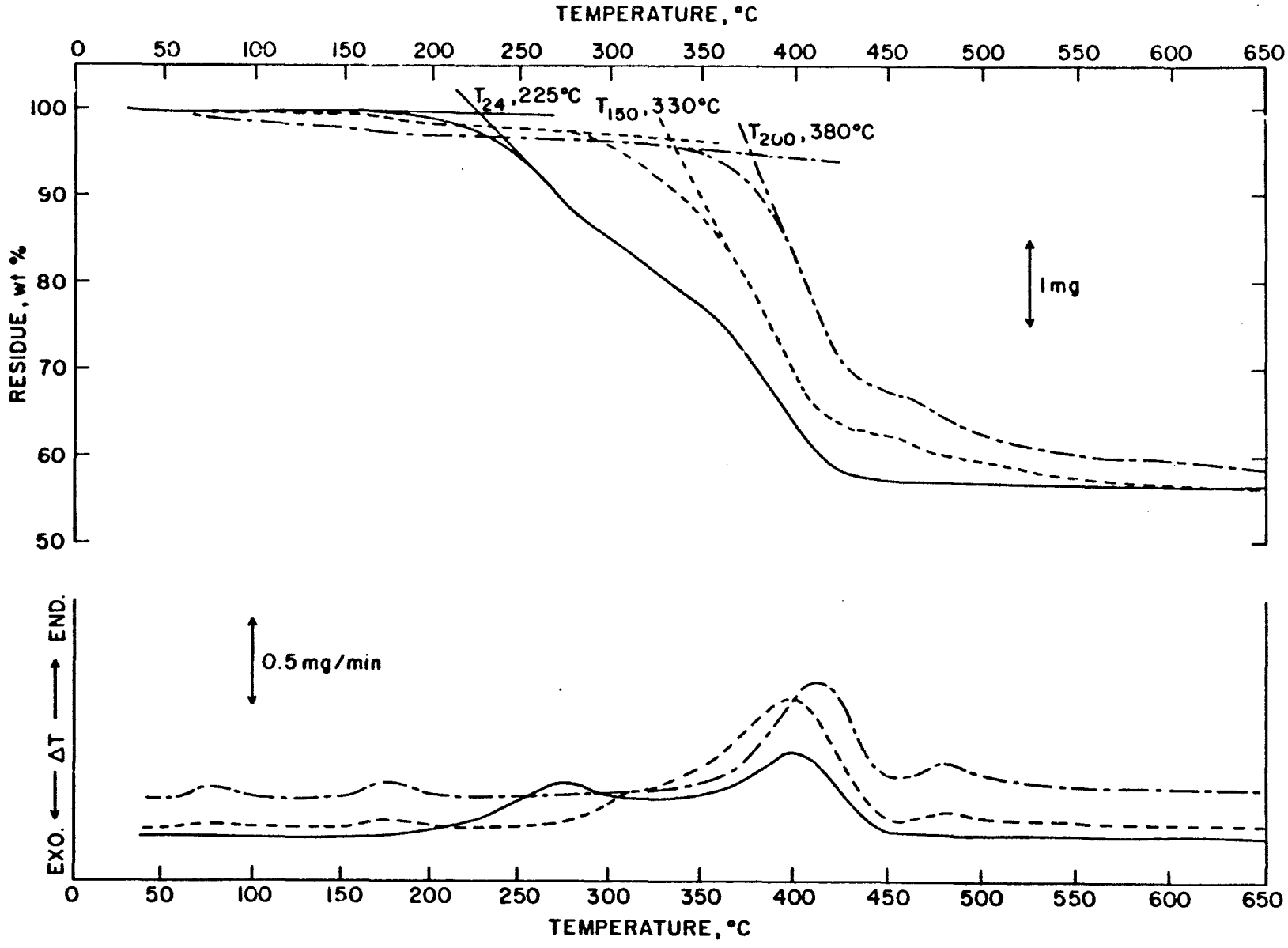

Figure 7. TGA and DTA curves for copolymer films with S/C 30/70 filler after exposure to water at temperatures of 24°C (——), 150°C (---), and 200°C (-·-).

The weight loss at ~175°C may be due to thermal dissociation of bound water, including the gel water combined with the hydraulic cement and the neutral H_2O molecules coordinated to Ca^{2+} ions in Ca^{2+} bridges. The amount of bound water was calculated to be ~0.1 g. The onset temperature for thermal decomposition of the 150°C sample was ~330°C, ~105°C higher than that of the control. The DTA curve shows that the intensity of its endothermal peak at ~300°C is much weaker than that for the control. This may imply that the chain rotation energy, which can be determined from the total area of the curve enclosed by the baseline, was reduced by the formation of salt complexes and by the inorganic macromolecules produced during the hydrothermal exposure.

Another weak peak appears in this curve at 480°C. This is due[30] to the dehydration of $Ca(OH)_2$ and is related to the slight weight loss between 480° and 540°C on the TGA curve. The $Ca(OH)_2$ formation of ~0.15 g was calculated on the basis of the distance between the onset of the two linear portions before and after the transition period, on the TGA curve. It amounts to ~3.72% by weight of anhydrous cement used.

The sample that had been exposed to water at 200°C lost ~0.18 g of water between the temperatures 50° and 110°C. The slight change in the slope of its TGA curve near 150°C is due to the presence of ~0.16 g of bound water, which is ~60% greater than that in the samples exposed at 150°C.

It is well known that the amount of water in a well-hydrated cement retained at 105°C is generally ~20% by weight of the anhydrous cement[31]. Thus, if ~0.16 g of bound water is assigned to the hydrated cement, this corresponds to ~4.1% by weight of the total anhydrous cement mass. It may, therefore, be interpreted that ~21% of the cement present in the copolymer matrix was completely hydrated. However, since some H_2O molecules coordinated to Ca^{2+} ions should also be contained as bound water, the amount of hydrated cement is actually <21%. These results seem

to suggest that the hydration products of cement are probably formed in a very thin superficial layer on the films, where they seem to protect the organic polymer from hydrothermal deterioration. On the other hand, the onset temperature of the major weight loss, as determined by TGA, was ~380°C. This was accompanied by a prominent endothermic peak at 425°C on the DTA curve. The high onset temperature, 50°C above that for the 150°C samples, seems to verify that the configurative combination between the highly formed salt complexes and the macromolecules contributes significantly to the improvement in the hydrothermal stability of the composite films. The temperature at which the film exhibited a 40% weight loss was ~600°C. DTA data also indicated the disappearance of the exothermal peak at ~300°C. Therefore, it appears that these formations enhance chain stiffness. On the basis of the change in the TGA slope at ~470°C, the amount of $Ca(OH)_2$ produced was estimated to be ~0.2 g, which corresponds to ~5.1% by weight of the anhydrous cement.

4. Wetting Behavior of Film Surface

Since the wettability relationship between water and a solid surface is considered to be a type of complex water-solid interaction,[32] the magnitude of the water wettability of a plane film surface can be estimated from the value of the work of adhesion, W_A (H_2O), which is a generally useful index of surface wetting. The value of W_A (erg/cm^2) was calculated by using the well-known classical expression originated by Young[33] and Dupre[34],

$$W_A\ (H_2O) = \gamma_{LV}\ (1 + \cos\theta) + \pi^s,$$

where γ_{LV} (dyne/cm) is the surface tension of water at 24°C, θ is the average value of the measurad contact angle on the solid surface, and π^s is the equilibrium spreading pressure of the adsorbed vapor on the solid. In many approaches to the theory of contact angles, π^s has been assumed to be approximately zero[35]. Fox and Zisman[36] showed that γ_{LV} (1 + cos θ) was a good approximation for W_A, the work of adhesion between liquid and solids which do not wet.

The film samples, containing fillers with various S/C ratios, that were used for contact angle and SEM measurements were exposed in hot water for 3 days at temperatures up to 150°C and then rinsed several times with distilled water and dried in the oven at 70°C for 24 hr. All the measurements were made at a temperature controlled at 24.0 ± 0.1°C, and 50% relative humidity. In measuring contact angles, because the angles on the dry film surfaces gradually increased during the first 10 to 20 sec, the static angles were recorded after the boundary of a sessile drop had been allowed to equilibriate for 30 sec after deposition.

A plot of W_A as a function of S/C ratio for films exposed at temperatures of 24°, 100°, and 150°C (Figure 8) shows that W_A is affected both by hydrothermal temperature and by S/C ratio. The W_A values for all samples exposed at 24°C were essentially constant, varying only from 83.0 to 85.9 erg/cm^2, showing that these films, which have a smooth surface, have a relatively low magnitude of surface wettability. In contrast, for the samples exposed in boiling water at 100°C, the W_A value rose sharply at S/C ratios >70/30, going up to 113.6 erg/cm^2 for non-cement-containing control samples. This value was 31.3% higher than that for the sample with S/C 70/30 filler, and 32.9% higher than that obtained from the same film surface at 24°C. The results suggest that the increase in surface wettability with lower cement concentration is probably due to an increase either in the number of hydrophilic groups or in their accessibility to water. The finding that W_A at S/C 30/70 was almost the same as at S/C 70/30 seems to demonstrate that the presence of >30% cement by weight of the total mix filler results in a low surface wettability.

The W_A plot in Figure 8 for films exposed at 150°C showed an interesting variation: the degree of wetting decreased sharply with increased cement concentration between S/C ratios of 100/0 and 70/30, and then increased somewhat with further lowering of the S/C ratio. The decrease in wettability in the S/C range of 100/0 to 70/30 is similar to the trend seen with the 100°C samples. The surface of the control samples had a W_A value of 120 erg/cm^2, and the lowest value (90 erg/cm^2) was for the

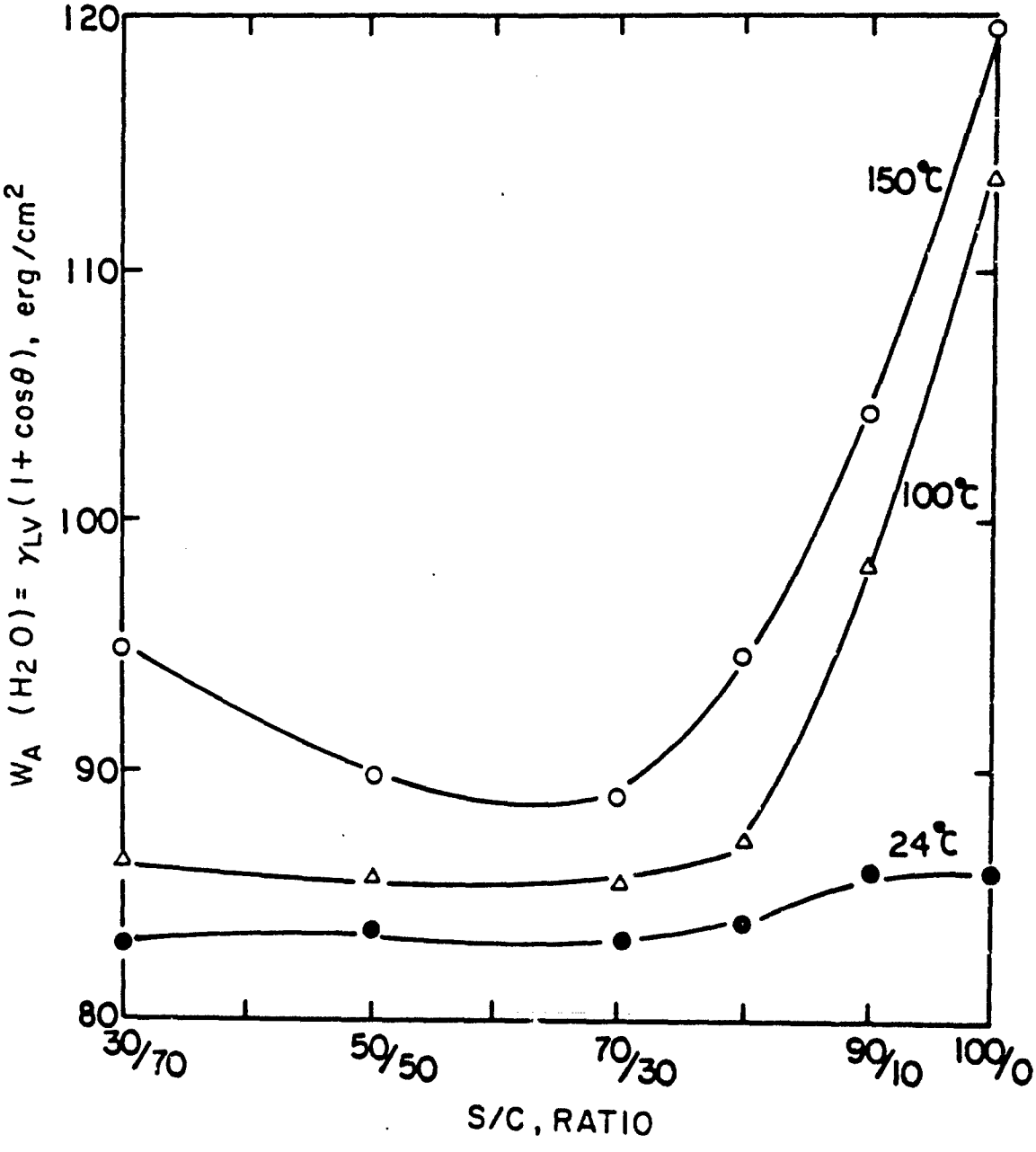

Figure 8. Work of adhesion (water) vs various S/C ratios at temperatures of 24°, 100°, and 150°C.

samples with S/C 70/30 filler. A possible reason for the increased wettability of films with S/C 50/50 (and lower) fillers is enhancement of the surface roughness by squeezing deformation of the films resulting from the increased concentration of hydration macromolecules in the amorphous copolymer matrix.

This can be further clarified by studying the relationship between cosine θ and the IR absorbance ratio for the $COO^-(Ca)$ at 1540 cm^{-1} frequency and the C=O groups at 1710 cm^{-1}. For samples that had been exposed to hot water at 150°C (Table 1), the tendency for the absorbance ratio to increase as the S/C ratio decreases is in agreement with that obtained from films exposed at 150°C. This implies that the hydrophilic carboxylate groups formed by hydrolysis of the carboxyl groups present in the polymer molecules are converted into hydrophobic Ca-complexed salt formations by ionic reactions with free Ca^{2+} ions released from the cement grains in an aqueous medium. Thus, reaction of the abundant Ca ions available from larger amounts of cement is thought to make the polar film surface less hydrophilic and more hydrophobic. On the other hand, cosine θ decreased as the cement quantity was increased from S/C 90/10 to 70/30 and then increased gradually with further decreases in the S/C ratio. In spite of being hydrophobic, the film surfaces may have enhanced wettability between S/C 50/50 and 30/70 because of heightened surface roughness and enlargement of their microcracking spaces. The latter results from the high internal stress concentration developed during growth of large hydrated macromolecules, which allows the transportation of more water.

To support the data on the wetting behavior, the surface free energy for the exposed film samples was determined by methods developed by Owens et al.[37] and Baszkin et al.[38] which are especially applicable to the surface characterization of polymers. Film surfaces that have high contact angles lack affinity for water and have a lower surface energy. Therefore, surface energy is one of the important factors affecting water permeability.

TABLE 1

Variation of Contact Angle and Absorbance Ratio as a Function of S/C Ratio for Samples Exposed at 150°C

S/C ratio	Cos θ (Water)	Absorbance ratio, 1540 cm^{-1} of $COO^-(Ca)$ / 1710 cm^{-1} of C=O
90/10	0.43	0.043
80/20	0.30	0.081
70/30	0.22	0.104
50/50	0.24	0.136
30/70	0.31	0.142

In measuring the total solid surface free energy γ_s, it is assumed that γ_s is the sum of two components: the dispersion forces γ^d and the dipole-hydrogen bonding forces γ^p. The geometric mean equation, proposed as a natural extension of the Fowkes[39] empirical formula by Owens et al.[37], was used to estimate these energy contributions for the high surface-energy systems:

$$\gamma_{SL} = \gamma_s^o + \gamma_{LV} - 2\sqrt{(\gamma_s^d \gamma_L^d)} - 2\sqrt{(\gamma_s^p \gamma_L^p)} \qquad (1)$$

where γ_{SL} is the interfacial tension at the solid-liquid interface, γ_{LV} is the surface tension of liquid on a free surface energy γ_s^o of the solid while under vacuum, and $\gamma_s^d \gamma_L^d$ and $\gamma_s^p \gamma_L^p$ refer to the dispersion forces and polar forces in the solid and the liquid. Generally, equilibrium at the solid-liquid interface depends on the four parameters governed by the following Young's expression:

$$\gamma_{LV} \cos\theta = \gamma_s^o - \gamma_{SL} + \pi^e \quad . \qquad (2)$$

In dealing with the adhesion of a liquid on a perfectly flat solid surface, the free energy of work of adhesion W_A is given by

$$W_A = \gamma_{LV} (1 + \cos\theta) + \pi^e \quad . \qquad (3)$$

By assuming that $\pi^e = 0$ for Eqs. (2) and (3), these equations can be combined and written as follows:

$$W_A = \gamma_{LV} + \gamma_s^o - \gamma_{SL} \quad . \qquad (4)$$

Accordingly, Eq. (1) can be reduced to the general form

$$W_A = 2\sqrt{(\gamma_s^d \gamma_L^d)} + 2\sqrt{(\gamma_s^p \gamma_L^p)} \quad . \qquad (5)$$

In Eq. (5), the values of γ_s^d and γ_s^p, which are needed to obtain the total solid surface energy γ_s, are unknown. They can be determined by the method of Owens et al[37] by measuring the contact angles with water (H_2O) and

methylene iodide (CH_2I_2). The latter is used because its molecules are much larger than H_2O and therefore cannot diffuse into the pores between the hydrocarbon chains in the film. Values of W_A for water and methylene iodide were computed from experimentally measured contact angle and surface tension values. Values for the parameters γ_L^d and γ_L^p were obtained from data reported by Fowkes[40]: γ_L^d = 21.8 erg/cm^2 and γ_L^p = 51.0 erg/cm^2 for water; γ_L^d = 48.5 erg/cm^2 and γ_L^p = 2.3 erg/cm^2 for methylene iodide.

Figure 9 shows γ_s^p, γ_s^d, and γ_s values plotted as a function of S/C ratios for composite films after autoclave exposure at 100° and 150°C. The values for γ_s^p at 100° and 150°C are essentially independent of S/C ratio between 30/70 and 70/30 and then increase with decreasing cement content. The highest γ_s^p value obtained from the non-cement-containing control samples indicated that the surface is composed of a hydrophilic monolayer of oriented polar groups. Conversely, the lower γ_s^p values correspond to a polar surface with a lower hydrophilic density. The shift in γ_s^d for the surfaces of samples autoclaved at 150°C indicated a trend similar to that for the W_A results discussed previously.

Values for γ_s^d were lowest at a 70/30 ratio and then increased rapidly with a further decrease in cement content. The changes in γ_s^d occurring between S/C ratios of 70/30 and 30/70 are considerably higher (48.4% vs 6.6%) than those for γ_s^p. This suggests that γ_s^d for high surface-energy solid film surfaces is more likely to be associated with surface roughness than with the inclination to polarizability of molecules. It should also be noted that over a wide range of S/C ratios, the variation in γ_s^d at 100°C is relatively small. Thus, the use of cement as a method for increasing hydrothermal stability of films seems to be most effective at ~100°C.

Since the total surface free enegy γ_s is the sum of the attraction forces γ_s^p and γ_s^d, its curve is similar to that for γ_s^d. The surface energies for the control, from the curve in Figure 9, were 53.61 erg/cm^2 at 100°C and 58.78 erg/cm^2 at 150°C, ~70% higher than those for samples with S/C 70/30 filler.

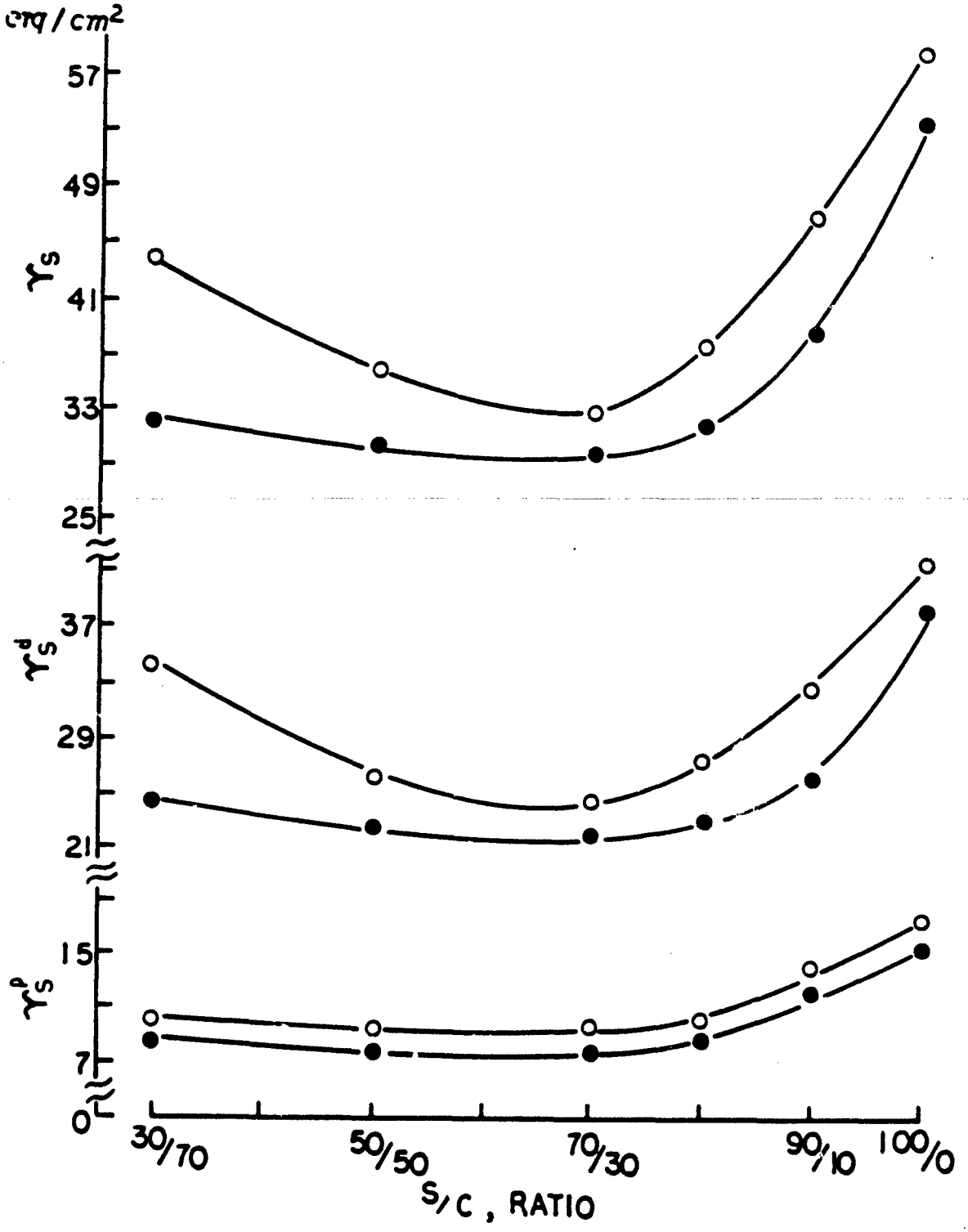

Figure 9. Components of surface free energy as a function of S/C ratio for samples autoclaved at 150°C (○) and 100°C (●).

The above results indicate that the hydrolysis of the pendent carboxyl groups in the superficial layer of the film enhances either the number or the accessibility of the hydrophilic groups formed from the functional carboxylate groups previously detected by IR. Furthermore, the increased roughness of the film surface due to the hydrothermal deterioration of polymer matrices and the presence of extraordinarily formed inorganic macromolecules significantly increase water wettability and thus allow the transportation of more water.

Scanning electron microscopy (SEM) is the best approach to characterizing the morphological features of the material surfaces. The microstructure and morphology of the composite film surfaces, before and after exposure to hot water at 150°C for 3 days, were studied by this technique. Figure 10 (X 204) shows a surface of an unexposed bulk copolymer film without any fillers. Its surface morphology is smooth, and evidence is lacking as to whether the microcracking in the middle is caused by shrinkage of the copolymer or by deposition of gold film on its surface. Exposure to hot water caused dramatic changes (Figure 11). The polymer molecules were strongly agglomerated by entanglement of the chain caused by severe hydrothermal deterioration, resulting in increased surface roughness. The agglomerate particles consist of approximately spheroidal and spherical granules of ~40 μm diameter. Since the amount of coalescent polymer aggregation is thought to increase progressively with extended exposure time, some of the agglomerate particles may be naturally removed from the material surfaces, which would reduce the weight of the films.

An exposed copolymer film with silica flour filler (Figure 12) had a heterogeneous solid surface exhibiting different areas with largely agglomerated polymer spheroids (A) and sharply protruding silica surfaces (B). The agglomerate particles appear very similar to those observed on the surface of the exposed homogeneous polymer. The roughness of this film surface indicates that the continuous copolymer layer formerly coating the surface of the silica grains was removed during the autoclave exposure. This surface texture results in increased surface free energies, weight loss, and water wettability. Figures 13 and 14 show the surface textures of films with S/C 80/20 filler before and after exposure in

Figure 10. Smooth surface of bulk MMA-TMPTMA copolymer before exposure in an autoclave..

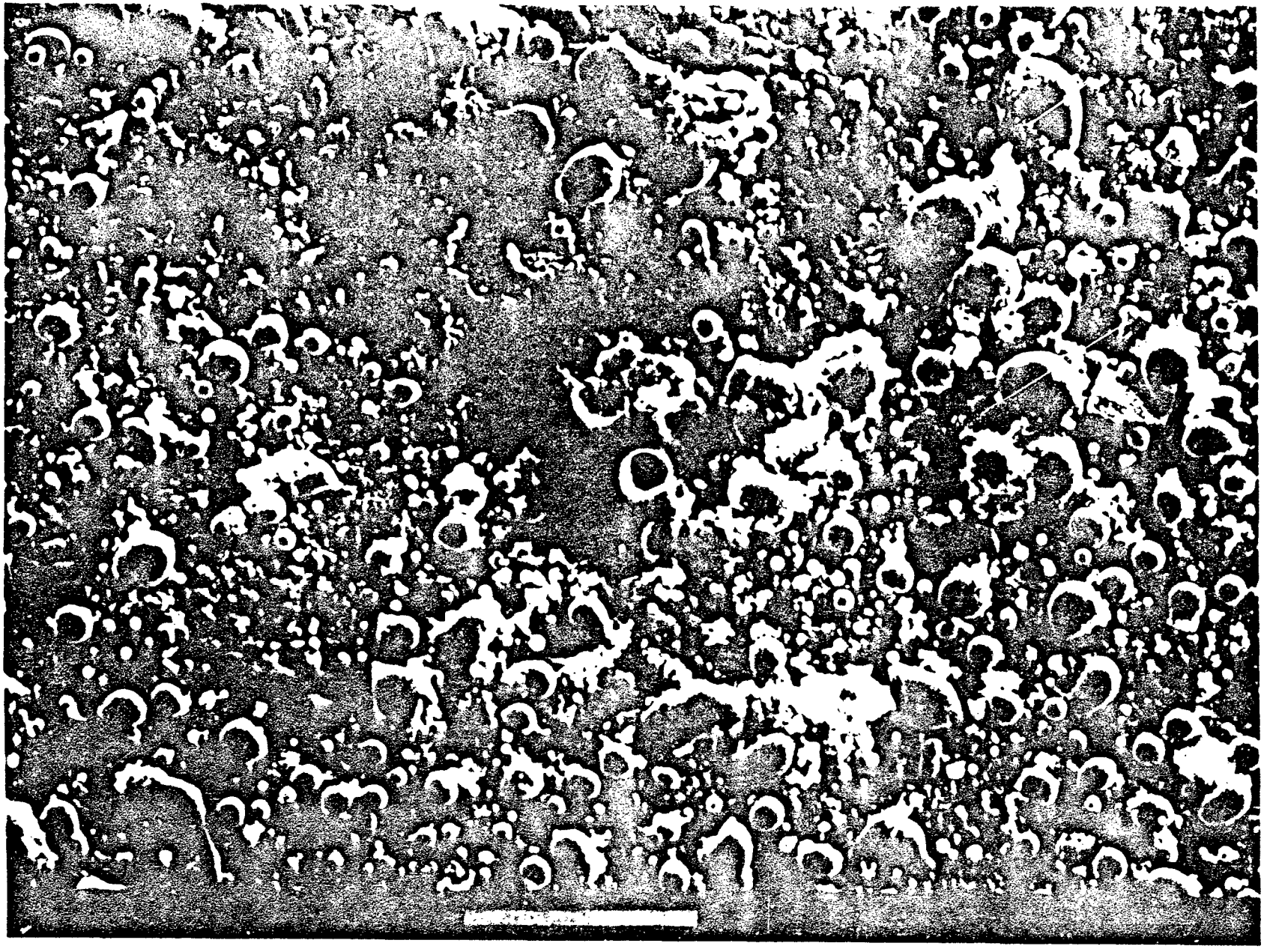

Figure 11. Micrograph of copolymer granule agglomerated during exposure for 3 days to water at 150°C.

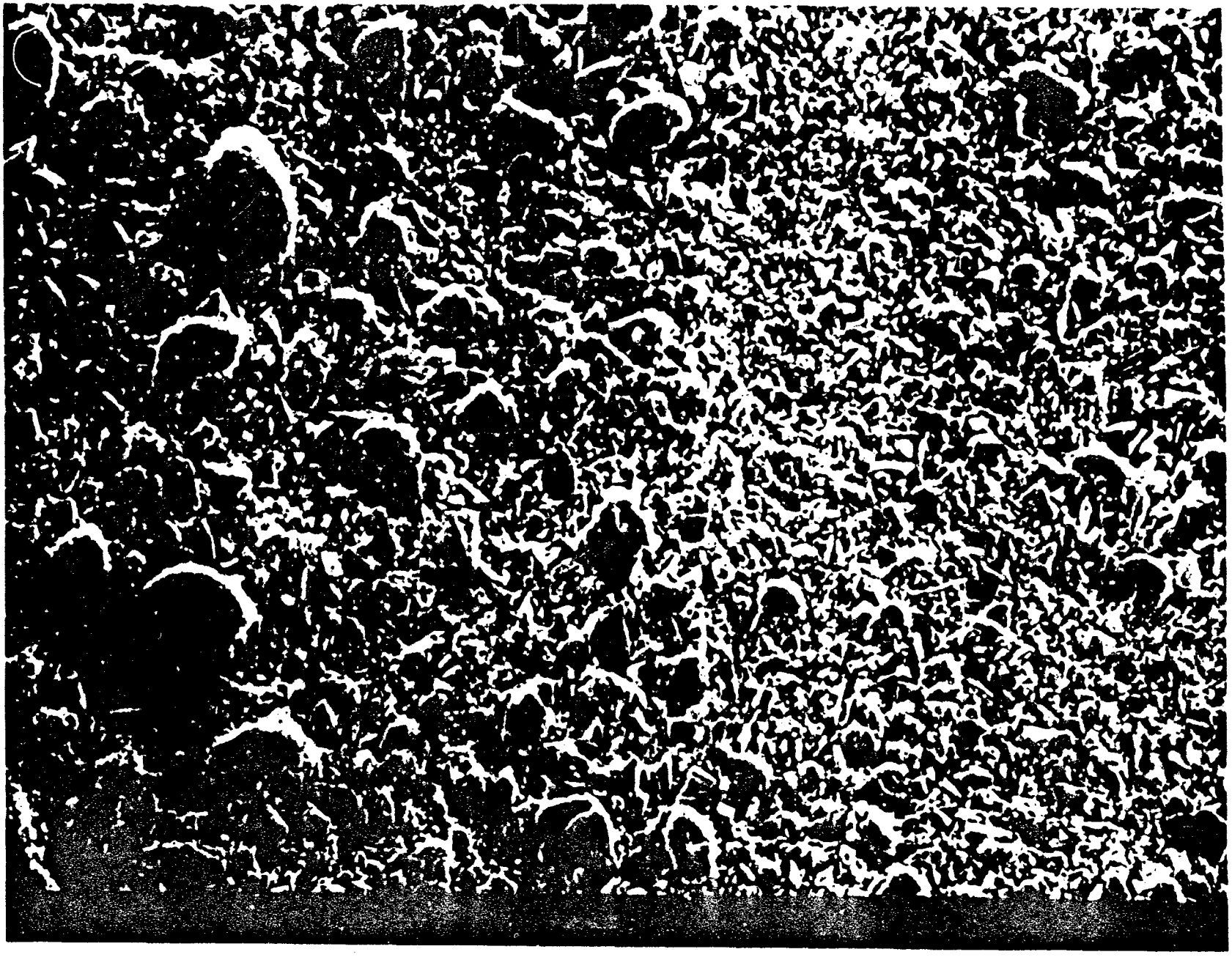

Figure 12. Rough surface of copolymer film with silica flour filler after exposure to hot water.

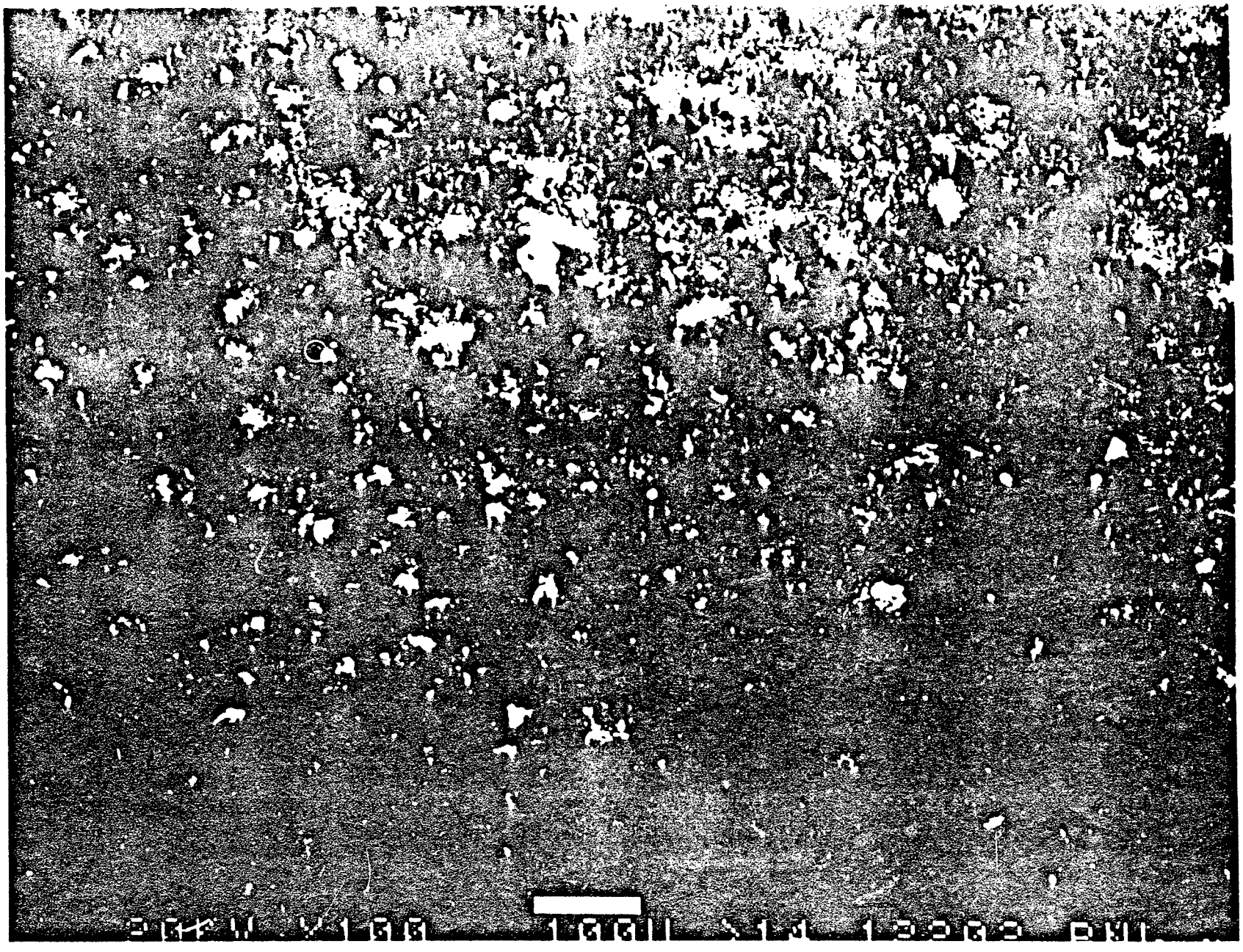

Figure 13. Surface of copolymer film with S/C 80/20 filler before exposure.

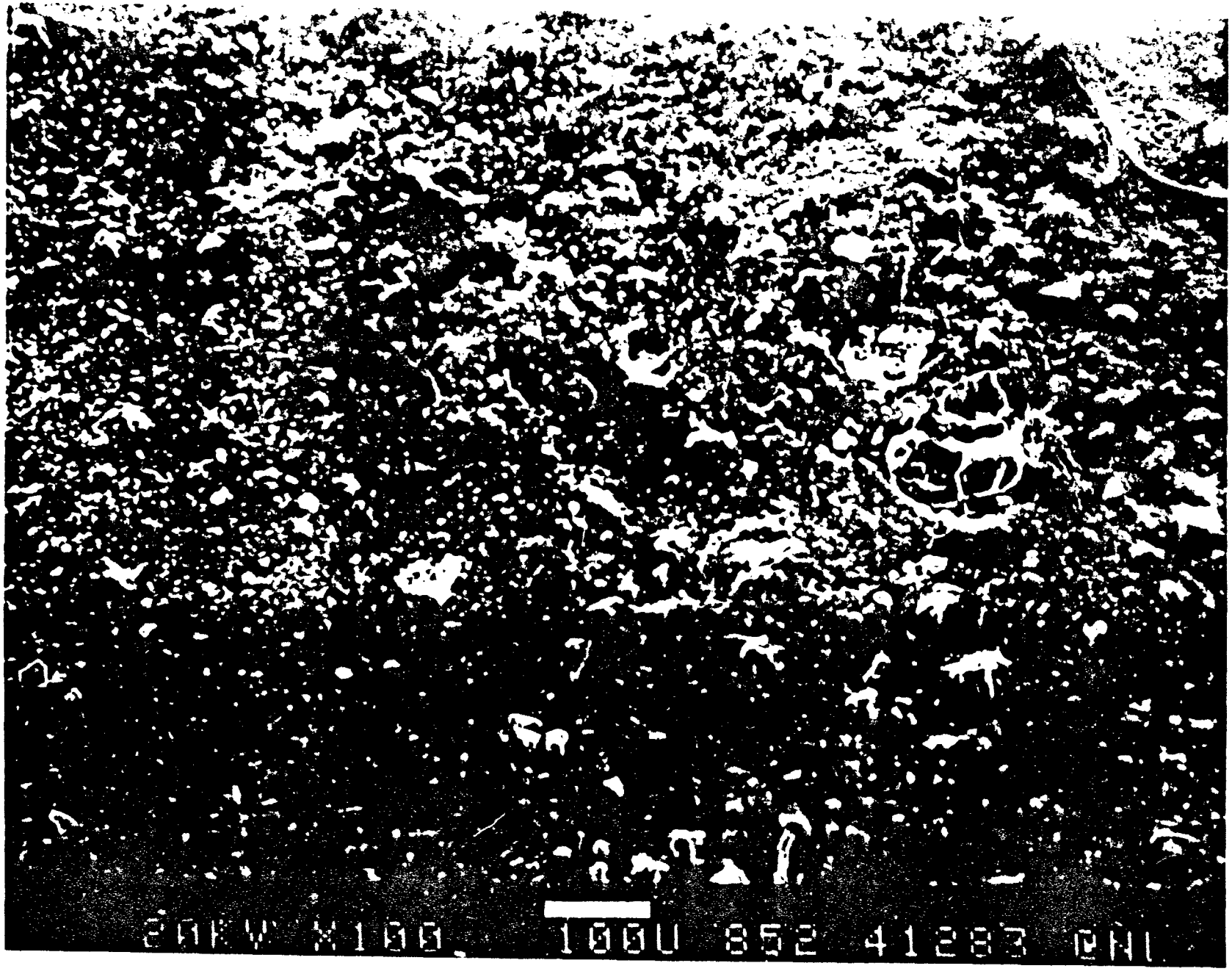

Figure 14. Surface of film with S/C 80/20 filler after exposure to hot water.

the autoclave. The former is characterized by a continuous layer of copolymer coating the surface of the original cement and silica flour grains. The anhydrous cement grains cannot be distinguished by their appearance. After exposure, some small pits were detectable, but in general the surface was much smoother than that of the exposed film with silica filler. This morphology verifies that the hydraulic cement prevents severe deterioration of the polymer by the attack of hot water. Although at low magnification the surface appeared smooth, enlargement to X 5000 disclosed that a number of knobs had developed on the surface (Figure 15). This may have been caused by the internal stress associated with the hybrid compounds of superficially formed Ca-complexed ionomer and hydrated cement macromolecules. The improvement of the hydrothermal stability of copolymer matrices by cement additives is apparent from the microstructure of film containing a large amount of cement. At a low magnification (X 48) the surface texture of a film with S/C 30/70 filler after autoclave exposure (Figure 16) shows numerous small cracks, in contrast to the agglomerated copolymers and silica particles seen on the films with silica filler (Figure 12). Formation of the Ca-complexed ionomer, which would be expected to be stable at ~150°C, is though to have prevented agglomeration of the copolymer. The cracking may be due to shrinkage of the hydrated cement macromolecules. This suggests that the superfluous cement contributes to surface roughness and thus increases surface free energy and wettability. Two different phases are seen in Figure 16, circular depression portions (C) and rough areas (D). The former are probably representative of the fresh composite surfaces disclosed by removing parts of a superficial layer of the Ca-complexed ionomer combined with the cement macromolecules.

Detailed examination of the superficially formed complex layers was accomplished by transmission electron microscopy (TEM). This analysis was helpful in the identification of the hydrated $CaO\text{-}SiO_2$ compounds. As illustrated in Figure 17, the image shows a fibrous structure that at higher magnification appears to be composed of dense masses of crystalline needles. The presence of both calcium and silica in this layer was confirmed by energy dispersive X-ray fluorescence (EDX) attached to the

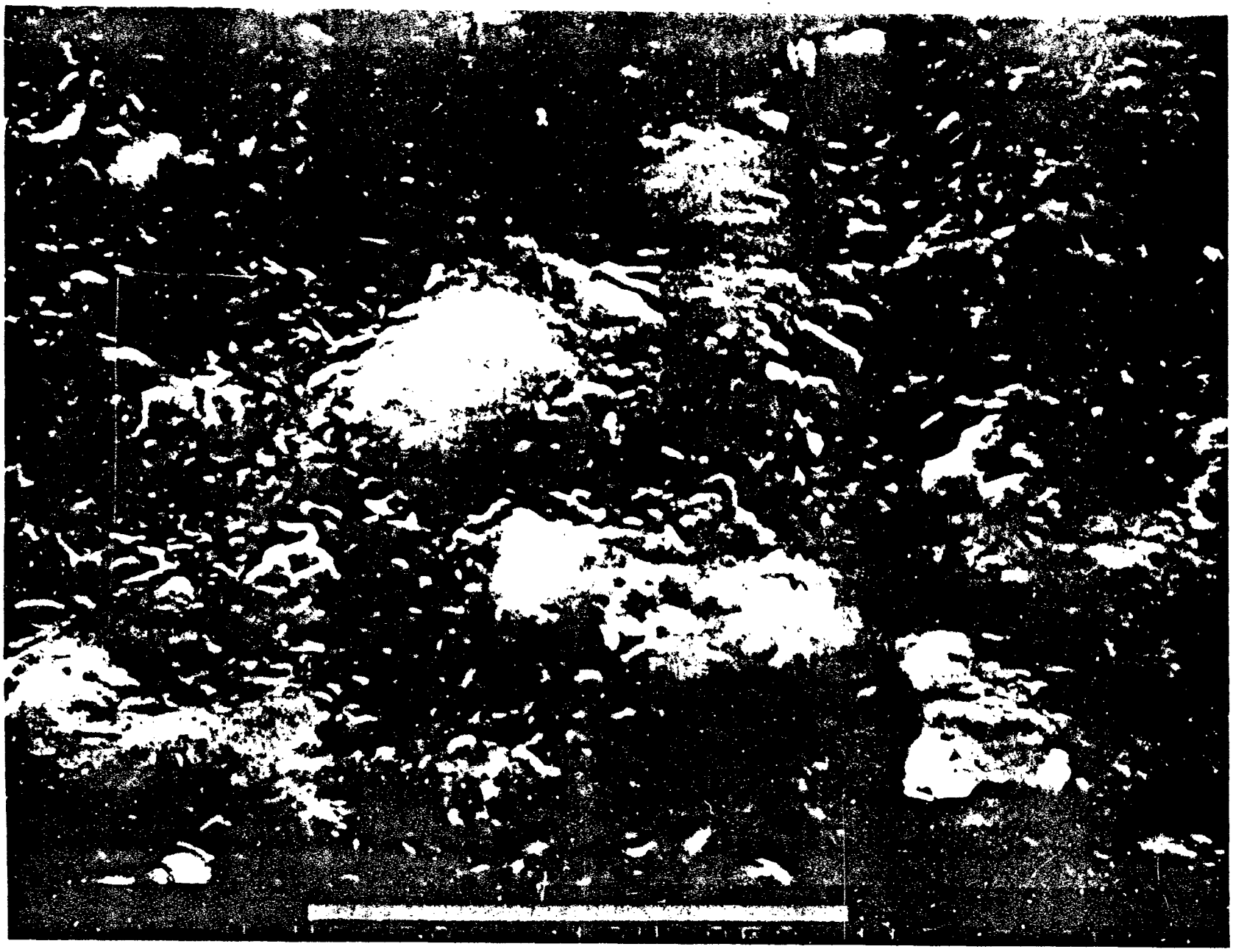

Figure 15. Surface texture of exposed composite film with S/C 80/20 filler at higher magnification (X 5000).

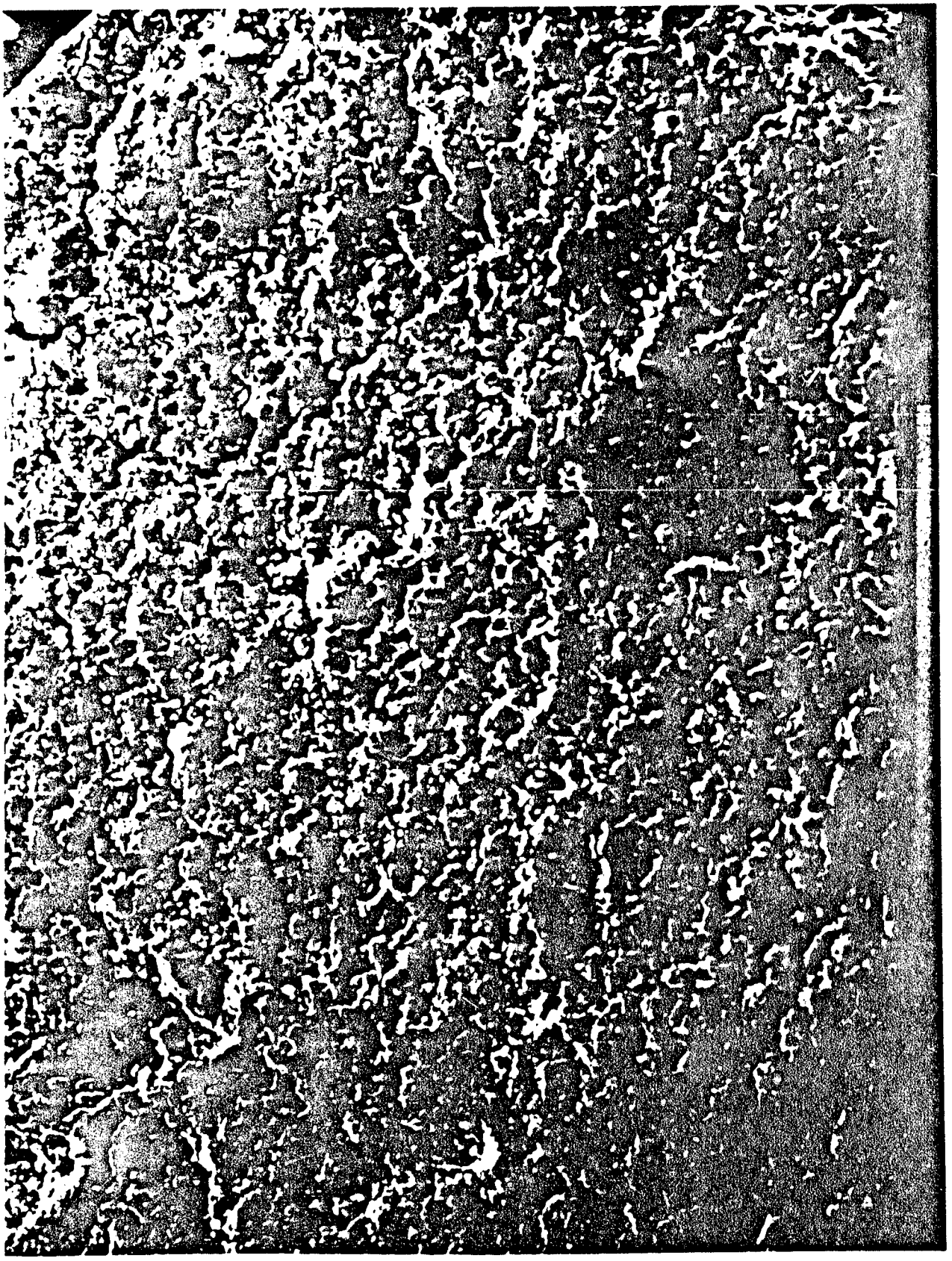

Figure 17. TEM micrograph showing fiber-like $CaO-SiO_2-H_2O$ crystal structure

SEM. In a further attempt to identify the hydrated compounds forming the fiber-like structures, X-ray powder diffraction analysis was performed. Consequently, the crystallized hydration compounds were identified from the broad peak at 3.03 Å to be calcium silicate hydrate (C-S-H). These fiber crystals which protrude from the ionomer surface as if from an arable land, are likely to function as a mechanical reinforcement for the ionomer matrix layers.

Accordingly, the ternary crystalline fiber formed after exposure for 3 days to water at 150°C must be regarded as a moderately crystallized C-S-H compound formed during setting of the cement. The amount of C-S-H formations growing outward from cement grains increases with exposure time, and such growth may fill the spaces between the original cement grains and between the cement grains and the complexed ionomers. Furthermore, the orientation of the closely packed gel structure may lead to the formation of the interconnecting cross-links between their surfaces, cementing the whole mass together. This seems to verify that the superficially formed inorganic macromolecule-complexed ionomer layers contribute significantly to the hydrothermal stability of the film.

5. Electrode Potential of Coated Metal Plates

Water permeation is one of the most important properties of films designed for protective coating applications. To estimate the water transport through the paint coatings, electrode potential measurements of coated metal plates were made after exposure for up to 25 days in an autoclave at 150°C. Samples in this test series contained fillers with S/C ratios of 100/0 and 70/30, and the thickness of the coatings was 10 and 25 mil.

Test results from these samples are given in Figure 18. Although the current flow through the coatings depends primarily on the film thickness and the exposure period, it is evident from the figure that the coatings with S/C 70/30 filler had a far lower current than those for the silica copolymer coatings. The current flow through the 10 mil coating with S/C 70/30 was 0.42 mA after exposure for 25 days. This value is ~80%

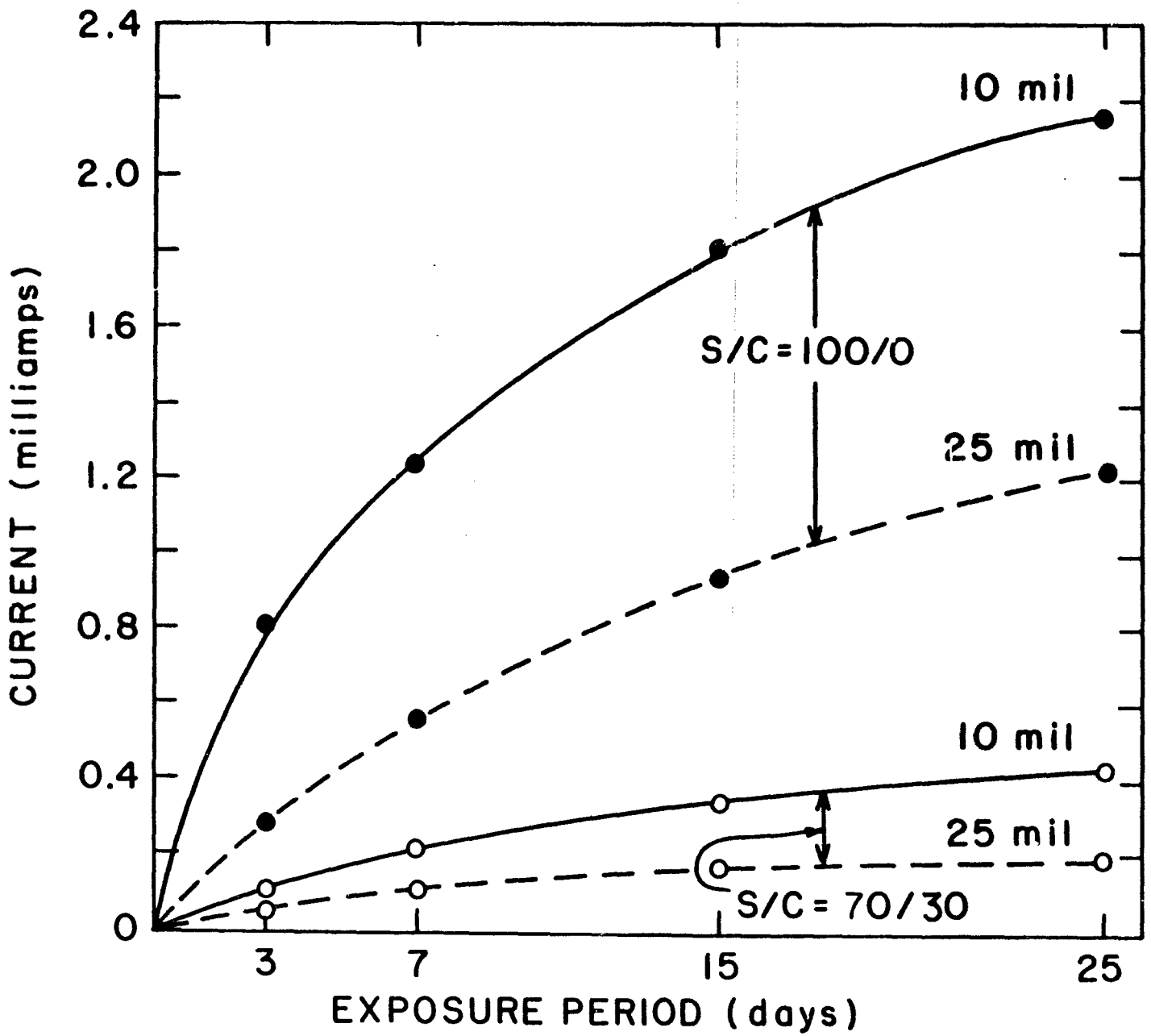

Figure 18. Current-exposure time curves for metal plates painted with S/C=100/0 and

less than that for the S/C 100/0 sample after the same exposure time. This seems to support the theory that the superficially formed $CaO-SiO_2-H_2O$ macromolecule-ion complexed copolymer layers are probably responsible for minimizing the permeability of the polymeric composite coatings to water.

From studies of the dipole-hydrogen bonding forces, dispersion forces, surface free energies, surface morphological features, and electrode potential changes discussed above, it is believed that the low water permeability of the exposed coatings is directly related to lower hydrophilicity, low-energy surface, and reduced surface roughness.

6. Conclusions

In studying the physico-chemical factors affecting the hydrothermal stability of hydrated inorganic macromolecule-ionomer composite materials for utilization as protective coatings on metals, the following generalizations can be conclusively drawn from the results described above. In the formation of the ionomer, the quantity of $COO^-(Ca^{2+})$ groups produced by ionic reactions occurring between the carboxylate anions and the nucleophilic Ca^{2+} ions during exposure to hot water increases with increasing hydrothermal temperatures and higher concentrations of the cement used as a source of divalent metallic cations. Evidently, the conformation of a Ca salt bridge not only acts to inhibit the scission of the polymer chains due to hydrolysis of the pendent groups, but also contributes significantly to the thermal stability of ionomer matrices near 300°C. This was indicated by TGA and DTA evaluations. SEM and TEM examinations of the morphology indicated that the ionomer composites combined with the hybrid macromolecules to form very thin superficial layers on the films. The major hydration macromolecules of cement formed during the 3 day exposure in the autoclave at 150°C were identified to be the C-S-H compounds moderately crystallized on the outward cement grains. These are primarily responsible for the mechanical enhancement since they act as a reinforcement for the protective ionomer layers.

Once these components become the constituents of a film, the film acquires some very interesting characteristics. One of inherent properties is that the glass transition temperature, T_g, tends to increase with increasing cement concentration. This affects the chain stiffness of the polymer molecules. A maximum T_g of 63.5°C was attained when 50 parts silica flour and 50 parts cement were used, and the addition of more cement decreased the T_g. Trends similar to those for the T_g were seen in the measurements of tensile strength of the films.

Analysis of the above data indicates that interactions at the interface between the configurated hydration macromolecules and the ionomer chains not only result in strong agglomeration and chain entanglement, but also are likely to contribute to incremental interfacial stresses which lead to chain enlargement occurring along with the growth of macromolecules.

Another characteristic observed is that the Ca-complexed ionomer films have a lower water permeability than the exposed films having silica flour filler without cement. A possible reason for this is as follows: The copolymer films with silica flour filler, after exposure to hot water, contain a larger number of hydrophilic carboxylate groups yielded by hydrolysis of the functional carboxyl groups in the polymer molecule. Contact angle measurements indicated a high surface free energy, γ_s, >50 erg/cm^2. In contrast, the complex ionomer films containing the Ca salt formation coordinated with 6 H_2O liganda are more hydrophobic. Thus, the total surface free energy for the films with S/C 70/30 filler after exposure to water at 150°C, was calculated to be ~34 erg/cm^2, ~42% lower than that for films with S/C 100/0 filler. Conversely, the production of excessive cement macromolecules results in an increase in surface energy. This is connected with changes in surface roughness due to the squeezing deformation of the film. The results suggest that the low water permeability of the exposed films is directly related to lower hydrophilicity, low-energy surface, and reduced surface roughness.

III. NATURE OF INTERFACIAL INTERACTIONS BETWEEN POLYMER AND PHOSPHATE-TREATED METAL SURFACES

Since one of the main factors affecting the durability of protective coatings is the adhesion force to metal substrates, it is very important to better understand the nature and role of adhesion mechanisms and how they affect the interfacial attractions between functional polymers and metal surfaces.

Generally, good bonding can be attributed to the following four elements: (1) mechanical interlocking associated with the surface topography of metals, (2) surface wettability of metal by the polymers, (3) strong chemisorption, and (4) type and degree of polymer-metal interfacial interaction. Two functional polymer systems, polyacrylic acid and levulinic acid-modified furan, were emphasized to obtain the above information. On the other hand, modifications to the metal surfaces are very important to successful bonding. Therefore, two types of chemically oxidized metal surfaces were evaluated in this study: (1) iron phosphating crystalline and (2) zinc phosphating crystalline layers.

A. Materials

Commercial polyacrylic acid (PAA), 45% solution in water, having an average molecular weight of 104,000, was supplied by Scientific Polymer Products, Inc. The pendent carboxylic acid (COOH) groups on the macromolecules were partially neutralized by adding the calculated amount of sodium hydroxide (NaOH). The degrees of neutralization used were 0, 20, 40, 60, and 80%.

Commercial-grade furan (FR) 1001 resin having a viscosity of 470 cP and a specific gravity of 1.22 at 24°C was supplied by the Quaker Oats Company. The condensation-type polymerization of the FR resin was initiated by the use of 4 wt% Qua Corr 2001 catalyst, which is an aromatic acid derivative. The gel time for a 200 g resin sample containing the initiator was ~15 min at 24°C. Commercial analytical-grade levulinic acid reagent (LA), $CH_3COCH_2CH_2COOH$, was employed to assemble the more reactive FR macromolecules.

The metal used in the experiments was nonresulfurized mild carbon steel consisting of 0.18 to 0.23% carbon, 0.3 to 0.6% manganese, 0.1 to 0.2% silicon, and <0.04% phosphorous. To deposit iron phosphate and zinc phosphate crystalline films onto metal substrate surfaces, the metal surfaces were polished with ultrafine emery paper and then chemically treated in an oven at 80°C for up to 24 hr. In the iron phosphate experiments, the polished metal surface was immersed in a dilute (pH ~2.5) solution of phosphoric acid (H_3PO_4). The zinc phosphate was deposited by immersing the metal in an acidic solution consisting of 9 parts zinc ortho phosphate dihydrate [$Zn_3(PO_4)_2.2H_2O$] and 91 parts 15% H_3PO_4 solution. The pH of this solution was ~2.0. After depositing the oxide film, the metal substrates were dried in an oven at 150°C for ~3 hr to remove any moisture from the film surfaces.

B. Measurements

The surface topography and morphology for the chemically treated metal adherends were analyzed by AMR 100 Å scanning electron microscopy (SEM) associated with TN-2000 energy dispersive x-ray fluorescence (EDX).

A Perkin-Elmer Model 257 Spectrometer was used for infrared spectroscopic (IR) analysis. To obtain the basic information regarding the interfacial reaction mechanisms, IR spectra were obtained for the samples prepared in the form of KBr discs. The samples were powdered before mixing and grinding with KBr.

The magnitude of the wetting force of the oxidized metal surfaces by modified and neutralized liquid resins was measured using a Contact Angle Analyzer in a 60% R.H. and 24°C environment. All of the data were determined within 30 sec after drop application.

X-ray powder diffraction (XRD) analyses were employed to identify the oxide compound layers deposited on the treated metal surface. To prepare the fine powder samples, the deposited oxide layers were removed by scraping the surfaces and were then ground to a size of ~325 mesh (0.044 mm).

The lap-shear tensile strength of metal-to-metal adhesives was determined in accordance with the modified ASTM method D-1002. Prior to overlapping between metal strips 50 mm long, 15 mm wide, and 2 mm thick, the 10 x 15 mm lap area was coated with the neutralized polyelectrolyte macromolecular adhesives. The thickness of the overlapped film ranged from 1 to 3 mil. The bond strength values for the lap shear specimens are the maximum load at failure divided by the total bonding area of 150 mm^2.

C. Surface Topography of Steel Prepared by Phosphating Solutions

Since the nature of the surface micromorphology[41,42] and the thickness[43,44] of the deposited oxide layers relate directly to the bonding forces at the interface, two different oxide film surfaces were examined by SEM and EDX. As illustrated in Figures 19 and 20, the micromorphology and topography yielded by these two surface preparations appeared to be very different. The topographical image of the H_3PO_4-treated surface (see Figure 19) seems to consist of two discriminable layers. Analyses of EDX peaks indicated that one of the layers consisted of irregularly deposited iron phosphate crystals and the other of iron oxide. The former was composed of crystals characterized by circular radiating and thin plate-like features. On the basis of the strong spacing at 3.28 and 3.60 Å on XRD patterns in the diffraction range 8.84 to 1.54 Å, the crystallized compound layer was identified as iron (III) ortho phosphate dihydrate ($FePO_4.2H_2O$). This was also confirmed by IR spectra analysis which will be discussed in later sections of the report. From SEM observations, it appears that the concentration of the crystal clusters of $FePO_4.2H_2O$ cover ~70% of the treated metal surface. Therefore, the H_3PO_4-treated surface appears to consist of a hybrid layer of $FePO_4$-Fe_2O_3-H_2O absorbed on porous Fe oxide.

Figure 20 shows large lamellate block crystal growths of zinc phosphate hydrate compound layers arrayed uniformly on all surfaces of the modified metal sites. The XRD patterns for these crystalline powder

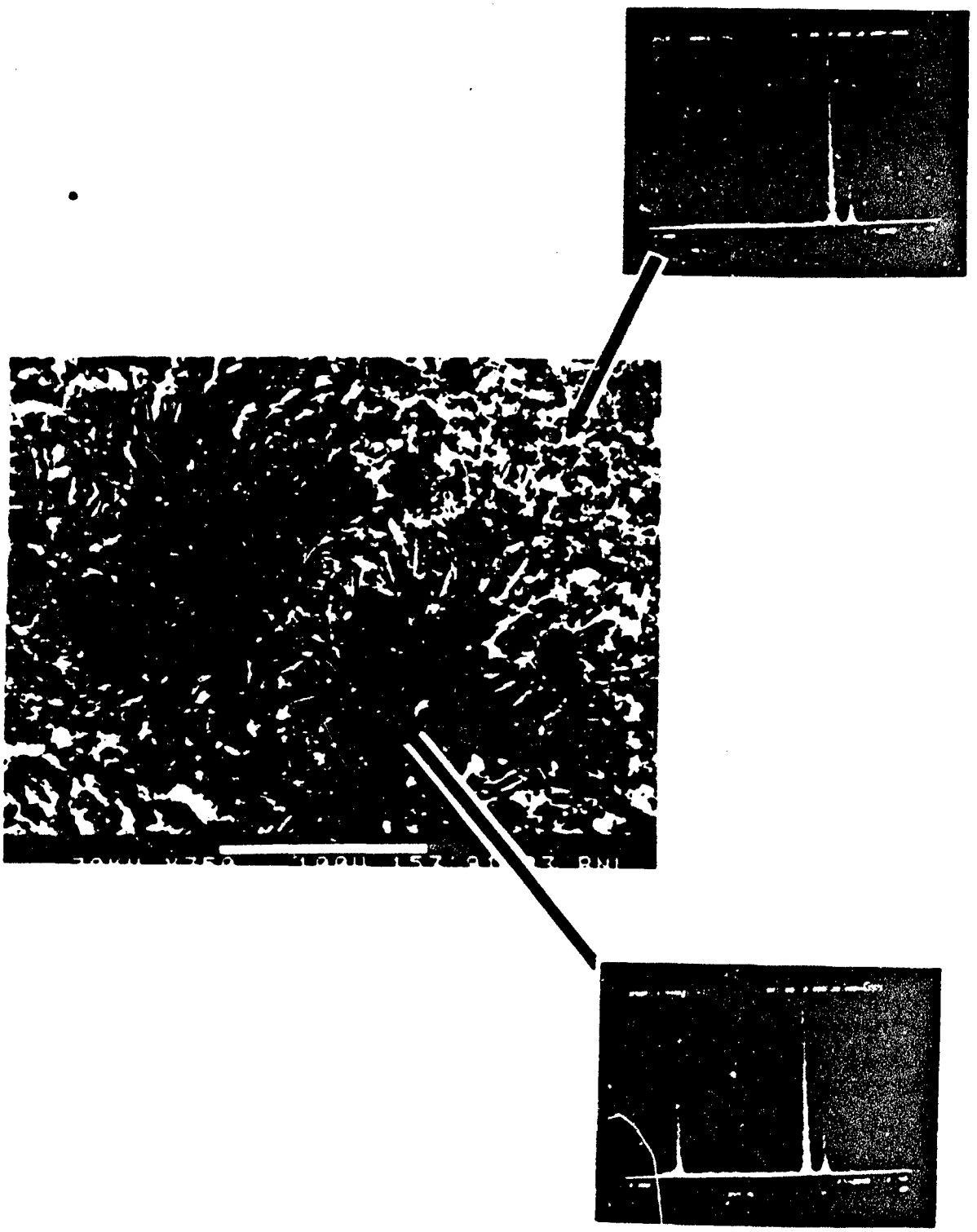

Figure 19. Scanning electron micrograph and EDX peak of H_3PO_4-treated metal surfaces.

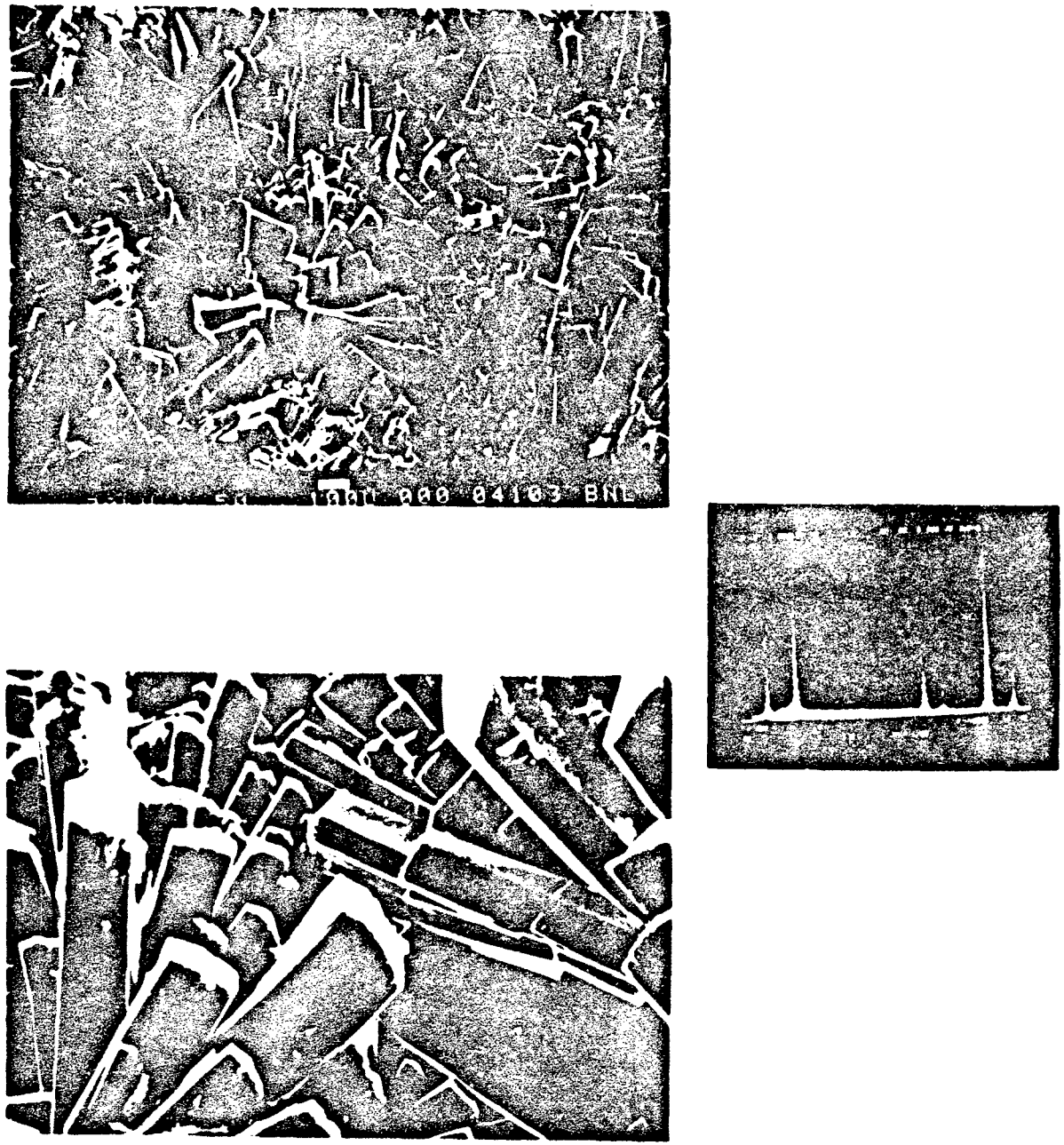

Figure 20. SEM photomicrograph and EDX diffraction peak of a lamellate block-like hopeite crystal prepared on metal.

samples disclosed a strong peak intensity at 4.57 and 2.83 Å. Accordingly, the highly crystallized layers indicated the formation of hopeite, $Zn_3(PO_4)_2 \cdot 4H_2O$. As seen in the figure, the main microstructure features of deposited hopeite films, compared with those for iron phosphate films, are extreme roughness, greater crystal thickness, and a more open surface structure. Because of these topographical features, it is expected that the regularly interlocked hopeite crystals will provide a larger surface area for bonding and give sufficient mechanical interlocking with adhesives. Also, penetration of adhesives into the pores on the open surface microstructure will help to enhance the bond at the polymer-hopeite interfaces. In addition to the information obtained from XRD, it appears from EDX peaks that some zinc is likely to be replaced by ferrous ions. By comparing the microstructure and surface topography of these two different hydrated oxide layers, work was initiated to define the micromorphological features that contribute to the adhesion behavior at the polyelectrolyte macromolecule-oxidized metal interfaces.

D. Polyacrylic Acid/Treated Metal Interface

1. Wetting Behavior

The wettability and the adsorption behavior of polyelectrolyte macromolecules on oxide layers were investigated on the basis of contact angle measurements made 30 sec after deposition on the test surfaces. For this work, a 10% PAA solution was prepared by diluting 45% PAA with distilled water. The primary purpose of this study was to evaluate quantitatively the degree of interfacial interactions of the functional COOH groups and to assess the correlations that may exist between the surface morphological features of oxide films and the dispersion forces of polyelectrolyte macromolecules. Both the conformation and orientation of the pendent polar groups in polyacid macromolecules will contribute to the magnitude of surface wettability and spreadability onto the oxide films. Thus, in order to describe how the regularly oriented macromolecule affects the dispersion function and efficiency, the pendent COOH groups were neutralized by adding NaOH. The changes in conformation of PAA molecules

neutralized in the range of 0 to 80% were apparently verified by the shift in IR spectra for these samples, as shown in Figure 21. The most pronounced changes in these frequencies were an increase in the peak intensity of two new bands at 1550 and 1400 cm^{-1} with an increase in the degree of neutralization. In addition, the carbonyl C=O group frequency at 1710 cm^{-1} tends to shorten with increased degrees of neutralization. The absorption bands at 1550 and 1400 cm^{-1} can be assigned to the asymmetrical and symmetrical stretching vibrations of carboxylic anions, COO^-. The spectra from the 80% neutralization sample indicates the almost complete disappearance of the conventional band at 1710 cm^{-1}. These results clearly demonstrate that salt complex formations having COO^- Na^+ groups were yielded by the acid-base reaction between the carboxylate anions formed by proton donor characteristics of the arrayed carboxylic acid groups and the active neucleophilic Na^+ ions dissociated from NaOH in the PAA solutions. These conformational changes contribute to the subsequent entanglement and coiling of the macromolecules. Since the extent of the intermolecule entanglement increases with the degree of neutralization, the loss of functional groups at available adsorption sites in the molecular chains may result in decreased dispersion and wettability forces on oxide surfaces by PAA polymers.

The improved wettability of metals by the macromolecules is attributed not only to interfacial interactions between the polar groups in the polymer and the oxide layers, but also to the enhanced activation of modified metal surface sites at which the energetics of adsorption are particularly favorable. The contact angles on the metal surface were measured as a function of the age of the chemical treatment. PAA solutions with 0, 20 and 40% neutralization were employed in this test series. The data, shown in Figure 22, indicate that the contact angles for both the H_3PO_4- and $Zn_3(PO_4)_2.4H_2O$-treated surfaces tend to decrease with increasing treatment times. When a non-neutralized PAA solution was used, the contact angles after a 24-hr surface treatment were reduced by ~63% and ~81% for the H_3PO_4- and $Zn_3(PO_4)_2.4H_2O$-modified surface layers, respectively, when compared with those from polished surfaces. Although the

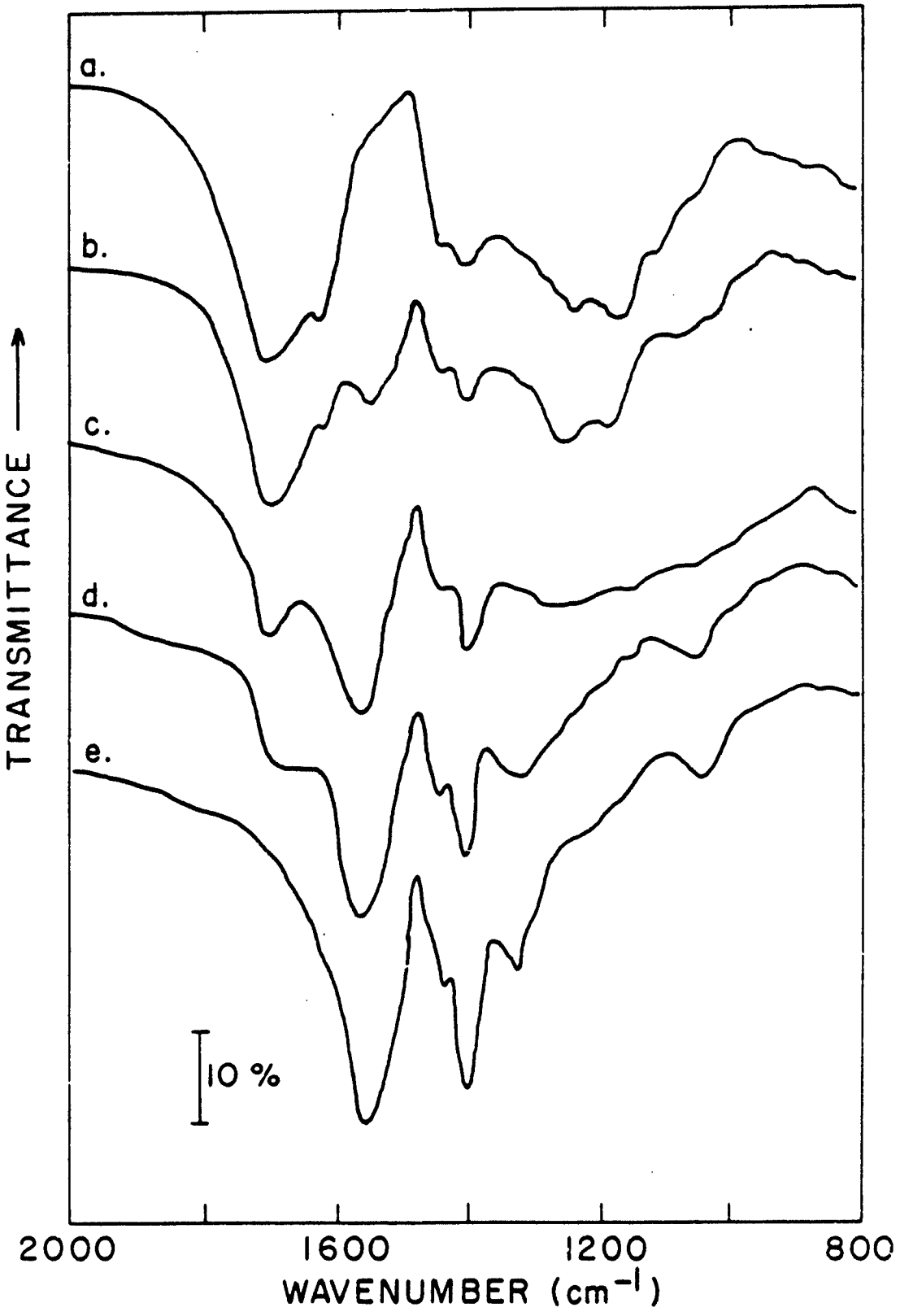

Figure 21. Infrared spectra of PAA polymers neutralized by NaOH; (a) 0%, (b) 20%, (c) 40%, (d) 60%, and (e) 80% neutralization.

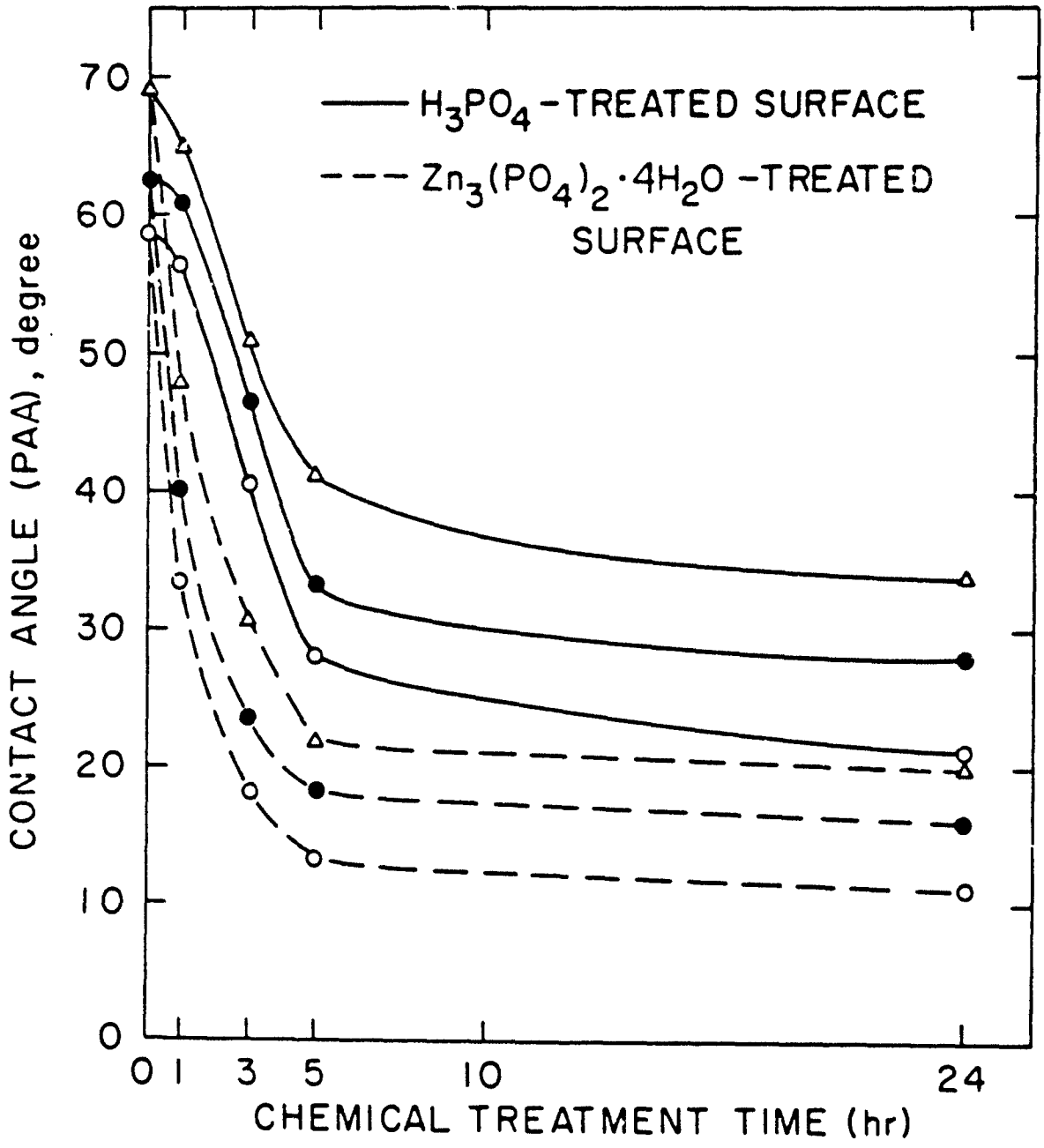

Figure 22. Changes in contact angle of oxide layers by non- and neutralized PAA as a function of the age of chemical treatment; (o) 0%, (●) 20%, and (Δ) 40% neutralization.

contact angles were measured using a neutralized PAA, the magnitude of the angle reduction for the $Zn_3(PO_4)_2.4H_2O$ layers is considerably higher than that for H_3PO_4-treated layers at the same age. This indicates that the open surface microstructure of hopeite crystals is easier to wet. The data further indicate that an increased degree of neutralization results in an increase in the contact angle. From these observations, it can be concluded that the migration of collectively entangled macromolecules leads to a decrease in the magnitude of the spreading and capillary forces, the magnitude of the interfacial wetting force is primarily dependent on the conformation changes in adhesive molecules and the surface topography of the deposited oxide films, and the presence of highly crystallized hopeite layers which have an open surface microstructure increases the wettability and despersion of polyelectrolyte macromolecules.

2. Chemisorption

The purpose of the chemical treatment is not only to increase the roughness of the metal surface, thereby enhancing mechanical interlocking bonds, but also to modify the surface chemical composition. Thus, it was considered that the increase in wettability discussed above may also have been due to interfacial interactions and conformation changes induced by chemical reactions between the functional COOH groups and the oxidized metal layers. To elucidate the nature of the interfacial chemical reaction mechanisms, these oxide layers were removed by scraping the metal surfaces, and the removed oxide metal powders were then ground to a size of ~325 mesh (0.044 mm). Samples were prepared by mixing PAA polymers with the finely powdered oxide compounds and subsequently curing them in an oven at 70°C for 10 hr.

Figure 23 shows IR spectra for iron phosphate compounds, bulk PAA polymers, and iron phosphate-PAA composites. IR analysis showed conspicuous bands at frequencies of 3400 and 1030 cm^{-1} in the spectra for the iron phosphating powder. These indicate the formation of iron (III) orthophosphate. The broad band near 3400 cm^{-1} can be ascribed to the vibration of the bonded hydroxyl (OH) groups of the hydrated oxide films, while the

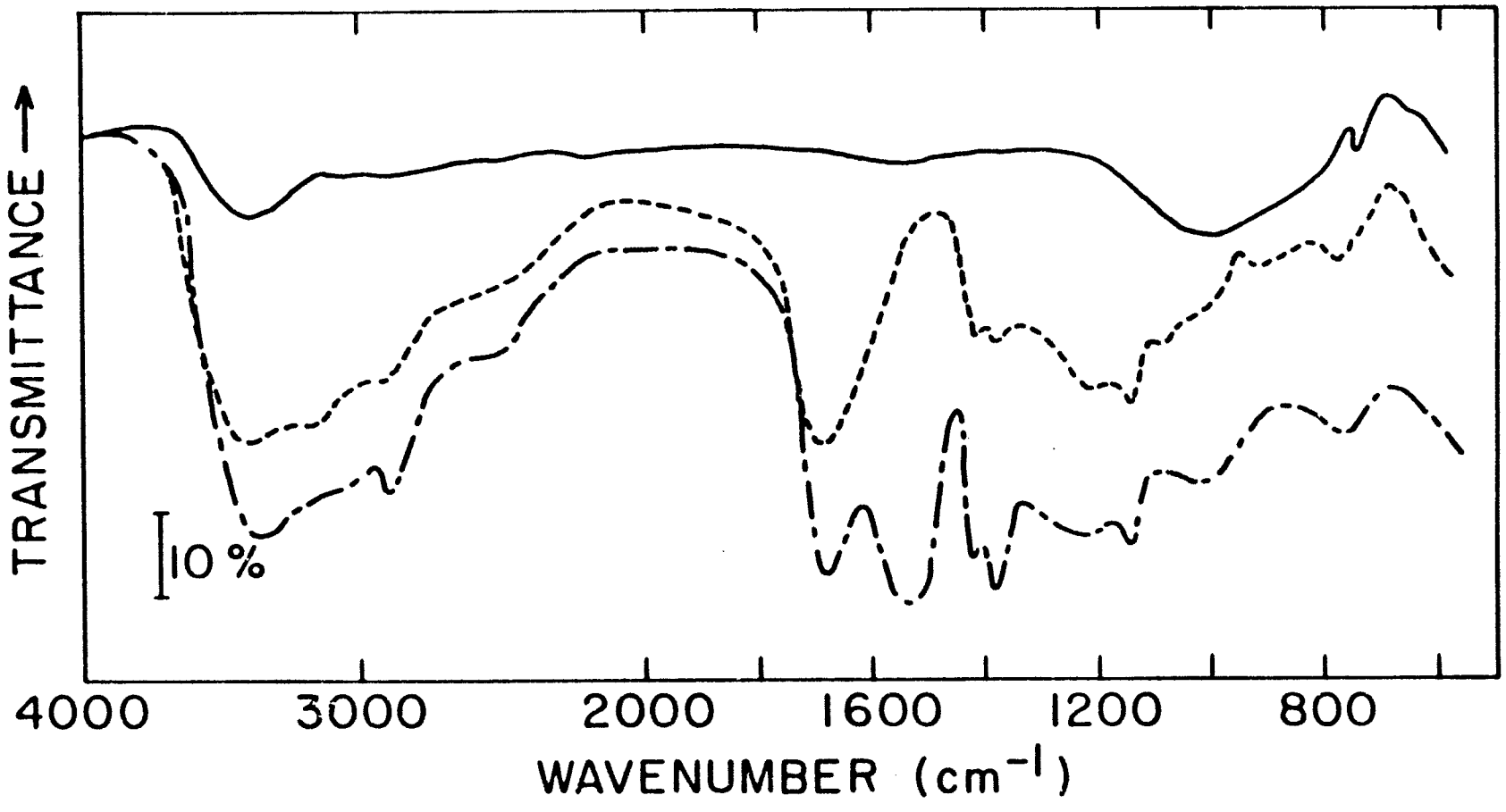

Figure 23. IR spectra of iron phosphate/PAA composite samples; (——) iron phosphate hydrate compounds, (----) bulk PAA polymers, and (— – —) PAA composites containing hydrated iron phosphate powder.

at 1030 cm^{-1} may be due to the vibration of PO_4^{-3} in $FePO_4.2H_2O$ compound formations. Although frequencies below 600 cm^{-1} are not shown in the figure, the presence of divalent Fe ions was confirmed by two adsorption bands at ~570 and 375 cm^{-1}.

The bulk PAA polymer samples exhibited major IR bands at frequencies of 3400, 1710, 1430, 1380, and 1160 cm^{-1}. The band around 3400 cm^{-1} is characteristic of O-H stretching. The adsorbance of carboxyl (C=O) groups is represented by the intense peak at 1710 cm^{-1}, and the bands at 1430 and 1380 cm^{-1} are associated with the dimeric OH in-plane bending coupled with C-O stretching, and the vibration of methyl groups, respectively. The band at 1160 cm^{-1} may be assigned to the O-H in-plane deformation mode.

When compared with the above two spectra, the spectrum for the iron phosphate-PAA composite samples was characterized by the pronounced presence of two new bands at 1550 and 1398 cm^{-1} and a shorter band intensity for C=O groups at 1710 cm^{-1}. Since these new peaks are attributed to the asymmetrical and symmetrical vibrations characteristic of carboxylate anion (COO^-) groups, it is presumed that interfacial interaction between the COOH groups and the hydrated oxide layers is due to the following two hypothetical mechanisms:

Type A: Acid-Base Surface Interaction Mechanisms

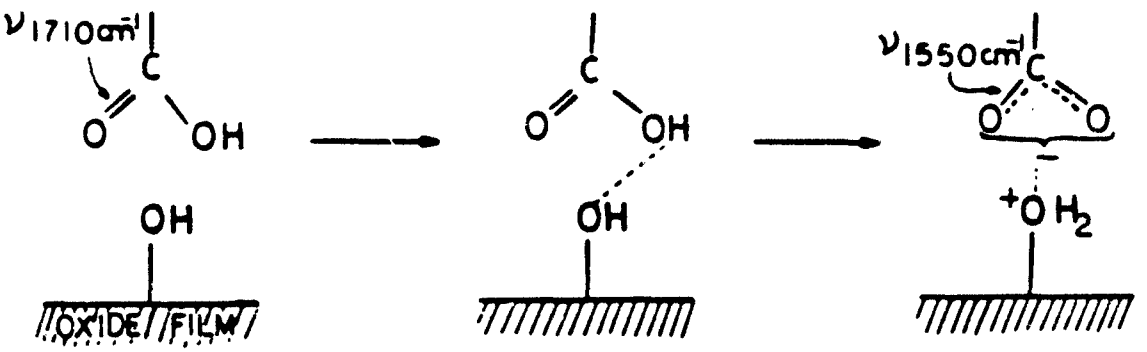

Type B: Salt-Bridge Intermolecular Reaction Mechanisms by Free Ferrous Ions

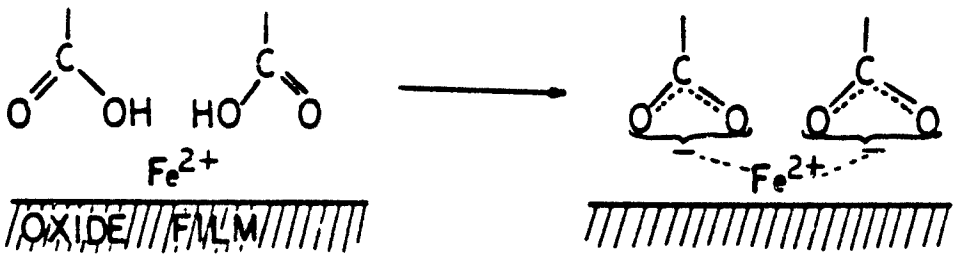

Type A consists of a strong ionic interaction associated with charge transfer bonding mechanisms which predominate over weaker dipole interactions. Thus, it is believed that the carboxylate anion (COO^-) produced by acid-base surface interactions occurring between the functional carboxylic acid (COOH) groups and the polar hydroxyl (OH) groups on hydrated oxide surface sites are strongly chemisorbed to oxidized metal surfaces. This significantly enhances the wettability and the bonding properties.

As an alternative possibility, mechanism B is the salt bridge formation brought about by ionic bonding between the free Fe^{2+} ions existing on the oxide surface sites and the COO^- anions. This formation leads to a substantial increase in the coil-up and the entanglement intermacromolecule density. The entangled molecules at the interface result in a decrease in the polymer adsorption values to metal surfaces. Accordingly, this spherical molecule phenomenon contributes to the formation of a weak boundary layer under the surface due to insufficient polymer filling of the cavities in the oxide film layers. However, the rate of the formation of the ionic interaction regions and the density of entanglement macromolecules at interfaces are not evident from the limited data. Nevertheless, there is no doubt that, when the reactive surface oxide layer chemically interacts with the orientated COOH groups to form metal-oxygen-polymer interfacial complex bonds, the yielded ionic bonds contribute particularly to an increase in adhesion.

IR spectra for the PAA-$Zn_3(PO_4)_2 \cdot 4H_2O$ composite systems are given in Figure 24. The vibrational frequency in inert hopeite powder is represented by the marked peaks at 3560, 3400, 1630, 1110, 1010, and 950 cm^{-1}. The bands at 3560 and 1630 cm^{-1} are assigned to the coordinated water expressed in terms of the hydration water. The latter band in particular can be taken as another important means of identifying water of crystallization. The 3400 cm^{-1} band is consistent with the hydroxyl stretching vibration of hydrated inorganic compounds. An absorption band in the region 1100 to 1000 cm^{-1} can be explained by assuming the presence of tetrahedral phosphate ions such as PO_4^{3-}, HPO_4^{2-}, and $H_2PO_4^-$ in the hydrated zinc phosphate compounds. Since the P-O-(metal) linkage appears to have the stretching frequencies for a P-O bond and an O-(metal) bond in the frequency range 1055 to 950 cm^{-1}, the two bands at 1010 and 950 cm^{-1} are likely to represent the stretching vibration of the P-O-(Zn) bond.

The spectrum for the PAA/hopeite composite samples indicates a new shoulder band at 1550 cm^{-1}, when compared with those for the hopeite and bulk PAA samples. The band at a frequency of 1550 cm^{-1} corresponds to an asymmetric stretching vibration of COO^- groups in accordance with Type A interaction mechanisms. As indicated by earlier SEM and EDX studies, very little, if any, free ferrous ions exist on the oxide film surfaces. The presence of free zinc ions would also act to inhibit the spreading forces of the oxide films by PAA polymer, thereby resulting in the entanglement of macromolecules. However, the concentration of the free zinc ions adsorbed onto the hopeite surface sites was not determined in this study. In addition, the charge transfer leading to the nature of acid-base reaction mechanisms between the polyelectrolyte macromolecules and the regularly oriented polar OH groups of hydrated oxide film sites, is more likely to be associated with the carboxylic anions converted from carboxylic acid groups rather than from the carbonyl group. Consequently, it was found that the presence of minimized divalent metallic ions at the interfaces not only tends to increase the magnitude of wettability and chemisorption of the oxide film by the functional macromolecules, but also enhances the evironmental durability of oxide-polymer bonds. In fact, the strong intensity band of C=O groups at 1710 cm^{-1} seems to suggest that

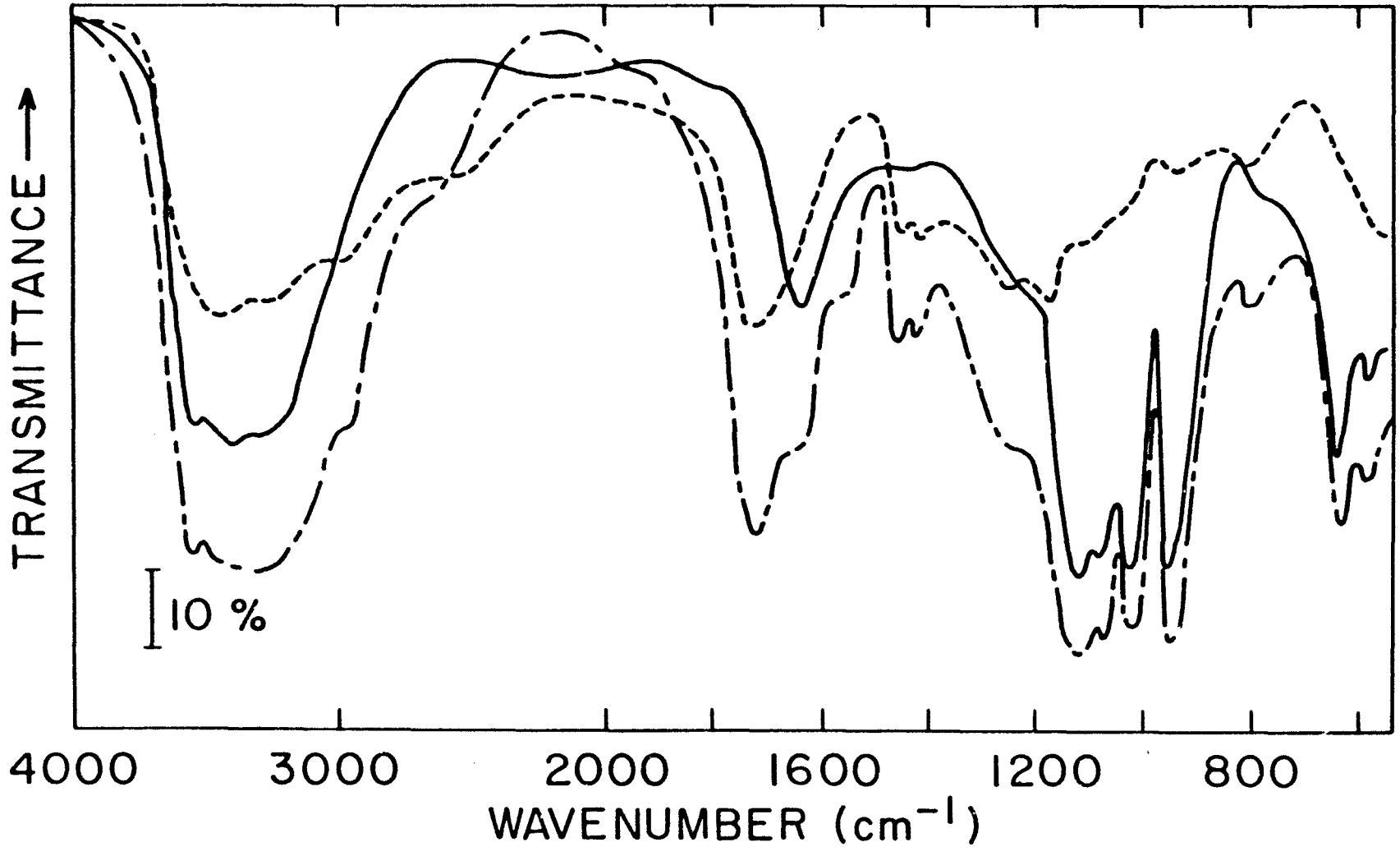

Figure 24. Comparison of IR spectra of (——) hopeite, (----) bulk PAA polymer, and (— – — –) PAA/hopeite composite.

even though oriented active COOH groups are present and may undergo acid-base interaction at all available -OH surface sites, the rate of the chemisorption at the interface regions will be small. Despite this small chemisorption rate, the energy evolved by the chemical interaction is enough to improve the interfacial bond forces.

3. Lap Shear Bond Strength

In support of the studies of the nature of the adhesion mechanisms and interfacial interaction processes described above, the lap shear bond strengths when PAA polymers with varying degrees of neutralization were used as metal-to-metal adhesives were determined. The average PAA adhesive thickness for the overlap ranged from 1 to 3 mil, and the tests on the lapped samples were performed after curing for 7 days at room temperature.

Figure 25 shows the lap shear bonding forces at the chemically treated metal-PAA polymer interfaces as a function of the degree of neutralization of the macromolecules. Correlations between the bond strength and the neutralization rate of COOH groups were found for both treated and untreated metal surfaces. In both cases, the bond strengths decrease with increasing NaOH neutralization of the PAA. As already noted in the earlier section on wetting behavior, the strength reduction is due to the poor spreading and adsorbing characteristics of PAA adhesives resulting from the increased density of conformational entanglement macromolecules. The spreading force is primarily dependent upon the degree of neutralization, but is independent of the degree of surface roughness of the deposited oxide films. In fact, the highest strength reduction rate of ~81% was obtained from the polished surface substrate bonded with 80% neutralized PAA polymers. Similar results were obtained for both treated surfaces. As an example, hopeite layers having a highly crystallized surface roughness exhibited a loss in strength of ~71% at the same degree of neutralization.

Without neutralization of the PAA, the adhesion force to the polished metal surface is low because of the absence of mechanical interlocking and chemical bonding at the interface. A stronger bond results when the metal

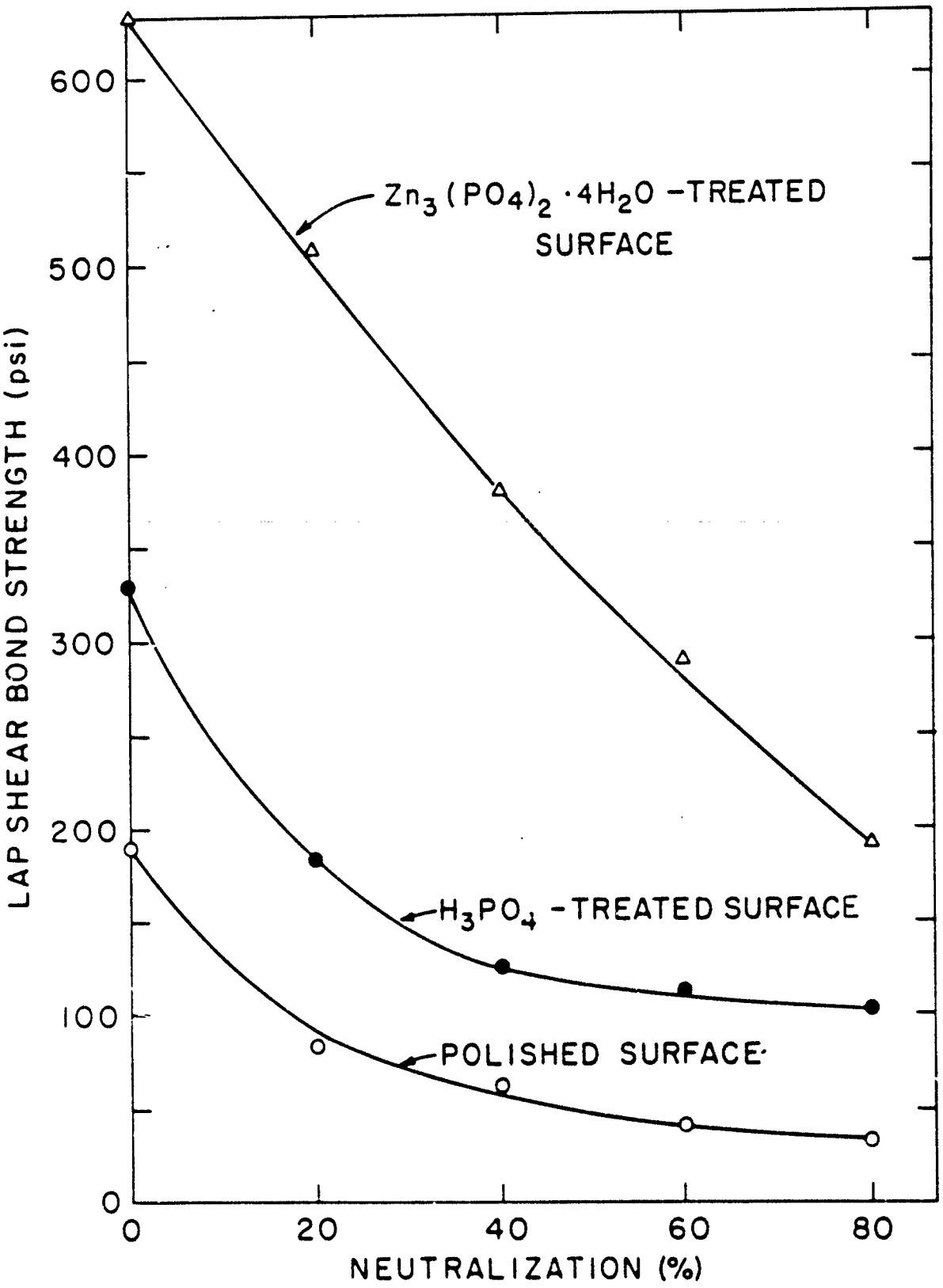

Figure 25. Lap shear bond strength change in chemically treated metal-to-metal PAA adhesives as a function of the degree of neutralization with NaOH.

faces are given a chemical treatment to produce a thick crystal surface oxide. The maximum bond streugth of 650 psi (4.48 MPa) in this test series was attained with the hopeite-deposited metal surface. This value corresponds to improvements of ~4 and ~2 times over those obtained from polished and H_3PO_4-modified surfaces, respectively.

To obtain further information regarding the polymer-hopeite interfacial bonding mechanisms, non-neutralized PAA polymer was applied to the hopeite surfaces and, after curing, the polymeric coating was physically stripped from the hopeite surfaces. Both the bonded surface side of the stripped polymer film and the coated hopeite side after stripping were studied by SEM associated with EDX. Since most of the thin polymer film remains on the hopeite surfaces, the presence of the joined pieces of hopeite crystals could be detected visually on the stripped polymer film surfaces. Morphological and energy-dispersive x-ray studies of the adhesive sites on the polymer films were therefore focused upon the bonded hopeite pieces which were randomly distributed on the film surfaces. As seen in Figure 26, the micromorphological image from the SEM resembles the surface microstructure of hopeite deposited on the metal surfaces turned upside down. The roughness of the polymer surface definitely verifies that the polyelectrolyte macromolecules adhere very well to hopeite surfaces.

The relatively modest technique of EDX has a high potential for detecting the distributions and concentrations of the major chemical constituents which exist at the solid material surface. When compared to the EDX peaks for hopeite itself (see Figure 20), it appears that the peak intensity for the Zn atom is stronger than those for P and Fe atoms. This may mean that although other transitional metal ions can be present, larger quantities of Zn atoms may be transferred to the polymer films from the hopeite surfaces.

In contrast, the coated side of the hopeite, as shown in Figure 27, displayed microstructure features completely different from those of the original hopeite crystal structures. EDX results indicated that the

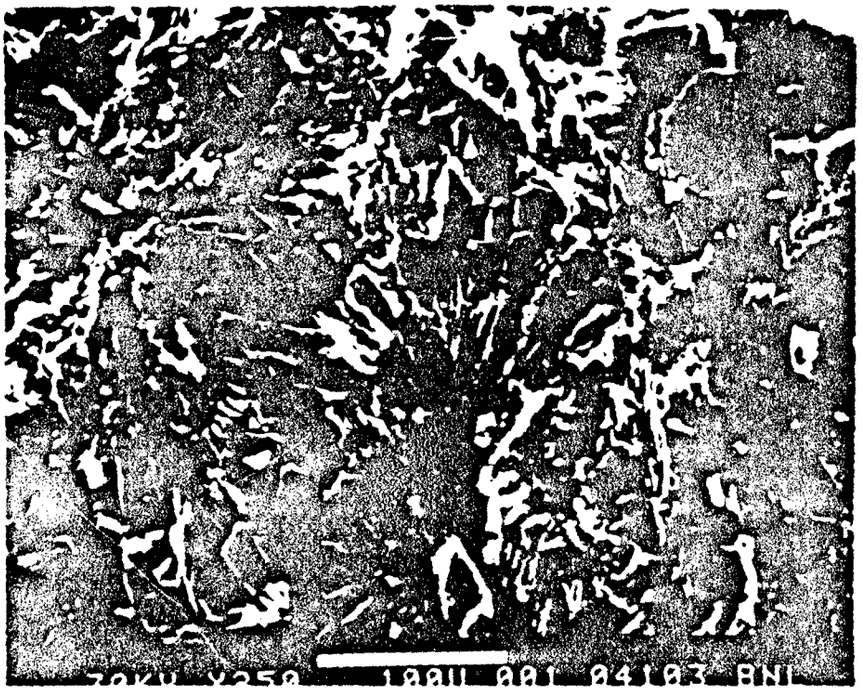

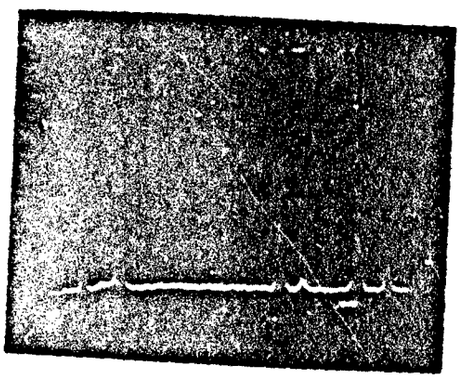

Figure 26. SEM image and ELX analysis of bonded surface side of PAA film.

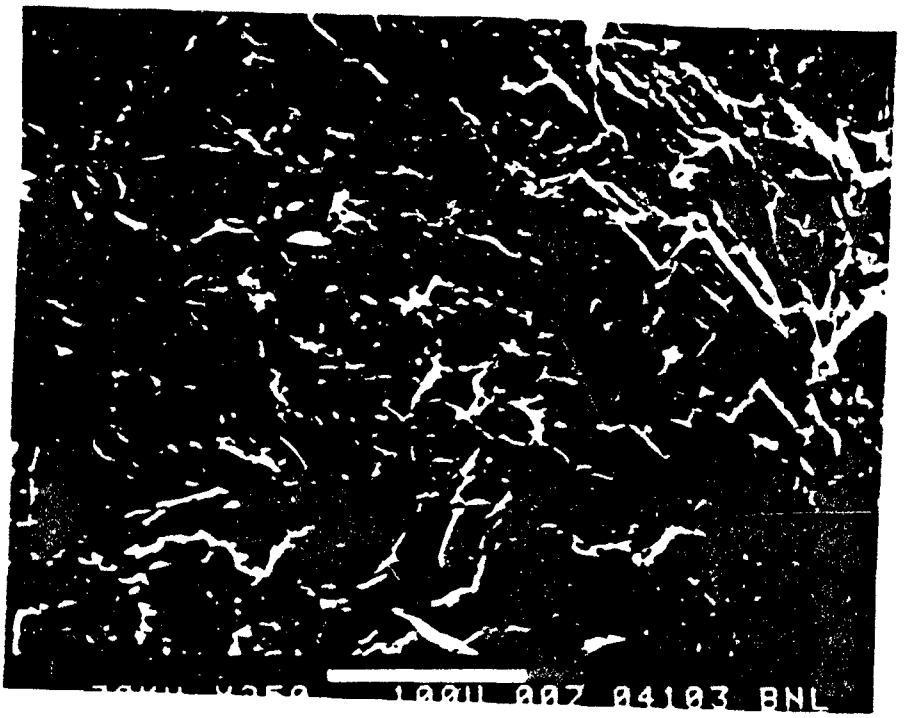

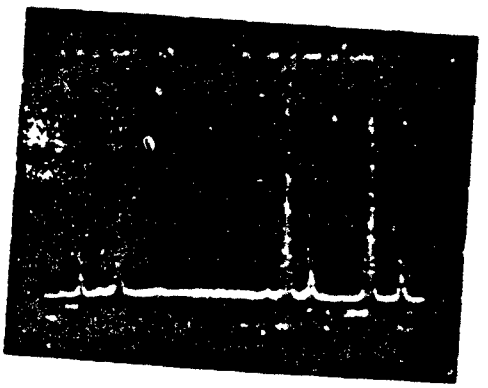

Figure 27. Surface topography with EDX peaks of coated hopeite layer site after stripping polymer.

ıtensity of Fe atom peaks increases significantly, whereas the Zn and P tom peak intensities become less. Consequently, an alternative hypothetical interfacial interaction mechanism consistent with the above bservation may be proposed.

ype C. Divalent Metallic Ion Crosslinking Reactions

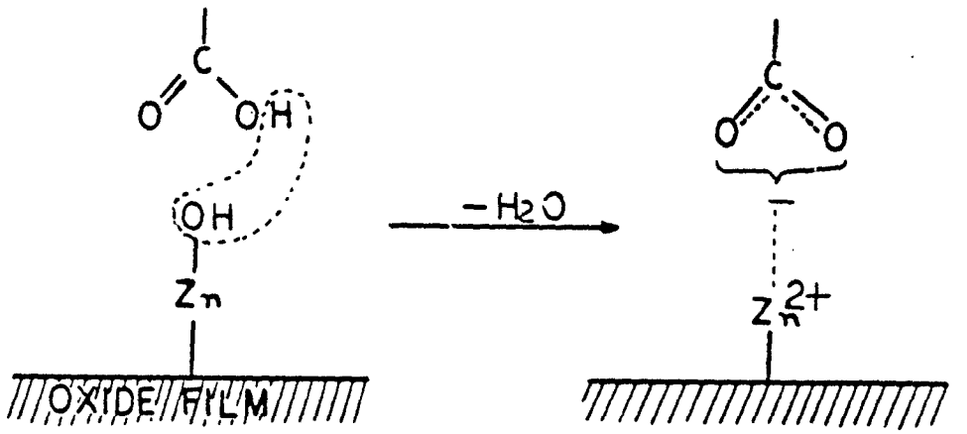

In the hypothetical Type C model, the carboxylic anion/hydroxyl group interfacial ionic bonds which have a relatively high mobility may be converted into more rigid divalent metallic bridge formations. From the results described above, the strong adhesion is essentially associated with the topography of the deposited oxide hydrate compound films, the nature of interfacial interactions, and the type of degree of chemisorption at the interfaces.

E. Modified Furan/Treated Metal Interface

1. Mechanical Interlocking Behavior

In general, good mechanical interlocking between a polymeric coating and an oxide substrate can be attributed to the following: 1) the nature of the surface topography and micromorphology of the deposited oxide layer, and 2) the physical properties of the adhesive and its ability to penetrate easily into the pores in the oxidized films. The former relates directly to surface activation factors, such as the highly crystallized oxide layer consisting of an open surface structure and an adequate

crystal thickness. These factors lead to an increase in the magnitude of the wettability and spreadability of polymeric adhesives on the oxide films. The second element is associated with the resins having low viscosity and surface tension.

On the basis of the above concept regarding the mechanical interlocking behavior, it is thought that the changes in the topographical features that occur during the growth of zinc phosphate crystals significantly affect the spreading and wetting behavior of the oxidized layers by the resin. Thus, it is very important to assess systematically any correlations that exist between the micromorphological nature of the aged oxide films and the adsorption rate of resin on the films. As a first attempt to obtain this information, the degree of crystallization of hydrated zinc phosphate compounds deposited on the metal surface as a function of the soaking time in the zinc phosphating solution was investigated by use of scanning electron microscopy (SEM).

Four steel panels which were polished with ultrafine emery paper, were immersed in the $Zn_3(PO_4)_2.2H_2O$-H_3PO_4-H_2O oxidizing solution at 80°C for 1, 3, 6, and 24 hr, respectively. SEM photomicrographs of the treated metal surfaces (Figure 28) show that the degree of deposition and the magnitude of the crystal growth increased with increased exposure to the oxidizing solution. The micrograph of the surface exposed to the solution for 1 hr indicates many distinctive tiny rings, but no significant crystal deposition on the surface is apparent. The crystalline rings may have been produced by erosion of the metal surfaces by the chemically aggressive oxidizing liquids. Closer examination reveals that the ring sizes ranged from 100 to 400 μm in diameter, and that the rings were slightly raised from the substrate surfaces. The microtexture of the metal surface changed dramatically from smooth to extremely rough after exposure for 3 hr. Its morphological features were characterized by the formation of a block-appearing coarse crystal ~280 μm in length, which was distributed randomly on all surfaces of the modified metal sites. It appeared from the SEM image after 6 hours' soaking (see Figure 28-C) that the coarse

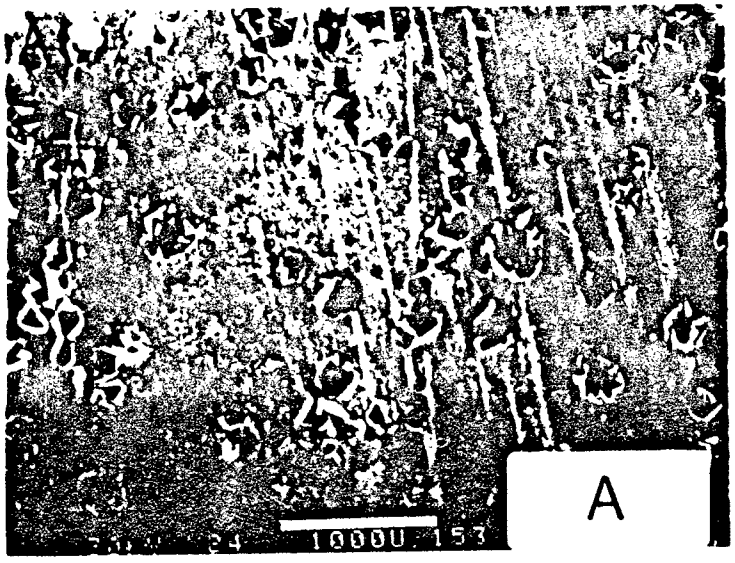
A

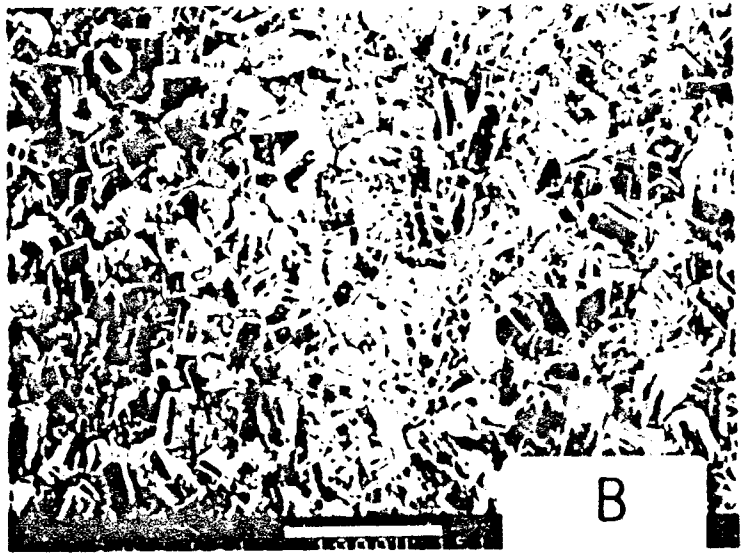
B

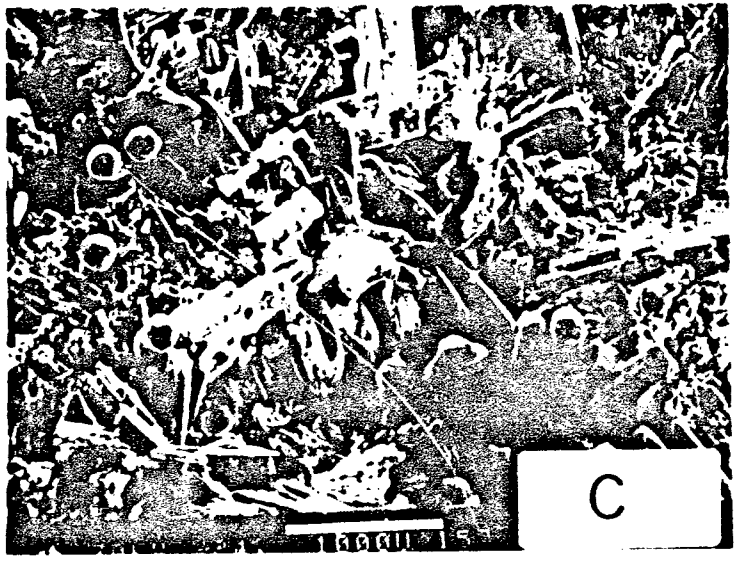
C

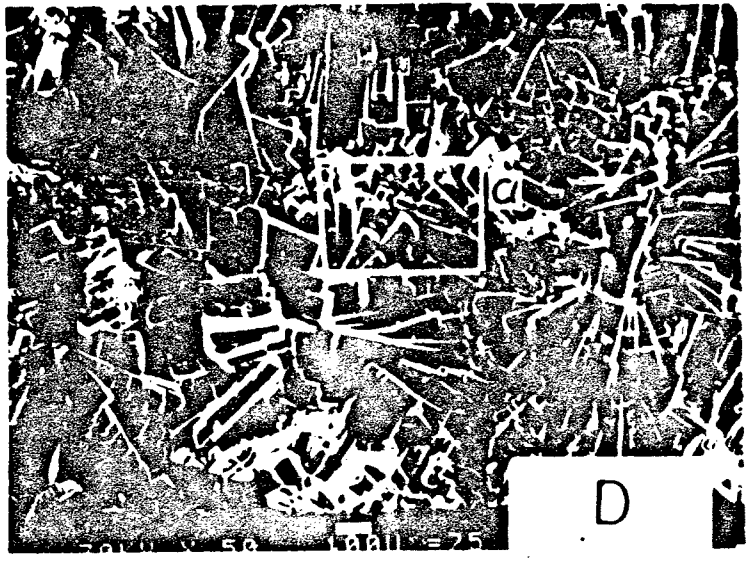
D

microstructure formed at age 3 hr was later converted into an almost rectangular crystal structure. As seen in the photomicrograph, the morphological features of the crystals formed at this age indicate a triclinic microstructure characterized by three unequal axes intersecting at angles oblique to each other. Further exposure (see Figure 28-D) resulted in the formation of a pronounced dendritic microstructure of triclinic hopeite crystals. The topography of the 24-hr-old hopeite film, as viewed by SEM, was comprised of a dense agglomeration of circular radiating rectangular zinc phosphate crystals. From this morphological image, it is expected that the uniformly interlocked crystals will provide a larger surface area for bonding and give sufficient mechanical interlocking with polymeric adhesives. When the adhesive penetrates into the open spaces on the interlocking surface microstructure, the rectangular crystals will become embedded in the adhesive phase and act as a reinforcement for the polymeric matrix.

SEM is particularly useful in preparing stereophotographs that can be viewed in three-dimensional relief with the aid of a stereoviewer and, hence it can be used to determine the approximate thickness of the crystals after various exposure times. These results are illustrated in Figure 29. The data indicate that, under the conditions employed, the oxidizing solution produces a film, the thickness of which increases almost linearly with time for exposure periods ranging up to 10 hr. Beyond that time, the rate of crystal deposition seems to decrease significantly. Highly crystallized hopeite layers ~200 μm thick can be produced by immersing the steel plate for ~15 hr in the phosphating solution at 80°C. From the above results, it is apparent that the prolonged exposure to the prescribed oxidizing mixture leads to the formation of highly dense interlocking crystals having an open surface structure. For a given crystal thickness, adhesion to more interlocked oxide films can be expected to be higher.

An increase in surface crystal thickness relates to an enhanced surface roughness and an increase in oxide surface area. The increased roughness will enhance the degree of wettability of the oxide film by the

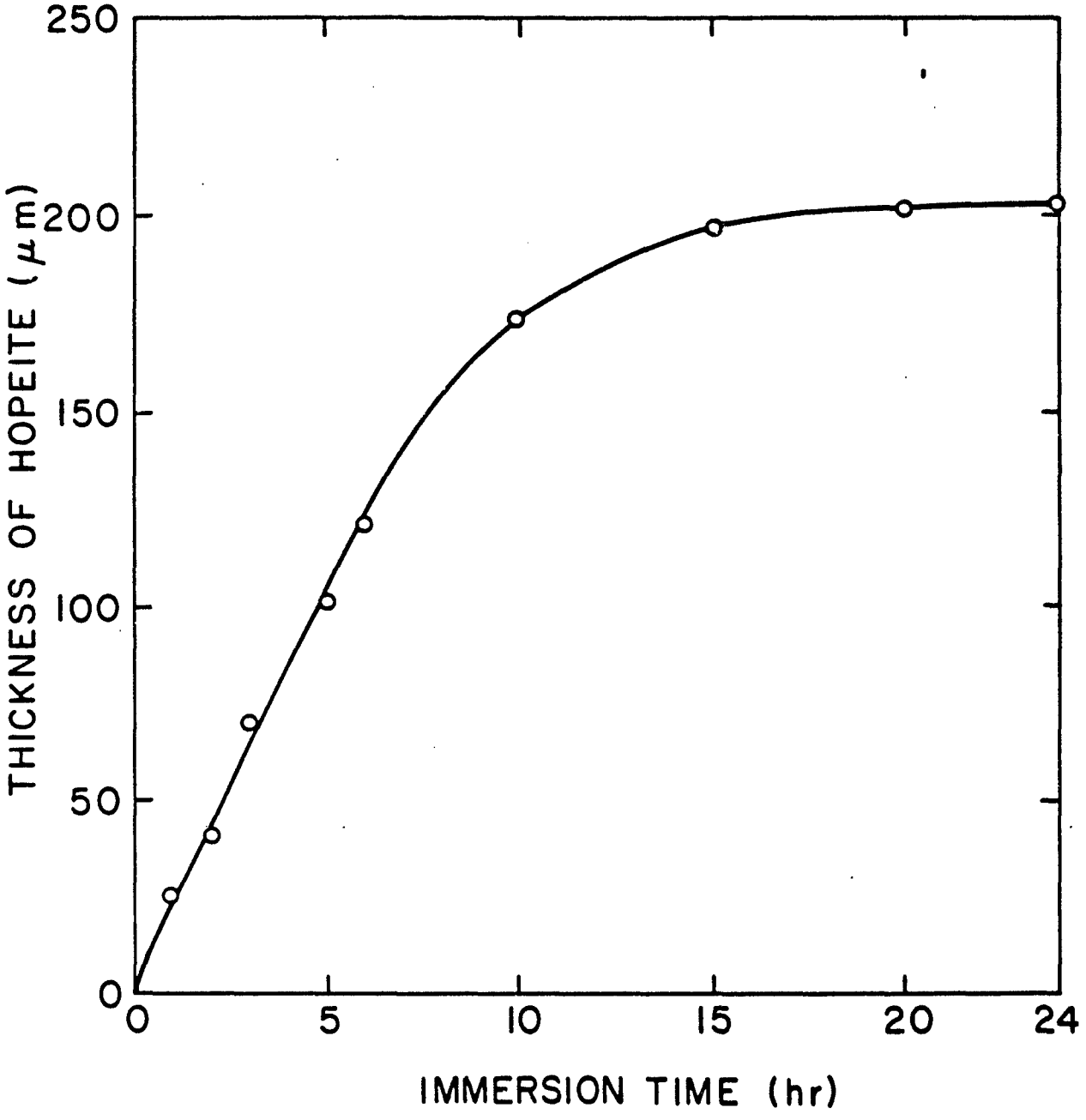

Figure 29. Thickness of hopeite crystals as a function of immersion time in zinc phosphating solutions.

liquid resin and increase the mechanical interlocking at the polymer-oxide layer interfaces. Experiments to obtain quantitative information regarding the magnitude of the wettability and the bonding forces were performed. In this work, determinations of the interfacial contact angle at the resin-oxide film boundary and the lap shear bond strength of metal-to-metal adhesives were made as a function of the immersion time for the metal substrate. A 95% furan - 5% levulinic acid resin system was used in this test series. The mixture had a viscosity of 420 cP and a surface tension of 37.4 dyns/cm at 24°C. The contact angles were measured within 30 sec after deposition of the liquid resin on the aged hopeite layers. The changes in contact angles and shear bond strength as a function of zinc phosphate treatment time are shown in Table 2. It was observed that the contact angle decreases as the treatment time in the phosphating fluid is increased up to ~24 hr, after which it remains constant. Since a lower contact angle results in an increase in the magnitude of the wetting force, it appears that the wettability of the hopeite films can be enhanced by increasing the crystal thickness. The value for the contact angle for the hopeite layer produced by immersion for 24 hr, corresponding to a crystal thickness of ~203 μm, was significantly lower (10.5° vs 30.8°) than that for an untreated metal surface. Although crystal thickness and surface roughness are major factors in the wettability of hopeite films, the unique topographical features of the dendritic structure of triclinic crystals and the facile penetration of resin into the open spaces in the interlocking rectangular crystals may also contribute.

As seen in Table 2, a strong correlation between the contact angle values and the shear bond strength seems to exist. The latter increases with decreasing contact angle for treatment times up to ~24 hr, and then levels off as the contact angle becomes constant. The adhesion to the polished metal surface (time = 0 hr) is poor because of the absence of interfacial interlocking. The failure region passes smoothly along the shear front and involves only a small amount of polymer in plastic deformation, giving a low shear bond strength of 140 psi (0.97 MPa). This low

TABLE 2

Contact Angles and Lap Shear Bonding Force as a Function of Treatment Time of Metal in Phosphating Solution

Treatment time, hr	Contact angle, deg	Lap-shear bond strength, psi (MPa)
0	30.8	140 (0.97)
1	28.9	250 (1.72)
3	24.7	390 (2.69)
6	19.0	510 (3.51)
15	13.0	680 (4.69)
24	10.5	720 (5.00)
35	10.7	700 (4.82)

strength for the untreated surfaces can be improved by a factor of 5.1 by the zinc phosphate treatment for 24 hr. An ultimate strength of 720 psi (4.96 MPa) was developed when the contact angle between the polymer and the hopeite crystal layer was 10.5°.

From the above results, it is apparent that the magnitude of the adhesion at the liquid resin-oxide film interface depends mainly on the area of resin contact, thereby resulting in an increase in the resin wetting capacity of the film surfaces. Thus, it is very important to estimate quantitatively the dynamic wetting feasibility which is expressed in terms of the rate of spreading. The primary objective in this work was to develop a spreading model for the wetting processes on the oxide film. A modified thermodynamic kinetics expression which may be rewritten in the following form was used to develop the model. This is as follows:

$$-\frac{d\left(\frac{\cos\theta_t}{\cos\theta_\infty}\right)}{dt} = k\left(1-\frac{\cos\theta_t}{\cos\theta_\infty}\right);$$

where θ_t is the contact angle at time t, θ_∞ is the contact angle at infinite time, and k refers to the spreading rate constant. The factor $\left(1-\frac{\cos\theta_t}{\cos\theta_\infty}\right)$ is defined as the rate of the contact angle fraction advanced at time t.

With this model, an attempt was made to obtain quantitative information regarding the rate of spreading on hopeite layers produced by the different zinc phosphate treatment times. Experiments were performed in which contact angles were measured as a function of time after the deposition of resin on the substrate surfaces at an ambient temperature of 24°C. Values for $\ln\left(1-\frac{\cos\theta_t}{\cos\theta_\infty}\right)$ plotted against the corresponding values of t are shown in Figure 30. Straight line relationships between the contact angle and elapsed time are evident. As a result, values obtained from the slopes $\Delta\ln\left(1-\frac{\cos\theta_t}{\cos\theta_\infty}\right)/\Delta t$ were used as the spreading rate

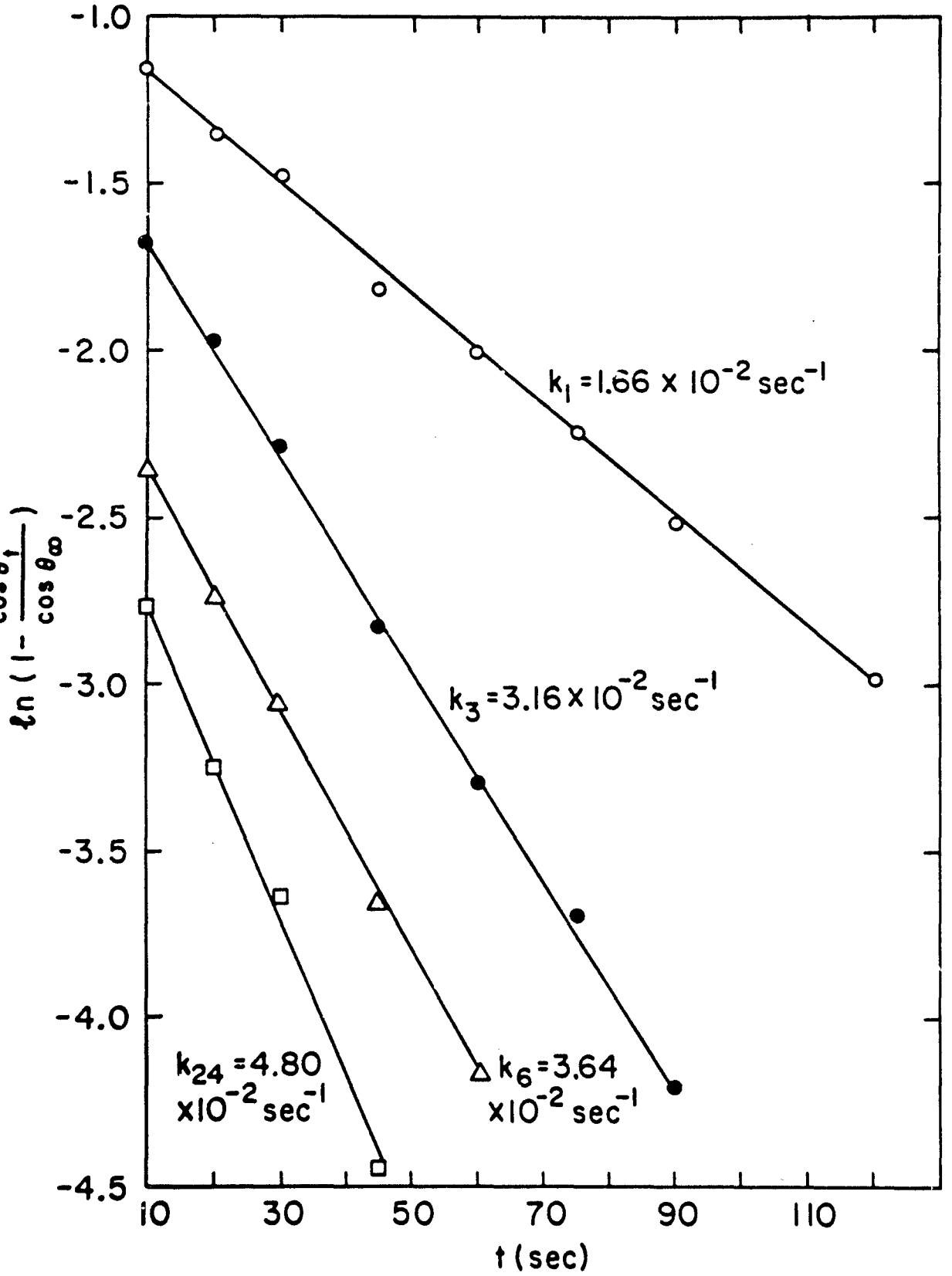

Figure 30. Comparison of spreading rate constant of resin on hopeite films at vario treatment ages; treatment time (o) 1 hr; (●) 3 hr, (Δ) 6 hr, and (□) 24

constant k. The influence of the surface oxide film on the spreading mobility of resins was evaluated by comparing the rate constant, k, for various treatment times. The data indicate that the k value increases as the treatment time of the metal surface is increased. The value of 4.80×10^{-2} sec^{-1} after a 24 hours' treatment was ~3 times greater than that at age 1 hr. This means that a film thickness of ~203 μm produced during a 24-hr immersion period has a more pronounced effect on the spreading processes than that produced during a 1-hr exposure. It apparently verifies that the boundary of a sessile drop is significantly advanced by the growing hopeite crystal layers. Consequently, the crystal thickness and the degree of surface roughness of the oxide film appear to have major roles in the resin spreading behavior.

In summary, it was found that hopeite films contribute to a good mechanical interlocking with polymeric adhesives. The bonding is attributed to the uniform topography of the dendritic array of triclinic rectangular crystals, the thickness of the crystalline film, interlocking micromorphology, and the large open surface microstructure. Anchoring of the polymer which penetrates into the open spaces in the interlocked crystal layers also acts to enhance the bond strength at interfacial regions.

2. Interfacial Chemical Attraction

The presence of functional groups, such as hydroxyl, ester, and carboxylic acid, in the levulinic acid-modified furan resin molecules may also contribute to the mobility to available adsorption polar hydroxyl (OH) groups on hopeite surface sites. The chemical treatment is intended not only to increase the rate of roughness of the metal surfaces, but also to modify the surface chemical composition. In fact, IR spectra for fine hopeite powders removed by scraping hopeite-deposited metal surfaces exhibited a strong sharp frequency at 3560 and 3400 cm^{-1}, which represents the presence of coordinated water expressed in terms of the hydration water. These strong bands represent the stretching vibration of OH groups of hydrated water. Water of hydration is also distinguished from OH groups by the presence of the H-O-H bending motion which produces a medium

band at ~1620 cm^{-1}. This band can be taken as another important means of identifying water of crystallization and it is very useful in the elucidation of inorganic structures. IR results suggest that water molecules in the hopeite molecular structure are present as simple water of crystallization and as coordinated water in hydrates. The fact that the highly crystallized hopeite formation contains a large number of polar OH groups in water molecules indicates that it should be possible to form strong hydrogen bonds to organic functional groups in polymeric coatings. Therefore, a study was performed to investigate the role of water in the interfacial chemical attraction between the functional resin and the hopeite layer. In an attempt to elucidate this role, composite samples were prepared by incorporating the modified furan resins with finely powdered hopeite which was removed from the metal surfaces, and then curing the mixture in an oven at 80°C for 10 hr. The composition of the hopeite-filled furan resin was adjusted by varying the concentration of the hopeite powder in the range of 0 to 70% by weight. After curing, the samples to be used in IR spectroscopic analyses were ground to a size of ~325 mesh (0.044 mm). IR analyses for these samples, prepared in the form of KBr discs, were conducted by interference techniques, using interfering discs containing various proportions of KBr and hopeite powders.

The resultant IR spectra indicate that the most pronounced changes in the peak intensity of IR absorption bands, as a function of hopeite concentration, take place in the frequency range of 1800 to 1350 cm^{-1}. As seen in Figure 31, the absorption spectra for bulk furan-levulinic acid-blend polymer showed a conspicuous band at a frequency of 1710 cm^{-1} and weak bands at 1560 and 1420 cm^{-1}. The prominent absorption at 1710 cm^{-1} is due to the stretch vibration of carbonyl groups (C=O) of levulinic ester formed by cleavage of furan rings and of reacted or unreacted levulinic acid. The peaks at 1560 and 1420 cm^{-1} are of approximate equal intensity and can be assigned to the asymmetric and symmetric stretching vibrations of carboxylate anion (COO^-) groups derived from the analogy of the ionized carboxyl groups. Of interest are the noteworthy changes in intensity at these frequencies that occur as the hopeite content in the

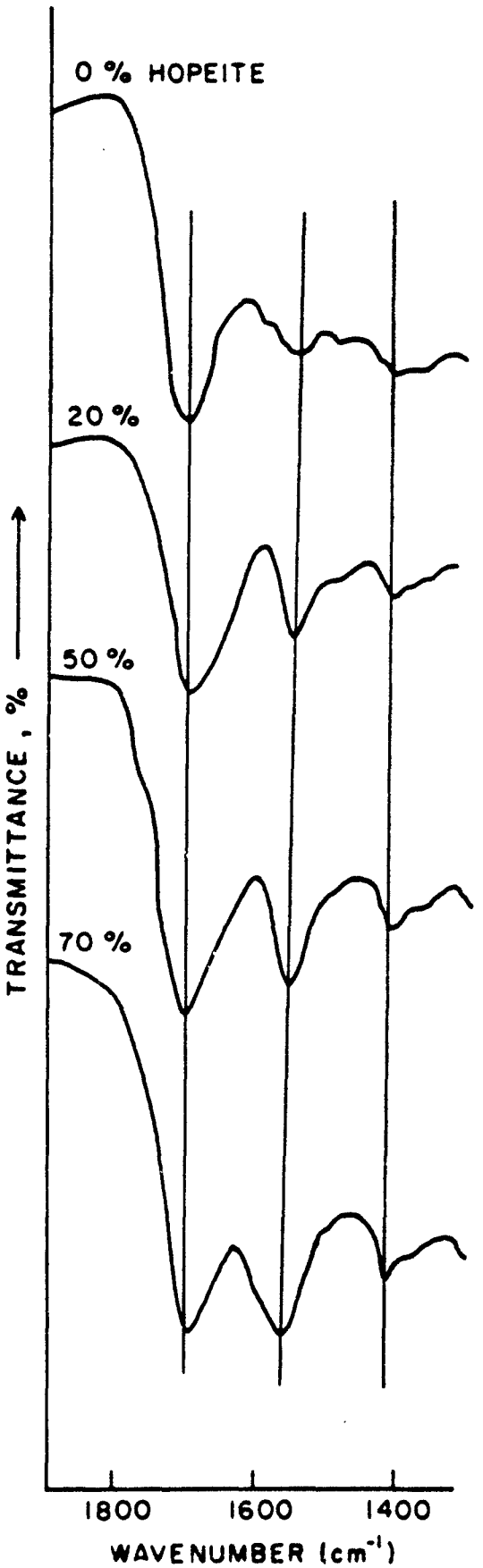

Figure 31. Changes in IR intensity at frequency of 1710, 1560, and 1420 cm-1 as a function of hopeite concentration in the composite samples.

composite systems is increased. As is evident from the figure, the intensities of COO^- bands at 1560 and 1420 cm^{-1} increase markedly with increased hopeite concentrations. Conversely, the C=O band at 1710 cm^{-1} tends to shorten with growth of the COO^- bands. From the viewpoint of interfacial chemical affinity, these results apparently demonstrate that OH groups on the hopeite surface can hydrogen bond with the carbonyl oxygen atom in the polymer molecules. Thus, the C=O stretching frequency of polymer decreases upon hydrogen bond formation through the carbonyl oxygen, whereas that of the asymmetrical and symmetrical stretching vibration of COO^-anion groups shifts to a higher frequency.

In practice, the rate of hydrogen bond formation between the C=O groups in the polymer and the OH groups on hopeite is directly related to the intensity of an absorption band or the absorbance at any given frequency. This bond rate as a function of hopeite content, from 0 to 70%, was quantitatively estimated by comparing the absorbance ratio of the C=O frequency at 1710 cm^{-1} with that of the COO^- at 1560 cm^{-1}. The absorbance at a given wave number can be calculated by using a Beer-Lambert law as shown below:

$$D_\lambda = \log (I_{o\lambda}/I_\lambda),$$

where D_λ is the absorbance at wavenumber λ, $I_{o\lambda}$ is the intensity of incident radiation, and I_λ refers to the intensity of transmitted radiation. For quantitative analysis by IR spectroscopy, the peak height or the area of the band is usually taken as the criterion of band intensity. Therefore, an accurate measurement of band intensity is required. The value of transmittance ($I_{o\lambda}$) at the base of an absorption band was determined by the use of the horizontal baseline connecting the two wings of the complex bands.

As shown in Figure 32, the plot of the absorbance ratio as a function of hopeite concentration exhibits a direct linear relationship. This indicates that the intensity of the band characteristic of COO^- formation becomes stronger as the C=O group band intensity decreases. Accordingly, it appears that the OH groups formed on the outermost surface of hopeite

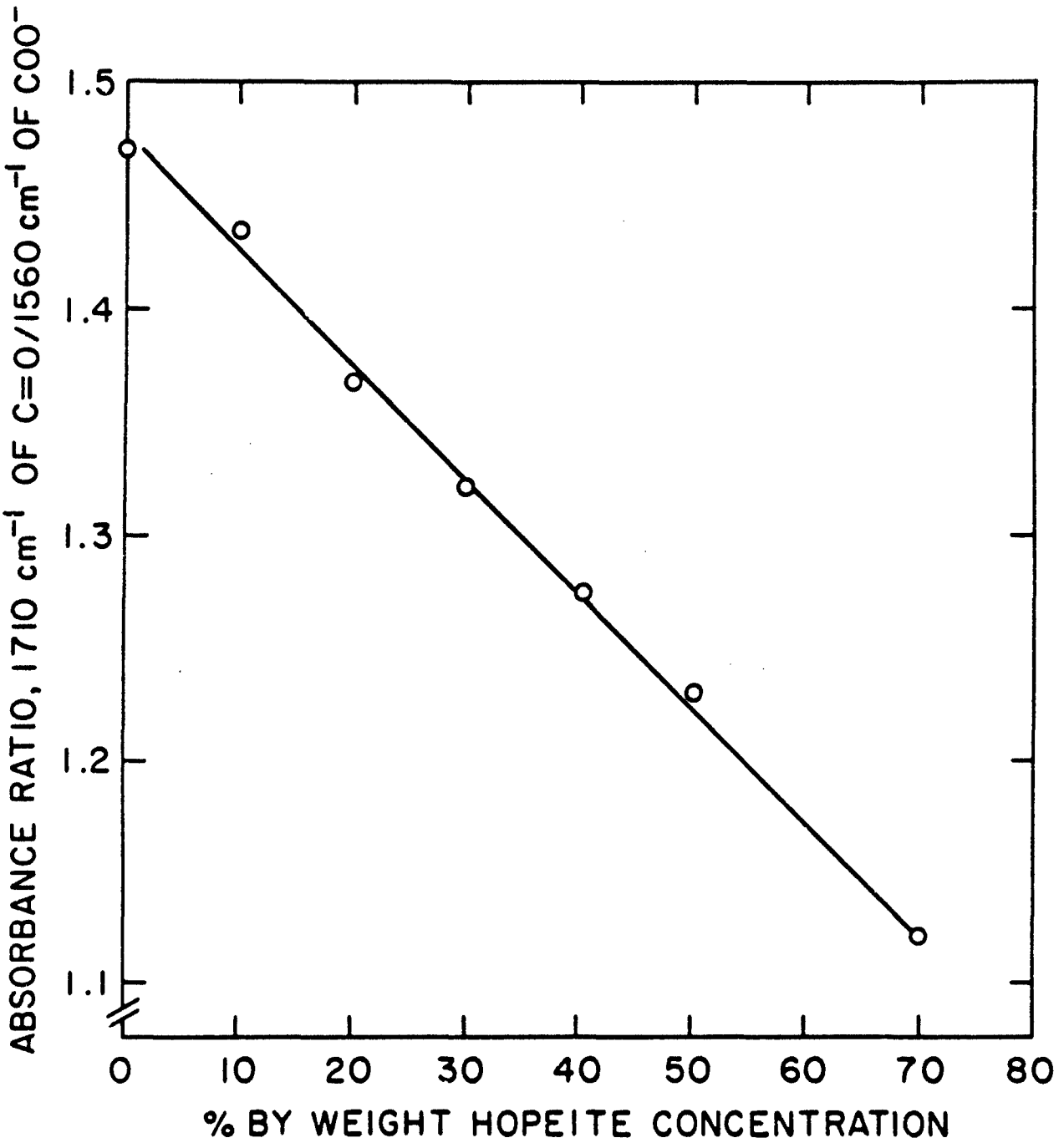

Figure 32. Correlation between absorbance ratio and hopeite concentration incorporated in furan resin system.

layers are accessible to electron donor-acceptor interactions to form hydrogen bonds. This fact further suggests that a large hopeite surface area, corresponding to the presence of a plentiful supply of polar OH groups on the outermost surface sites, is more strongly chemisorbed by the functional resin than a smaller surface area. This effect leads to an increase in the strength of the mechanical bonding at the interfaces.

A possible interpretation for the facile resin mobility at the liquid resin-hopeite interfacial regions can be developed from the nature of hydrogen bond mechanisms. When a resin, initially in a liquid state, is brought into contact with the hopeite films, the functional groups in the liquid resin are mobile enough to migrate to the polar OH group sites on the film where the energetics of adsorption to form the hydrogen bonds are particularly favorable. This behavior may be explained using a model for a charge transfer bonding mechanism which predicts that the functional groups will bond strongly to an oxygen atom forming metal-oxygen-resin complexes. Charge transfer leading to the formation of chelate-type complexes is much more common and seems to occur on most C=O containing resin surfaces. These C=O groups can stem from carbonyl, carboxylate, ketone, or other functional groups.

A study was conducted to elucidate the role of crystallized water, often called hydrates, in hydrogen bond behavior. The water molecules of crystallization are stable enough to remove water vapor from ordinary air at ambient temperature. As mentioned earlier, the presence of these thermally stable water molecules can be identified by the IR frequency at 1620 cm^{-1} which is assigned to the bonding vibration of water crystallization. Therefore, the rate of hydrogen bond formation of the water molecule with the C=O groups in the copolymer may be estimated on the basis of data obtained from quantitative analysis by IR spectroscopy. The analytical work was focused upon the changes in the absorbance ratio of C=O bands at 1710 cm^{-1} and H_2O bands at 1620 cm^{-1}. The samples for IR studies were prepared by mixing equal parts of initiated furan-levulinic acid blend resin and hopeite powder. To study the hydrogen bond reaction of C=O groups and H_2O groups, the concentration of levulinic acid reagent in the blend

resins was varied, ranging from 0 to 40% by weight of total resin mass. IR spectra were recorded for samples prepared in the form of conventional KBr discs.

Figure 33 shows the changes in absorbance ratio which are calculated from the peak intensities at the two frequencies (1710 and 1620 cm^{-1}), as a function of the levulinic acid concentration. The data indicate that the absorbance ratio gradually increases with an increase in the amount of levulinic acid. The absorbance ratio for the sample containing 40% levulinic acid was more than three times greater than for the sample without the levulinic acid. The reduction in the intensity of the H_2O frequency at 1620 cm^{-1} with increased C=O groups is due to a lowering of the H-O-H bond order by formation of the hydrogen bond, -C=O-----H_2O. As is evident from the above results, an interesting speculative possibility is that the water crystals formed on the hopeite layers play an essential role in binding the oxide film-polymeric coating units together, thereby producing good adhesion. All available crystallized H_2O at the outermost sites of the hydrated hopeite surfaces reacts chemically with the numerous functional groups modified by addition of the levulinic acid to the furan. Subsequently, the proton-donating ester and carboxylic acid groups chemisorbed strongly with the polar OH groups are converted into carboxylate anions which induce hydrogen bonding as a result of acid-base and charge transfer interactions. It should be noted that the rate of hydrogen bond formation between the functional groups and the H_2O groups can be estimated by determining quantitatively the reduction rate of the IR peak intensity at 1620 cm^{-1}.

F. Conclusions

It appears that for a metal substrate surface to achieve good bonding with polyelectrolyte macromolecules, the interface and interfacial regions should have the following surface activation elements: (1) a highly crystallized oxide layer consisting of an open surface structure, (2) an adequate crystal thickness, (3) the presence of rich polar hydroxyl groups formed on the metal oxide surfaces, and (4) minimal free divalent metallic ions on the oxide films.

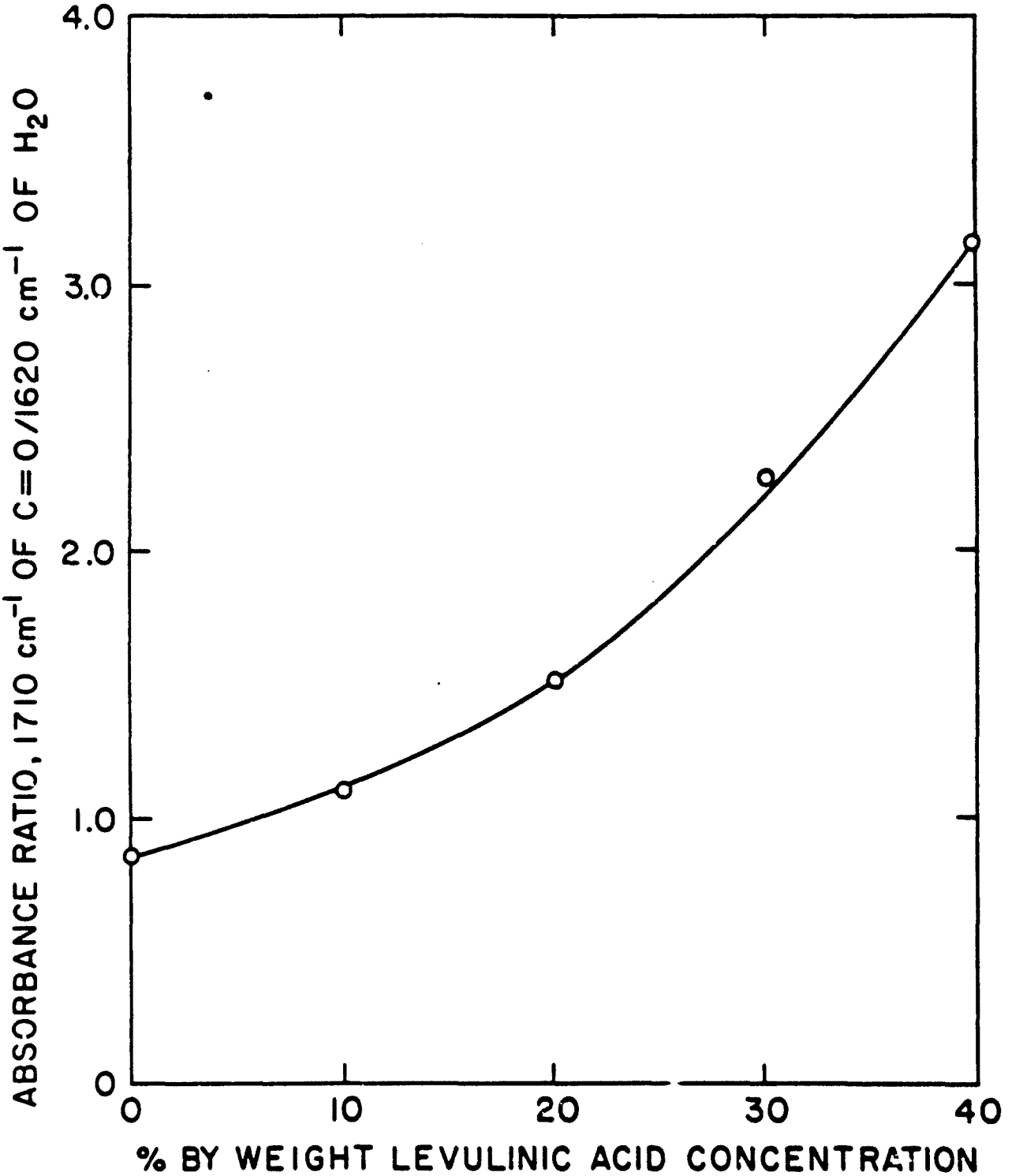

Figure 33. Absorbance ratio obtained from 1710 and 1620 cm^{-1} absorption bands vs levulinic acid concentration.

An essential prerequisite for attaining good adhesion of macromolecules to hydrated oxide metal surfaces is that macromolecules having regularly oriented pendent COOH groups must continuously wet the rough surface by spreading on and penetrating into the open surface microstructure and microfissures of the oxide films. Subsequently, the proton-donating COOH groups chemisorbed strongly with the polar OH groups at hydrated oxide surface sites must be converted into carboxylic anions which induce strong ionic bonding as a result of acid-base and charge transfer interaction mechanisms. The mechanical interlocking and chemical ionic bonds formed at the pore wall, which are normal to the oxide hydrate films, are primarily responsible for the molecular orientation. The preferred macromolecule orientations in the polymer layer contribute significantly to the development of the interfacial bond strength, whereas the conformation change caused by the free-ion-complexed molecular structure, resulting in coiled-up macromolecules, is likely to result in a decrease in interfacial bonding forces.

On the basis of the experimental results and analysis, the following physico-chemical factors significantly affect the adhesion of levulinic acid-modified furan polymer to crystalline hopeite films deposited on metal surfaces. The nature of the interfacial attraction which can be modified to achieve good bonding at the hopeite film-modified furan polymer interfaces, was influenced by the following three elements: 1) mechanical interlocking bonds which are provided by the degree of the surface roughness of the substrates, 2) spreading forces of the deposited hopeite polar film by the functional liquid resins, and 3) chemical intermolecular attractions.

The highly crystallized triclinic hopeite has a considerable deposition weight, and a typical surface topography comprising a dendritic microstructure array of an interlocking rectangular crystal was confirmed. This structure was found to be the primary factor contributing to the increased mechanical interlocking forces associated with the mechanical anchoring of the polymers yielded by penetrating liquid resin into the open surface microstructure and microfissures of the films. The extent of hopeite-polymer interlocking depends mainly on the thickness of the

hopeite crystals, the polar H_2O groups at the crystal surface sites, and the reactive molecular structure of the liquid adhesives. The coordinated and crystallized H_2O molecules existing at the outermost surface of the films were found to play an essential role in wetting the furan blend resin containing a levulinic acid admixture which has functional carboxylic acid groups in the molecules. Thus, the presence of a plentiful supply of polar H_2O groups on a hopeite film surface with a crystal thickness of ~200 μm acts as a good spreading key in promoting mobility of the functional resins. The ability of furan coatings to interact chemically with the hopeite surfaces can be modified by incorporating an adequate amount of levulinic acid. Hopeite-to-functional blend polymer chemical affinity is due mainly to the intermolecular attraction resulting from the formation of strong hydrogen bonds, $COO^-....H_2O$, between the carboxylate groups derived from levulinic ester or acid and the water molecules of hydration at the hopeite surface sites.

IV. CHARACTERISTICS OF POLYELECTROLYTE-MODIFIED ZINC PHOSPHATE CONVERSION PRECOATINGS

Although zinc phosphate treatments are considered to be effective for protecting cold-rolled steel plates, the crystalline zinc phosphate (Zn·Ph) conversion precoats deposited on the substrate surfaces are often porous, and as a result, ineffective. In addition, the resultant crystal structure and film thickness play major roles in restraining physical deformation failures of the metals. Increased coating thickness results in increased brittleness, thereby enhancing the potential for failure during flexure or other deformation.

The introduction of polyelectrolyte macromolecules into the zinc phosphating liquid was found to significantly improve the stiffness, the ductility, resistance to moisture permeability, and the paint adherent properties of Zn· Ph conversion layers. Therefore, an aim in the study was to comprehensively elucidate how the polyelectrolyte containing Zn·Ph conversion crystal film contributes to the improvement in the controllability of crystal thickness, the wettability by liquid resin, and the adherent properties to polymeric topcoat systems.

A. Materials

The metal used in the experiments was nondesulfurized mild carbon steel consisting of 0.18 to 0.23% C, 0.3 to 0.6% Mn, 0.1 to 0.2% Si, and $\leq$0.04% P. Fine crystalline polyacrylic acid (PAA) complexed zinc phosphate hydrate films were deposited onto the metal substrate surfaces. The zinc phosphating liquid consisted of 9 parts zinc orthophosphate dihydrate and 91 parts 15% H_3PO_4, and was modified by incorporating a PAA polymer at concentrations ranging from 0 to 4.0% by weight of the total phosphating solution. Commercial PAA, 25% solution in water, having an average molecular weight in the range of 5×10^2 to 5×10^5, was supplied by Scientific Polymer Products, Inc. The PAA- Zn·Ph composite conversion film was deposited on the metal substrates by immersing the metal for 10 hr in the modified zinc phosphating solution at 80°C. After depositing the composite conversion films, the substrates were left in a vacuum oven at 150°C for ~5 hr to remove any moisture from the film surfaces and to solidify the PAA macromolecules.

Commercial-grade polyurethane (PU) M313 resin, supplied by the Lord Corporation, was applied as an elastomeric topcoating. The polymerization of PU was initiated by incorporating a 50% aromatic amine curing agent M201. Furan (FR) 1001 resin employed as a glassy topcoating system was supplied by the Quaker Oats Company. The condensation-type polymerization of the FR resin was initiated by the use of 4 wt% QuaCorr 2001 catalyst, which is an aromatic acid derivative. These initiated topcoatings were cured in the oven at a temperature of 80°C.

B. Measurements

The image analysis of surface microtopography, measurement of crystal thickness, and quantitative multi-element analysis of subsurface composition for the chemically treated metal surfaces were conducted with an AMR 100-Å scanning electron microscope associated with TN-2000 energy dispersive X-ray spectrometry.

A Perkin-Elmer Model 257 spectrometer was used for internal reflection infrared (IR) spectroscopic analyses. To detect the presence of the functional organic polymers in the conversion complex films and to estimate the concentration, IR spectra were obtained for samples prepared in the form of KBr discs. The samples were powdered before mixing and grinding with KBr.

Quantitative elemental information and identification of chemical states at the surface of PAA-zinc phosphate composite crystal layers can be obtained on the basis of the peak heights, precise determination of bonding energies, and peak shapes deduced from x-ray photoelectron spectroscopy (XPS) analytical techniques. XPS spectra of sample surfaces were taken using a CLAM 100 Model 849 Spherical Analyzer operating in a vacuum of 10^{-8} to 10^{-9} Torr. Measurements were made with Al Kα radiation.

X-ray powder diffraction (XRD) analyses were employed to identify the Zn·Ph compound layers deposited on the treated metal surface. To prepare the fine powder samples, the deposited oxide layers were removed by scraping the surfaces and were then ground to a size ~325 mesh (0.44 mm). The magnitude of the wetting force of the modified metal surfaces by furan resin coatings was measured using a Contact Angle Analyzer in a 60% R.H. and 24°C environment. All the data were determined within 30 sec after drop application.

In the support of XRD data, a DuPont 910 Differential Scanning Calorimeter with a heating rate of 10°C/min in N_2 gas was used to determine the thermal decompositions of the identified Zn·Ph compound phases.

In an attempt to evaluate the mechanical properties of the layers, the stress-strain relation and modulus of elasticity in flexure were determined using computerized Instron Flexure Testing Systems, operating at deflection rates of 0.5 to 0.05 mm/min. The determination of the stress-strain curve was made on the tensile zones of metal plate specimens, 6.2 cm long by 1.3 cm wide by 0.1 cm thick, subjected to three-point bending at a span of 5.0 cm.

Modulus of elasticity, tensile strength, and elongation tests for the cured topcoat polymers were performed on dumbbell-like samples 7.0 cm long and 0.5 cm wide at the narrowest section. Stress-strain diagrams were obtained with a tensile tester having a cross-head speed of 0.5 mm/min. All strength values reported are for an average of three specimens.

Peel strength[45] tests of adhesive bonds at the polyurethane topcoat modified metal substrate interfaces were conducted at a separation angle of ~180° and a crosshead speed of 5 cm/min. The test specimens consisted of one piece of flexible polyurethane topcoat, 2.5 by 30.5 cm, bonded for 15.2 cm at one end to one piece of flexible or rigid substrate material, 2.5 by 20.3 cm, with the unbonded portions of each member being face to face. The thickness of the polyurethane topcoat overlayed on the complex crystal surfaces was ~0.95 mm.

The lap-shear tensile strength of metal-to-metal rigid furan adhesives was determined in accordance with the modified ASTM method D-1002. Prior to overlapping between metal strips 5.0 cm long, 1.5 cm wide, and 0.2 cm thick, the 1.0- x 1.5-cm lap area was coated with the initiated furan adhesive. The thickness of the overlapped film ranged from 1 to 3 mil. The Instron machine was operated at a cross-head speed of 0.5 mm/min. The bond strength values for the lap shear specimens are the maximum load at failure divided by the total bonding area of 1.5 cm^2.

C. Deposition Weight and Thickness

The investigation to determine the ability of PAA polyelectrolyte macromolecules to decrease the quantity of crystalline Zn·Ph conversion deposits was conducted using the following test procedures: the PAA macromolecules in amounts ranging from 0 to 2.0% by weight of total zinc phosphating liquid were dissolved in the phosphating solution by stirring. The polished metal plates were then immersed for up to 20 hr in the phosphating liquid with and without PAA at 80°C. Immediately after immersion, the plates were placed in a vacuum oven for 10 hr at 130°C. The surface of the dried plate was then washed with acetone solvent to remove the

multiple-layer PAA polymer coating from the deposition films and then rinsed with water. The deposition weight, expressed as mg/cm^2 of treated metal surface, was consequently determined by a method in which the conversion crystal film was removed by scraping the surface of a weighed plate, and the plate was reweighed.

The results from the above tests are given in Figure 34. The resultant weight vs immersion time curves indicate that the coating weight produced from the PAA-modified phosphating or unmodified liquids tends to increase with soaking time. For the oxidizing solution without PAA, the coating weight after a 1 hr phosphate treatment was increased by a factor of 2.7 by extending the immersion time to 20 hr. As is evident from the figure, the coating weight can be reduced by adding PAA, and the amount seems to correlate directly with the PAA concentration. At a phosphating age of 20 hr, the addition of 2.0% PAA produced a coating weight of 7.9 mg/cm^2. This is 30% less than the value obtained using a phosphating solution without PAA for the same period of time. Thus, the presence of PAA macromolecules in zinc phosphate treatment processes reduces the coating weight, which could be economically desirable.

To further clarify the effects of PAA macromolecules on the coating weight, the extent of the conversion crystal growth deposited on metal surfaces was assessed using scanning electron microscopy (SEM). This technique is particularly useful since, with the aid of a stereo viewer, the crystals can be viewed in three-dimensional relief. Samples measuring 6 x 2 x 1 mm were used to determine the approximate thickness of the crystals produced by zinc phosphate treatment lasting 7 hours. The specimens were prepared by cutting a center portion of a larger-size metal plate with a diamond wheel. The SEM examination was focused primarily on the edge view of sliced sections. Figure 35 shows SEM photomicrographs of

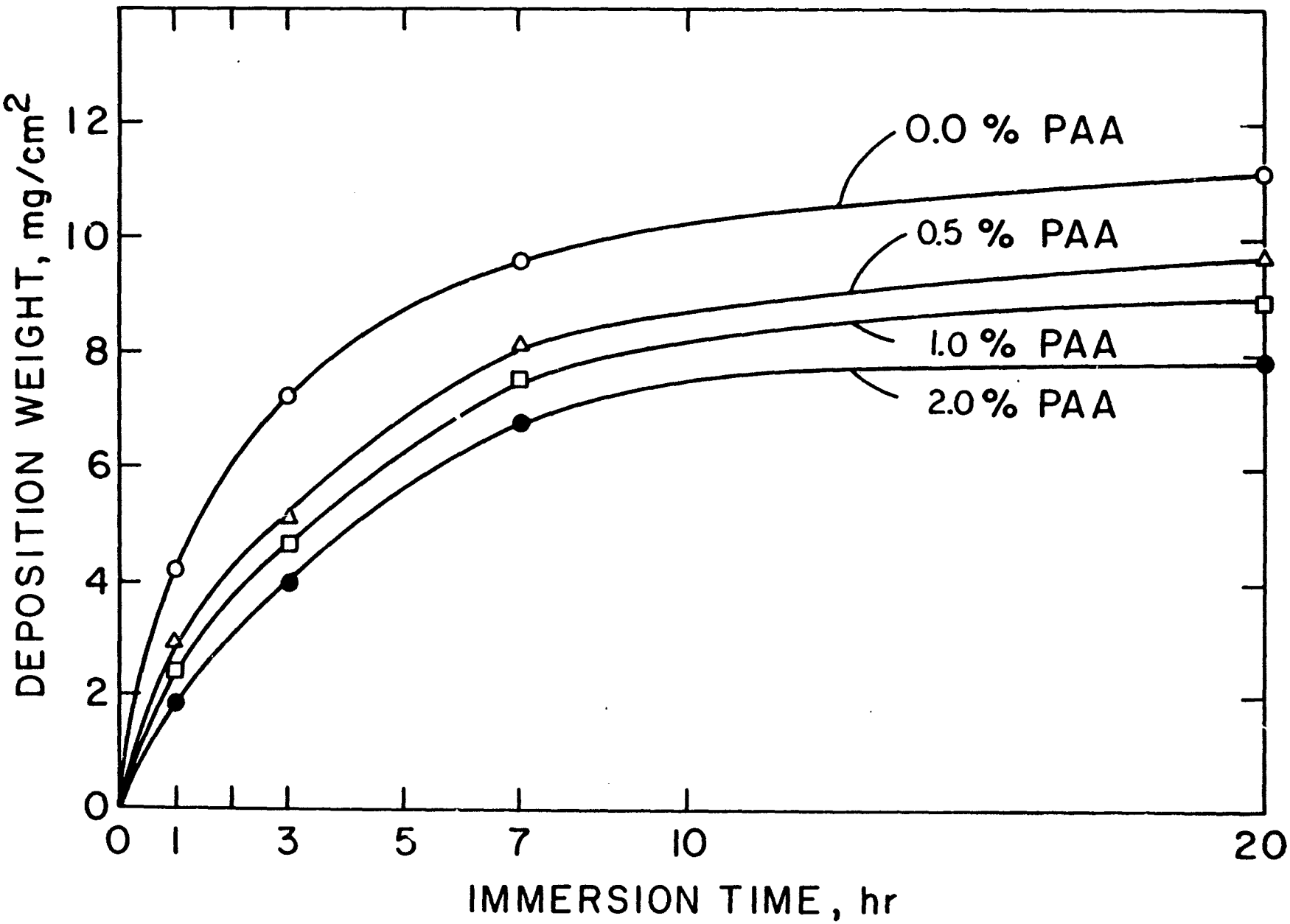

Figure 34. Effect of PAA macromolecules on the coating weight of zinc phosphate deposition.

crystalline films deposited on metal surfaces treated with PAA-modified and un-modified phosphating liquids. The coarse crystals (Figure 35-a) produced by immersing the metal substrate in the conventional phosphating liquid for 7 hr were ~120 μm thick. In contrast, the coating deposited from a solution containing 3.0% PAA was considerably thinner and was comprised of relatively fine crystals (see Figure 35-b).

A curve of average crystal thickness as a function of PAA concentration was prepared by direct SEM observation of edge views in accordance with the procedures described above. This curve is shown in Figure 36. The zinc phosphate treatment time for all specimens used in this study was 7 hr at 80°C. As is evident from the figure, the conversion crystal thickness decreases dramatically with an increase in the PAA concentration in the conventional phosphating liquid. Over a PAA concentration range from 0 to 4.0%, thickness varied between ~120 and ~35 μm. The presence of 4.0% PAA in the solution reduced the thickness to less than 30% of that from the conventional liquid. Although not shown in the figure, it was not possible to deposit a coating on the metal substrate when 7.0% PAA was added. It is apparent that when water-soluble polyelectrolyte macromolecules having an average molecular weight of 104,000 are used as a deposition-reducing admixture, the concentration of the macromolecules in the phosphating liquid must be carefully estimated in order to produce a crystal film of the required thickness and coating weight.

The amount of the PAA polymer deposition on the metal substrate surfaces can be estimated by using IR absorption spectroscopy. Since the conversion of the PAA solution to a solid polymer is essentially completed during the process of drying the deposited film surfaces at 150°C, the powder samples for IR studies were made by scraping the formed PAA-zinc phosphate composite crystal surfaces. IR spectra were then recorded for the samples prepared in the form of conventional KBr discs. The composition of the PAA-modified phosphating liquid was adjusted by varying the concentration of the PAA solution in the range of 0 to 3.0%.

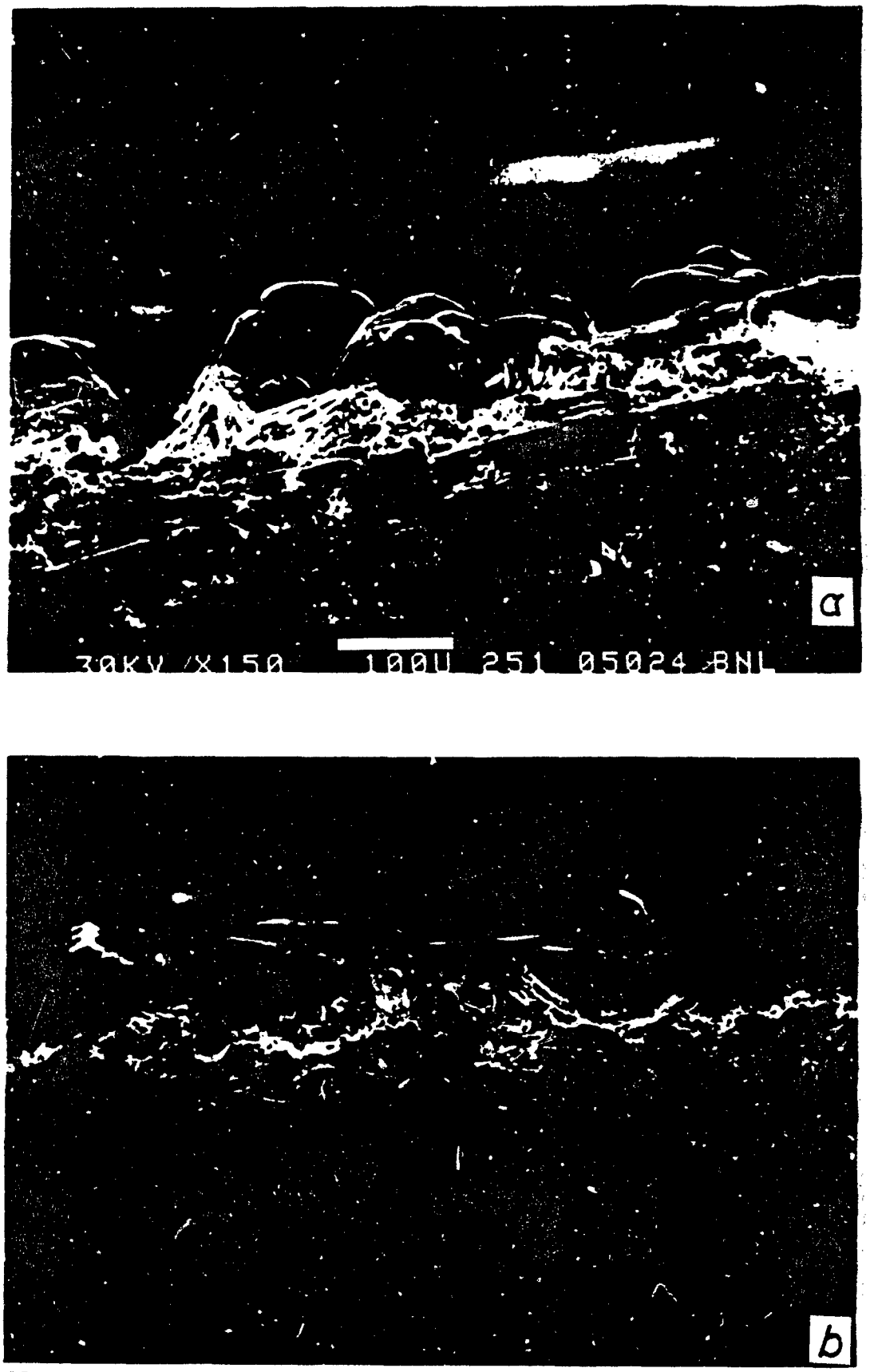

Figure 35. SEM micrographs of edge views of zinc phosphate crystal sections: metal surface treated with conventional phosphating solution (a), and surface produced with a 3.0% PAA-modified phosphating liquid (b).

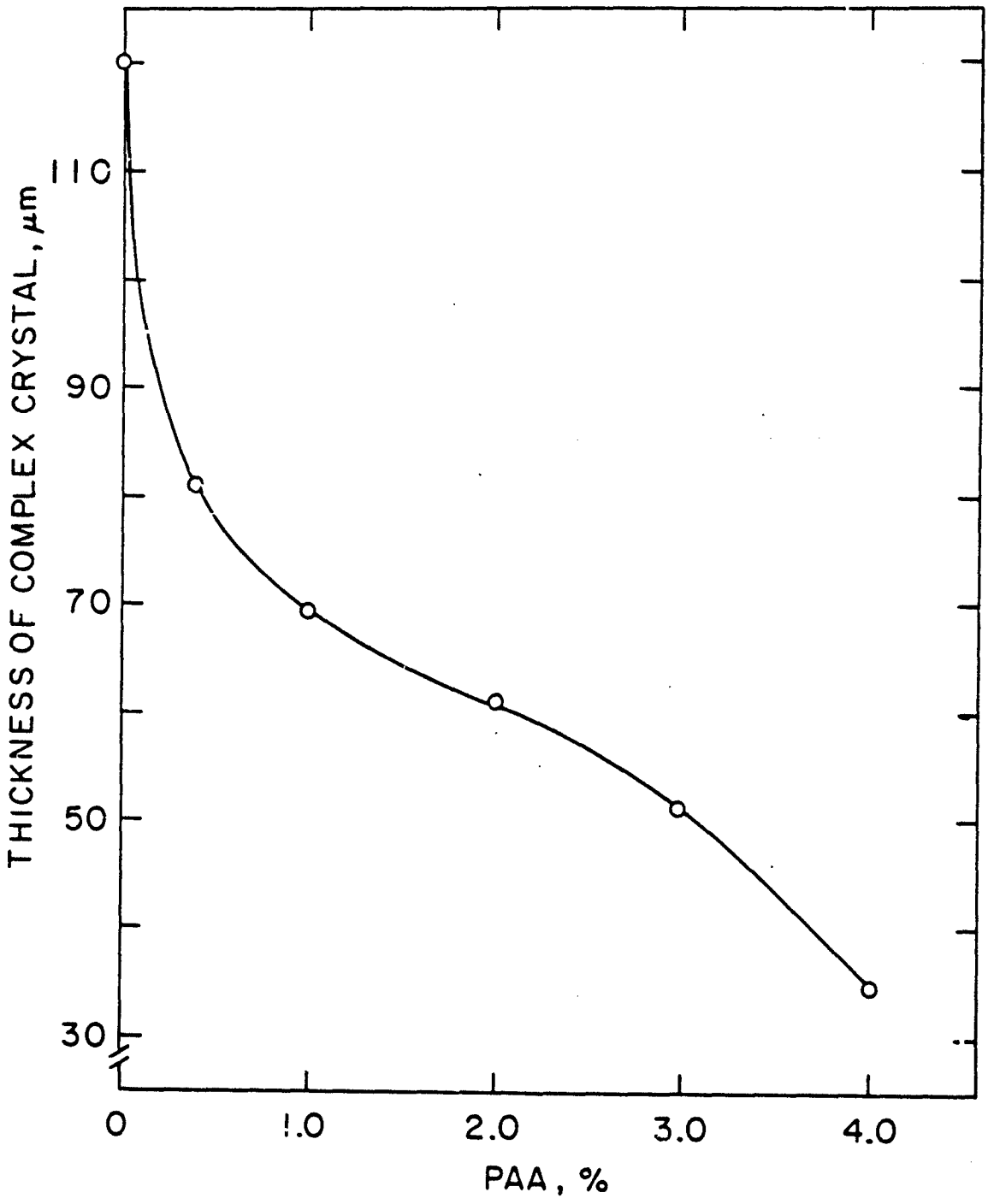

Figure 36. Thickness of complex crystal vs PAA concentration.

The analytical work to compare the quantity of the deposited PAA polymers was focused on the changes in band intensity of the carbonyl C=O at 1710 cm^{-1} and the CH of saturated methylene at 1440 cm^{-1} which represent the pendent and main chain groups in the PAA polymer structure. Figure 37 shows the resultant IR spectra for these specimens over the frequency range of 1900 to 1300 cm^{-1}. Referring to the figure, the conspicuous band at 1630 cm^{-1} for all specimens is assigned to the crystallized water of Zn·Ph hydrate films. Also, the intensities of the peaks at 1710 and 1440 cm^{-1} gradually increase as the PAA concentration is increased. This implies that the quantity of PAA polymer deposited is directly proportional to the amount added to the phosphating liquids.

D. Surface Microtexture

The nature of the microtexture of the surface of the unmodified and the PAA-modified Zn·Ph crystal coatings was studied by use of scanning electron microscopy (SEM). Figure 38 shows electron micrographs of the surface microstructure of the deposition compounds prepared by soaking the metal substrate in the conventional and PAA-modified phosphating liquids for ~20 hr. The conversion coating produced with the conventional liquid (see Figure 38-a) is characterized by the formation of a pronounced dendritic microstructure of triclinic Zn·Ph crystals. This morphological image indicates an interlocking structure of rectangular-like crystals which produces an extremely rough surface texture. In contrast, the metal specimens treated with PAA solutions had a much smoother surface. Figures 38-b and c show microtexture views of 0.5% and 2.0% PAA-treated metal surfaces, respectively. As seen in the photomicrographs, the topographical features were progressively changed from rough to smooth by increasing concentrations of the PAA solution. This is probably due to the multiple PAA polymer layers forming continuously on the surface of the conversion crystal film. However, the thickness of the overlaid PAA polymer films was not determined in this study.

It was presumed that the cured PAA polymers would produce a mechanically stable coating due to the formation of strong interlocking forces associated with the anchoring of the polymers into the open surface

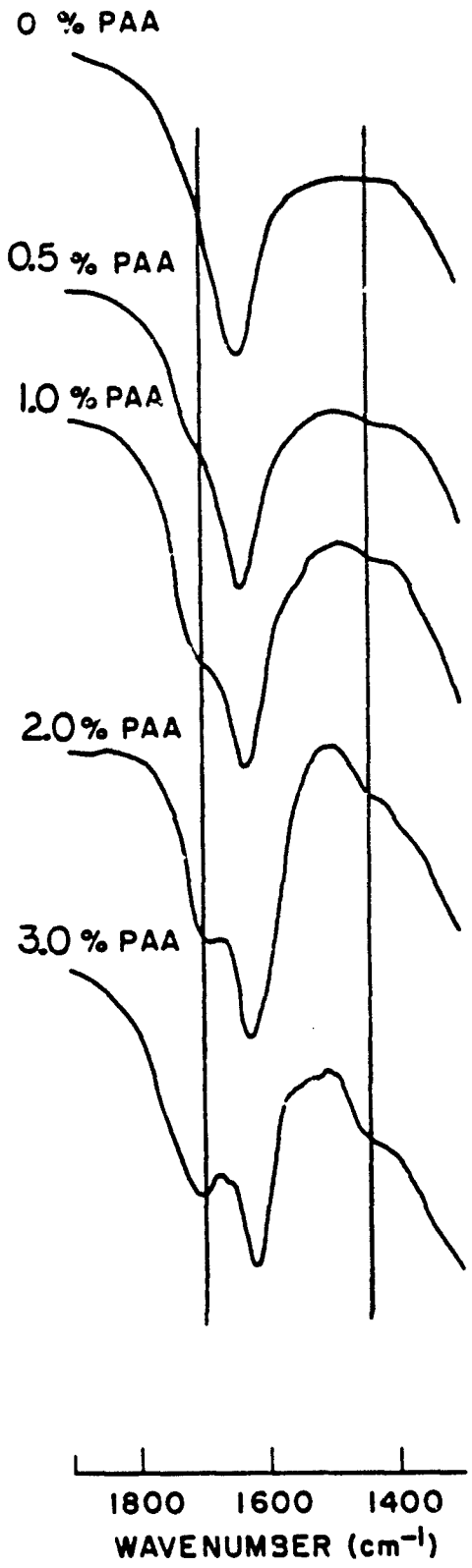

Figure 37. Infrared spectra of zinc crystal films modified with PAA.

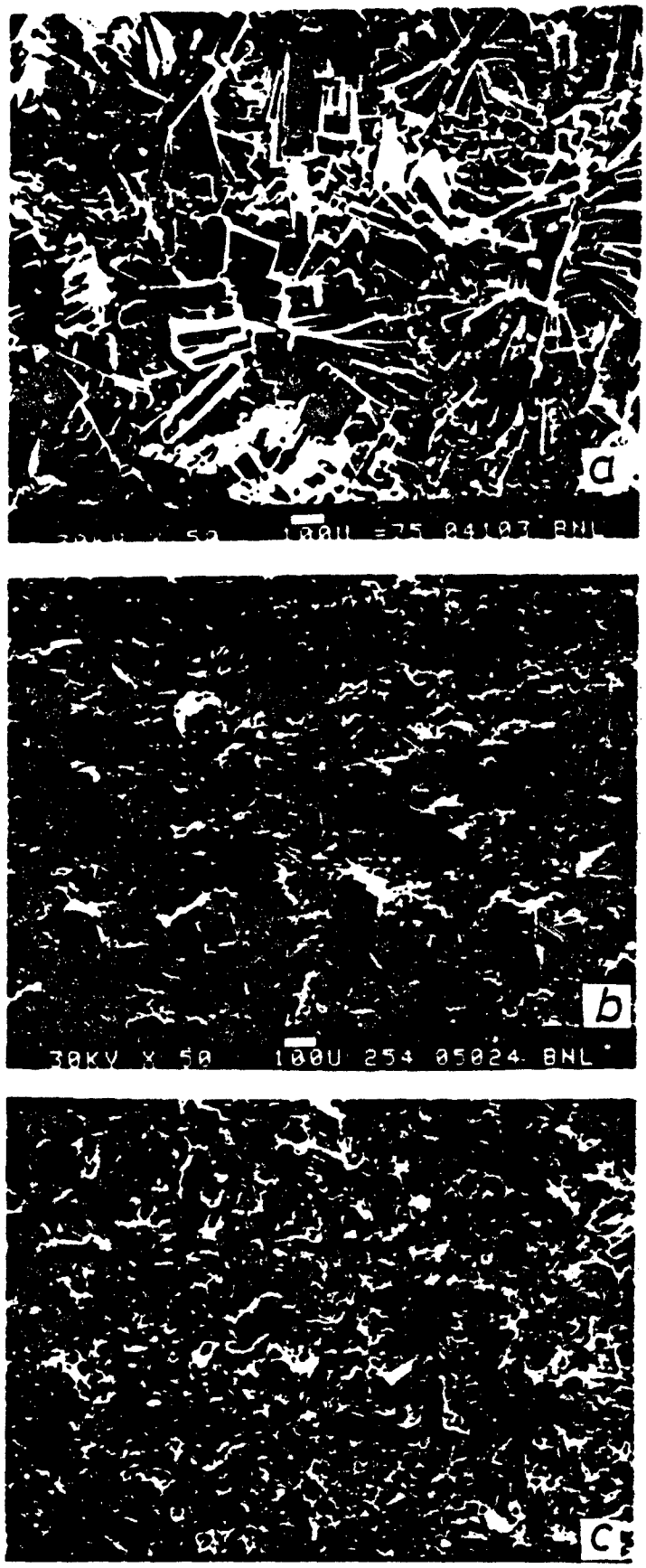

Figure 38. Photomicrographs of metal surfaces treated with conventional and PAA-modified phosphating liquids: 0% PAA (a), 0.5% PAA (b), and 2.0% PAA (c).

microstructure and microfissures of the crystal films, and the formation of chemical intermolecular attractions with the conversion Zn·Ph compounds. Detailed information regarding the latter will be discussed later in this paper. The thin PAA film formed on the crystals may also act to enhance the adherent properties of protective polymer topcoat systems because of the presence of functional carboxylic acid groups in the PAA molecular structure.

Since the PAA overlayers can be removed by rinsing with an organic solvent, considerable attention was given to the contrast between the surface topographical features of the conversion coatings after the PAA was removed. Metal surfaces used in the test series were treated with 0, 0.5, 1.0, and 3.0% PAA-modified phosphating liquids, and then washed with acetone to remove any PAA polymer, rinsed with water, and dried in a vacuum oven at 150°C. Resultant SEM photomicrographs are presented in Figure 39. Visual comparison of these micrographs, shows the dimensions of the deposited crystals to decrease with increasing quantities of PAA in the conventional phosphating liquid. The micrograph of the conventional surface treatment (see Figure 39-a) indicates a dense agglomeration of rectangular-like crystals ~420 μm in length. Short rectangular-shaped crystals, ~320 μm in length, are produced by the addition of 0.5% PAA (Figure 39-b). With 3.0% PAA, the crystal size is ~240 μm, ~43% smaller than the conventional crystal. Unfortunately, the reason for this is not evident. From the viewpoint of surface topographical features, examination further indicated that the uniformly configurated conventional Zn·Ph crystal is converted into randomly distributed fine crystals as the PAA concentration is increased. This may be due to the chemical transformations of the conventional crystals by polyelectrolyte macromolecules.

E. Chemical States of Surface and Subsurface

The energy-dispersive x-ray (EDX) spectrometer coupled with SEM has a high potential for the quantitative analysis of any selected elements which exist at solid composite material subsurfaces. Its application can greatly enhance the results as well as facilitate the interpretation of SEM studies. EDX spectra for conventional Zn·Ph and 3.0% PAA-modified

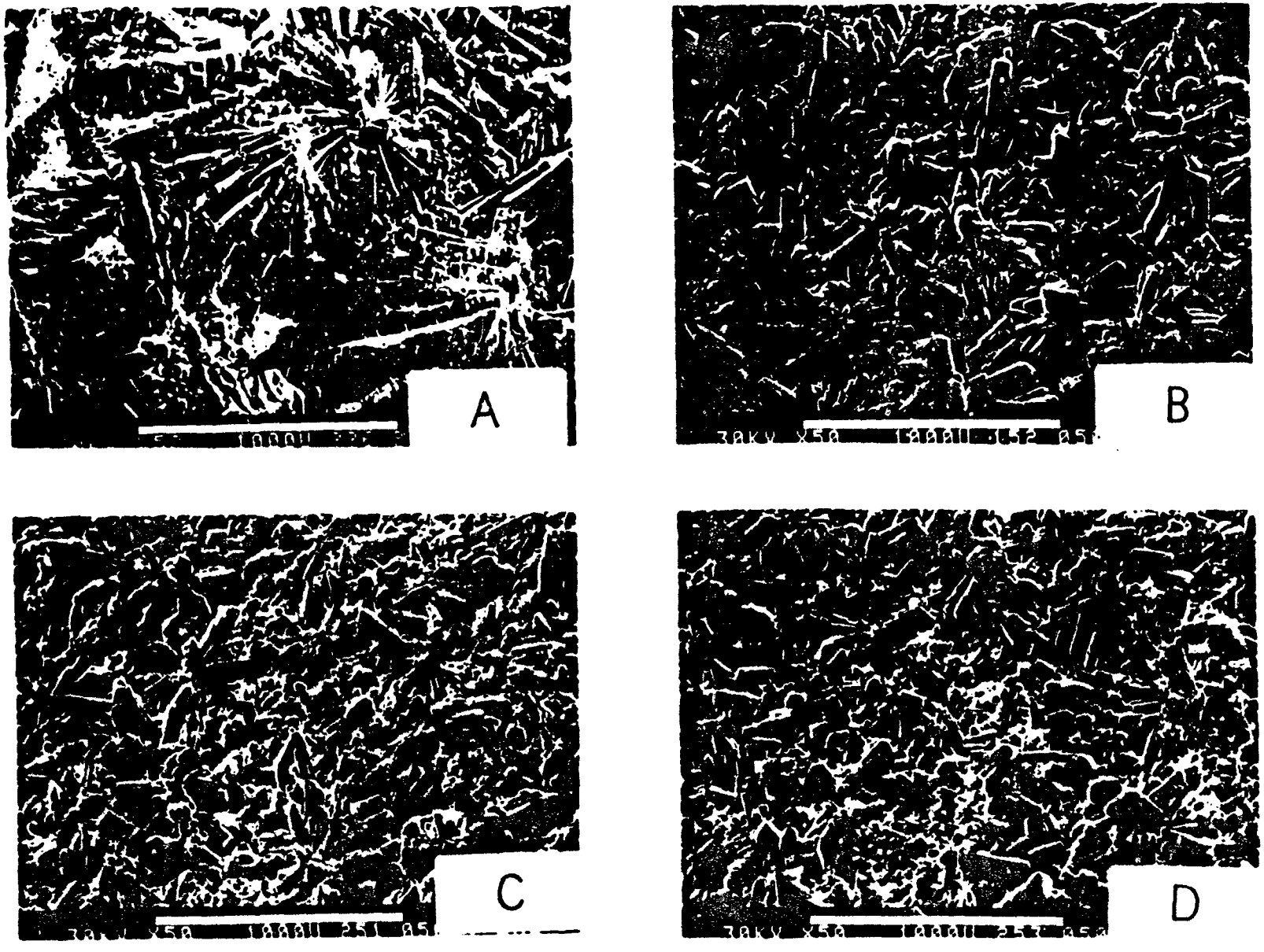

Figure 39. Alternation in the conventional crystal size by PAA polyelectrolyte macromolecules: 0% PAA (A), 0.5% PAA (B), 1.0% PAA (C), and 3.0% PAA (D).

Zn·Ph composite film surfaces are shown in Figure 40. The abscissa of the spectrum is the x-ray energy characteristic of the element present, and the intensity of a gross peak count is related directly to the amount of each element present. As seen in the figure, it appears from the two strong peak intensities that the predominant elements in either the single or the composite conversion coatings are Zn and P atoms. Comparison of count rates for the Zn and P peaks indicates that there is more Zn in the coating system than P. Detailed information regarding the Zn-to-P count ratio as a function of PAA concentration will be discussed later. The spectra also exhibited a weak peak of Fe, which is produced by the oxidation of metal surfaces. Since photo-excited EDX is useful for the elemental analysis of layers which are several micron thick, the Fe peak suggests that some Zn at distances up to several microns from the composite film surface is likely to be replaced by Fe.

Changes in the peak intensity of Fe by varying PAA concentrations are also of interest. In Figure 40-b it is apparent that the Fe peak frequency for the 3.0% PAA composite layer is much stronger than for the conventional phosphate coating. Although not illustrated in the figure, the Fe frequency was observed to grow with an increasing PAA concentration. This implies that the thinner crystal deposition layers produced by incorporating large amounts of PAA solution consist of hybrid compounds of zinc and ferrous phosphate hydrates.

The EDX studies were also focused on the variation in Zn and P peak intensities for composite subsurfaces before and after rinsing with acetone solvent. Figure 41 illustrates EDX survey spectra for unrinsed and the acetone-rinsed 4.0% PAA composite subsurfaces. The spectrum for the untreated composite layer (Figure 41-a) is characterized by the conspicuous frequency of Zn which is the dominant element in this system. In contrast, the spectrum for the subsurface composite disclosed by removing the PAA macromolecular overlayer from the crystal surfaces (Figure 41-b), exhibited a noticeable transmutation, namely, the intensity of the Zn peak became much weaker compared to that of P. Even when smaller concentrations of PAA were used to modify the conventional Zn·Ph layers, similar spectral features were recorded for the acetone-treated composite coating

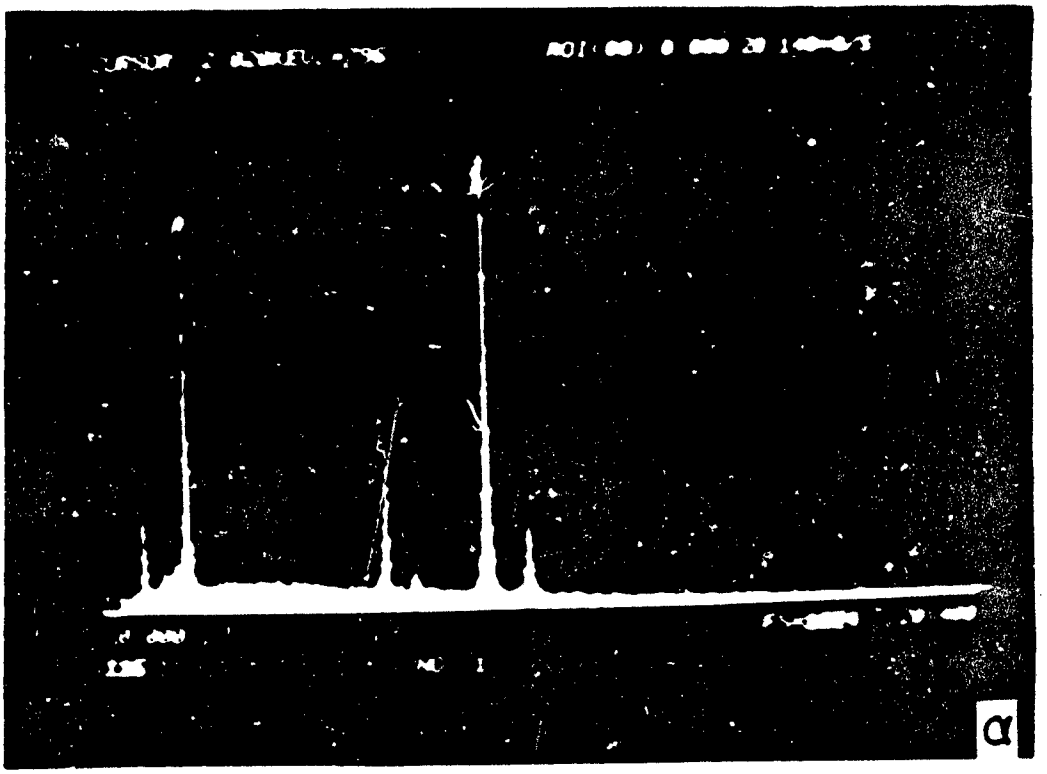

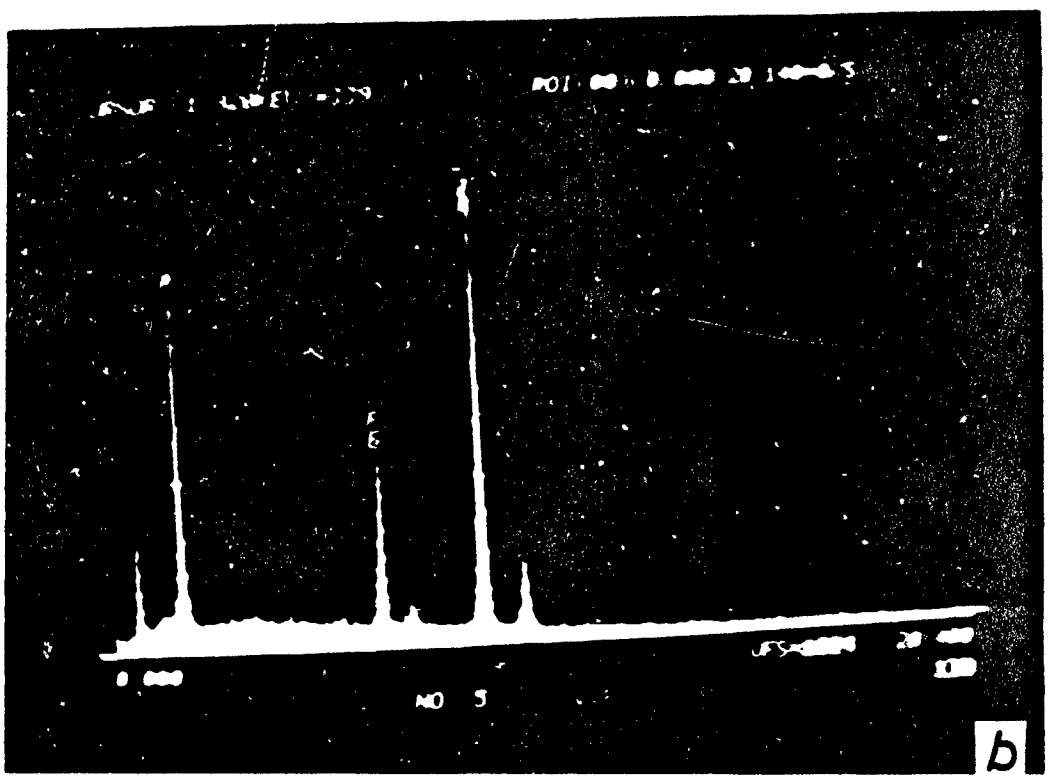

Figure 40. EDX analysis of unmodified (a), and 3.0% PAA-modified zinc phosphate (b), conversion coating surfaces.

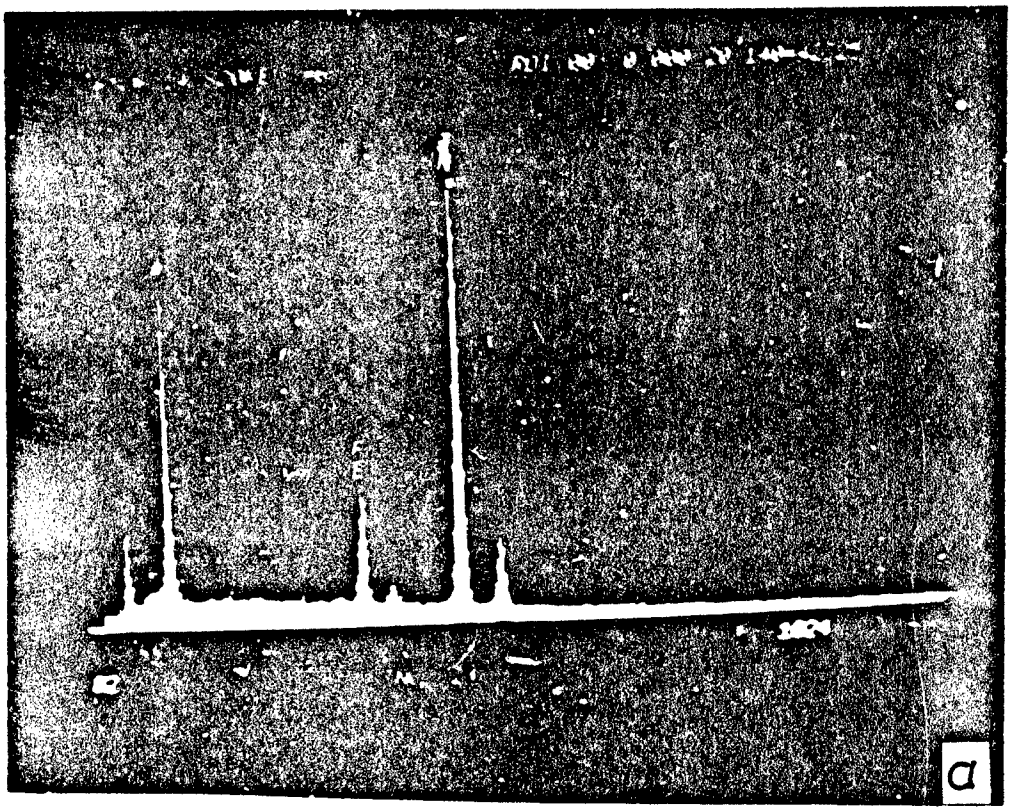

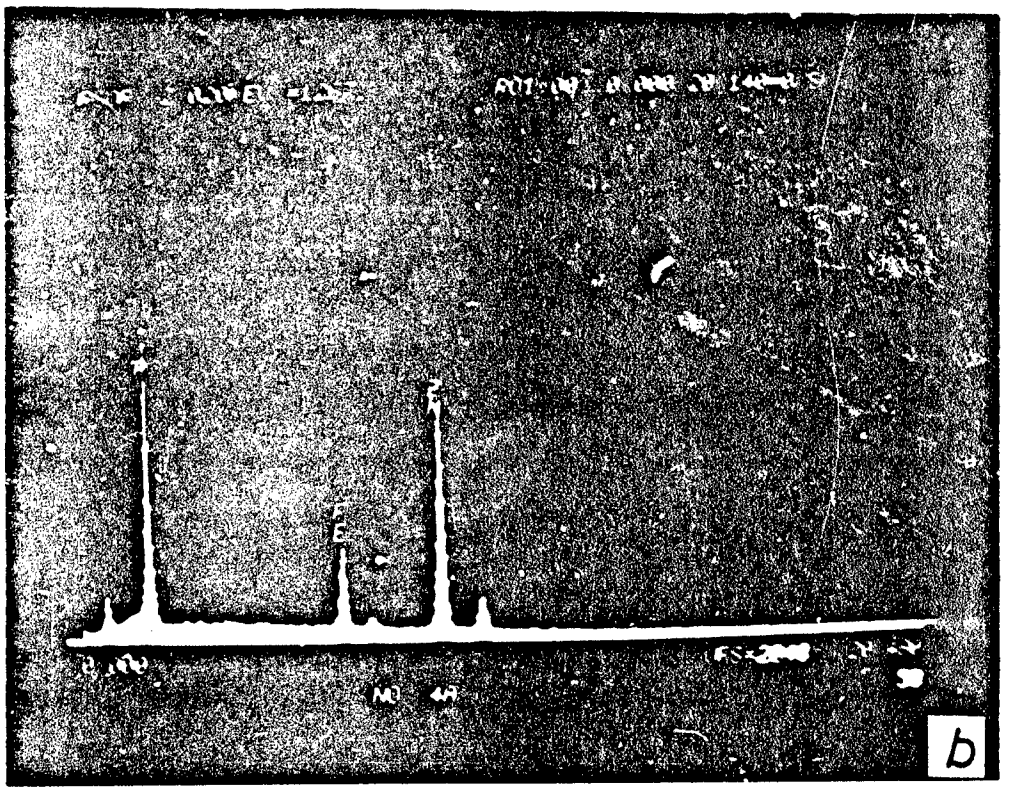

Figure 41. EDX spectra of untreated (a), and acetone-treated 4.0% PAA-modified zinc phosphate composite coating surfaces (b).

subsurfaces. This surprising result seems to demonstrate that a certain amount of Zn is transferred to the interfacial contact layers of PAA macromolecules from the outermost Zn·Ph surface site. Hence, it was concluded that the transitional Zn element existing in the Zn·Ph molecular structure results in strong interfacial intermolecular attraction with the functional groups of PAA polymers.

The degree of the chemical attraction between the PAA and the Zn element can be quantitatively analyzed by comparing the ratio of Zn to P atom peak counts for the acetone-treated composite surfaces. An aim in the acetone treatment for the composite surfaces was to remove not only the bulk PAA polymer overlaid on the crystal surfaces, but also the PAA-based reaction products formed at the interface. For comparison purposes, Zn to P count ratios for untreated surfaces were also computed. These analytical results are listed in Table 3. For the untreated composite layers, the data indicated that the Zn/P count ratio did not change very much with increased PAA concentration. Ratios ranged from 1.28 for the conventional zinc phosphate layers to 1.34 for 2.0% PAA-modified composite coating surfaces. In contrast, the Zn/P ratio values for the acetone-rinsed composite surfaces appear to be affected by the PAA content. As is evident from the table, the Zn/P ratios tend to decrease with an increase in PAA macromolecules. The value of 0.77 at 2.0% PAA is ~40% lower than that for samples without PAA. This correlation suggests that the polyelectrolyte macromolecules have a stronger chemical affinity for Zn than for P. Consequently, the Zn bound chemically to the PAA migrated as a result of the rinsing with acetone. From these observations, it can be speculated that when the polyacid is introduced into the zinc-phosphating liquid, an appreciable number of divalent Zn ions are preferentially taken up by the functional carboxylic acid (COOH) pendent groups in the PAA macromolecules which appear to act as a miniature ion-exchange system. The binding of the Zn ions may be essentially electrostatic in character, since ordinary equilibrium considerations cannot account for the binding quantitatively.[46] Hence, the reversible salt complex formation consisting of COO^- Zn^{2+} coordinated groups could be obtained by a charge transfer interaction between the carboxylate anions (COO^-) formed by the proton

TABLE 3

Ratio of Zn to P Atom EDX Gross Peak Counts for PAA-Zinc Phosphate Composite Films Before and After Rinsing With Acetone.

PAA, %	Zn/P Ratio	
	Untreated composite layers	After rinsing with acetone
0.0	1.28	1.28
o.5	1.39	0.87
1.0	1.30	0.81
2.0	1.34	0.77

donor characteristics of the COOH groups and the active neucleophilic Zn^{2+} ions dissociated from $Zn_3(PO_4)_2 \cdot 2H_2O$ in the phosphating solutions. The formation of the complex structure which involves intramolecular pairs of COO^- groups associated with Zn ions in the zinc phosphate depositing stages may play a key role in restraining the conversion crystal growth, resulting in the production of a finely crystalline Zn·Ph deposition.

Accordingly, considerable attention was given to understanding the nature of the interaction at PAA-Zn interfaces during the transformation from a solution state to a solid conversion film. Assuming that the formation of the interfacial bonding is a local phenomenon involving only a few atom layers of PAA and Zn, a highly sensitive analysis technique such as x-ray photoelectron spectroscopy (XPS) was considered as appropriate for obtaining reliable information regarding the chemical interfacial interactions. XPS can be used to identify the chemical states and to obtain quantitative elemental analyses of thin surface layers ranging from 5 to 50 Å. Identifications can be made from precise determination of binding energies, peak shapes, and other spectral features. Quantitative analyses are made from XPS peak heights or areas. In our approach to the interface, it was considered desirable to investigate the interface before the occurrence of mechanically or chemically induced failure. Therefore, the surfaces of compcsite layers containing the PAA overlayers were studied to determine the nature of chemical interactions. Three coating surfaces, conventional zinc phosphate and 1.0% and 2.0% PAA-modified Zn·Ph, were employed in this test series.

Resultant XPS spectra indicated only four elements--Zn, P, O, and C--to be present on the composite coating surfaces. On the basis of the binding energies (eV) of their XPS lines, the chemical states of Zn and P are assigned to the zinc and phosphorous compounds and carbon is attributed to the organic PAA polymers. Oxygen is present in both the inorganic compounds and PAA layers. The presence of Fe in the several-micron-thick crystal layer, which was clearly confirmed by EDX spectra, could not be identified on the XPS spectrum. This indicates that Fe atoms do not exist within 5 Å of the top surface of the composite coatings.

Figure 42 shows typical survey spectra of the zinc $2p_{1/2}$ and $2p_{3/2}$ core levels and illustrates differences in peak shape and peak intensity between unmodified and PAA-modified phosphate layers. The spectrum of the control surface is characterized by photoelectron peaks at two levels of adsorption in the binding energy ranges of 1048 to 1046 eV and 1024 to 1023 eV. It is of interest that these double peaks were shifted to single peaks by the incorporation of PAA. The spectra also show that the relative peak intensity tends to decrease with increasing PAA concentrations. In contrast, no significant changes in peak intensity and binding energy were observed from the phosphorus 2p core level spectra of the PAA-Zn·Ph system layers. This is shown in Figure 43. The phosphorus 2p peak shapes for 1.0% and 2.0% PAA-modified composite layers are quite similar to the peak shape of the control layer and have adsorption levels at ~135.5 and ~134.3 eV. These results clearly suggest that the functional PAA macromolecules are more strongly bound to the surface Zn atom rather than to an inert P atom. Figure 44 exhibits XPS signatures of oxygen 1S core levels. For the control layer, the peak at 532.9 eV assigns to the oxygen as P-O and Zn-O bonds. However, it is not yet clear whether it will be possible to distinguish the oxygen from either P-O or Zn-O. As is evident from the figure, the oxygen peaks associated with the presence of PAA are shifted slightly to higher in binding energies. The shifting peak was 0.8 eV higher than the control layer. This difference implies that the oxygen induced from the PAA-overlaid composite layers is related to that of COOH groups located in the pendent sites in the PAA molecular structure. For the O_{1s} peak for the PAA composite layers, the peak intensity at 2.0% PAA is fairly weak compared to that for 1.0% PAA. This seems to suggest that the presence of a large number of COOH groups leads to a stronger chemical affinity for the zinc atoms.

The chemical accessibility of the COOH groups to the Zn atom can be estimated from the shift in binding energy of carbon 1S at ~290 eV which ascribes to the polar C=O groups. To obtain this information, two different PAA-Zn·Ph composite layers were used. One was a PAA-modified phosphate crystal conversion film produced from a 0.5% PAA-zinc phosphating mix liquid; the other was a PAA-coated crystal layer formed by means of vacuum vapor deposition of the PAA solution on a preformed phosphate

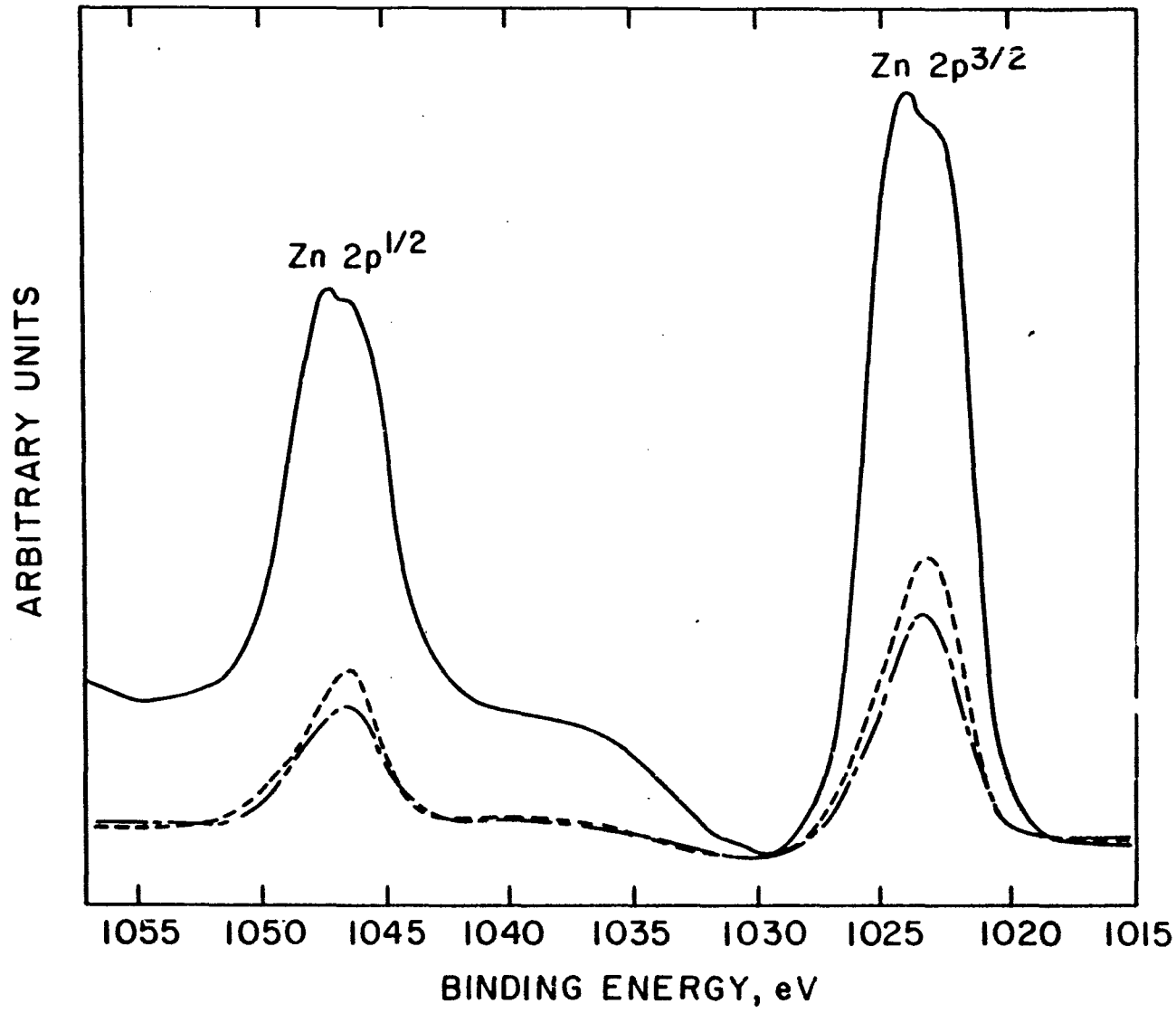

Figure 42. Photoelectron spectra of Zn $2p_{1/2}$ and $2p_{3/2}$ in unmodified and PAA-modified zinc phosphate layers; (——) 0% PAA, (----) 1.0% PAA, and (— — — —) 2.0% PAA.

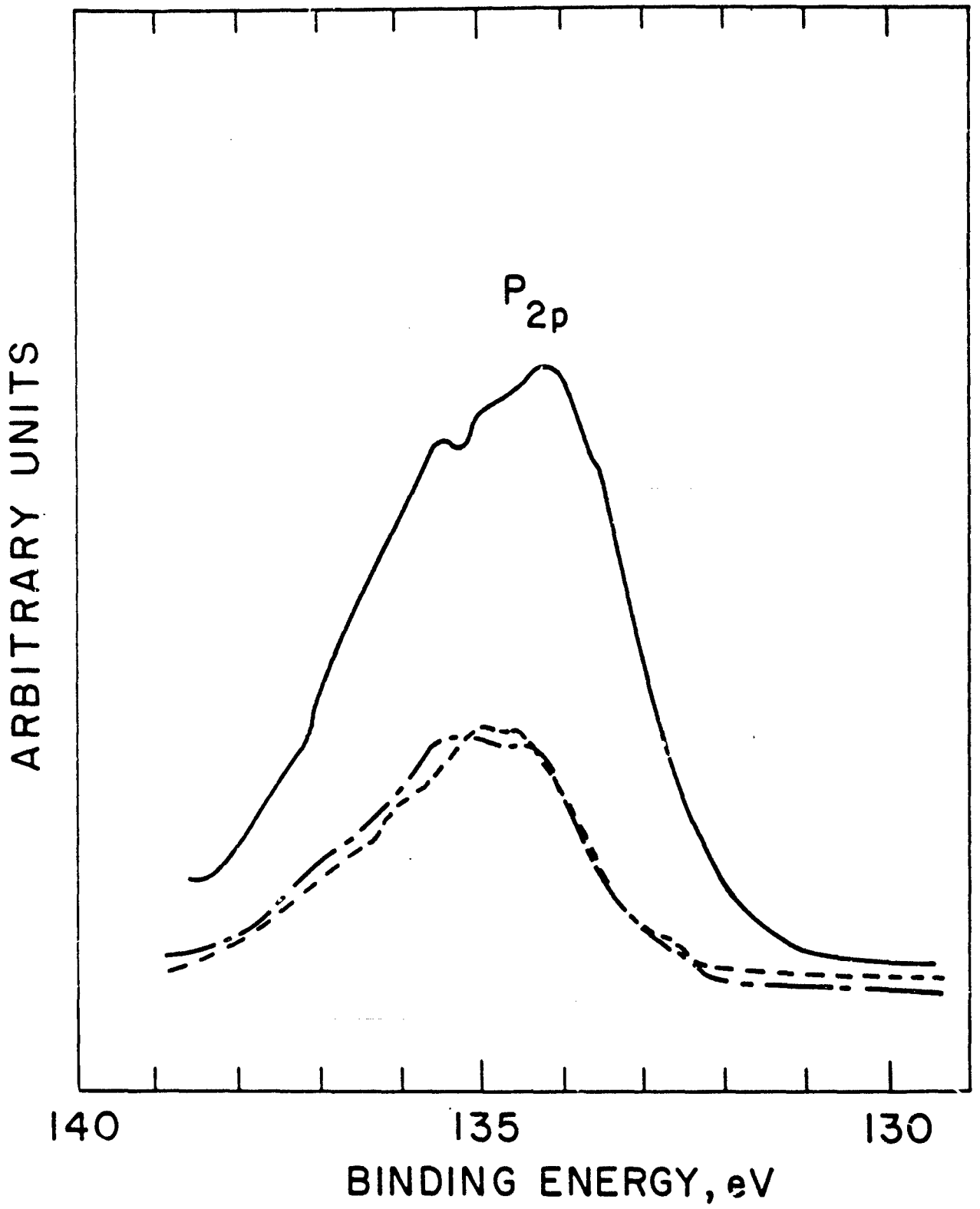

Figure 43. P_{2p} region of conversion coating surfaces; (____) 0% PAA, (----) 1.0% PAA, and (— – — –) 2.0% PAA.

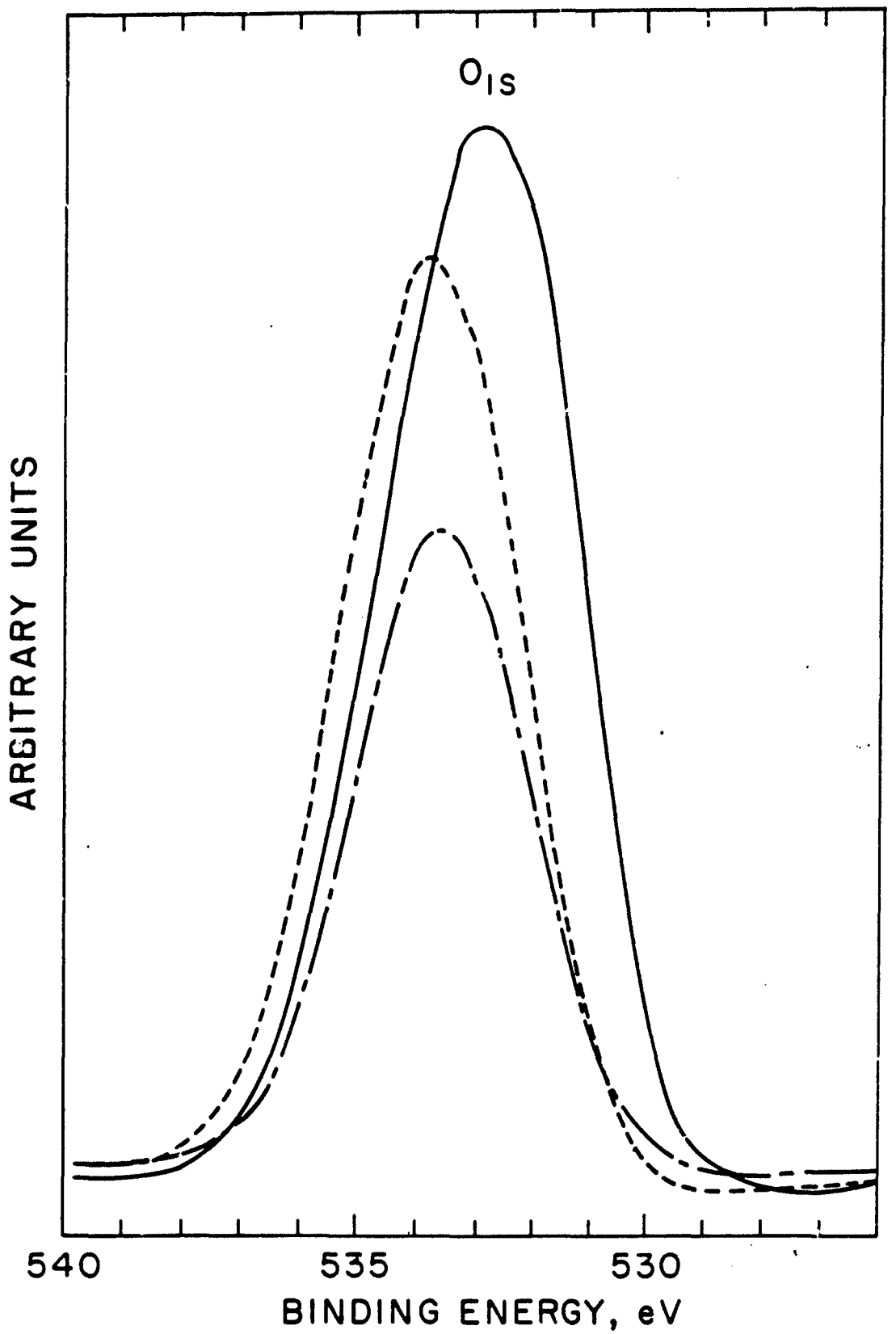

Figure 44. Oxygen photoelectron peaks of (____) control, (----) 1.0% PAA-, and (__ _ __ _) 2.0% PAA-modified zinc phosphate film surfaces.

crystal surface. The latter was prepared on the assumption that a strong chemical interaction at PAA-Zn atom interfaces would not occur. Two C_s spectra for these layers are illustrated in Figure 45. The spectrum for the PAA-coated layer exhibits a predominant peak at 284.9 eV and a minor peak at 289.8 eV. The former binding energy is associated with the characteristic alkane line contribution expressed in terms of the backbone carbon, and the latter reveals the C=O in the pendent COOH groups. When compared to the two peaks for the coated layer, conversion layer peaks are shifted significantly to a high binding energy. The difference between the binding energy values was 1.4 eV for the alkane line and 0.6 eV for the C=O. The figure also shows that the peak intensity of the alkane line for the conversion layer is approximately the same as for the coated layer. In contrast, it appears that the peak intensity of the C=O is considerably greater than for the coated layer. This change in peak shape and increase in binding energy is probably due to the strong accessibility of the functional side COOH groups to the metallic atoms. On the other hand, the strong increase in bonding energy of the alkane line for the conversion layer is likely to represent changes in conformation of the linear backbone chains which are assumed to be planar or zigzag.

From the results of the above EDX and XPS spectra analyses, it is speculated that the interfacial interaction between COOH and Zn which transforms the PAA-zinc phosphate solution into solid composite films is due to the following hypothetical mechanisms: the proton-donating functional COOH groups chemisorbed strongly with the Zn atom at the outermost surface sites of Zn·Ph crystal layers are converted into COO^- anions. These anions induce strong ionic interactions associated with charge transfer bonding mechanisms. Subsequently, the converted COO^- groups are transformed into unique bridge formations through a cross-linking reaction with Zn atoms. Hence, increased amounts of PAA will increase the degree of the cross-linking reaction. This also suggests that the chemical effect of the surface Zn atoms results in intermolecular bridging, which acts to connect the PAA macromolecular and the zinc phosphate layers. On the other hand, the newly formed CUO-Zn bond may act to break the original zinc-oxygen bond in the zinc phosphate molecular structure. In fact, as

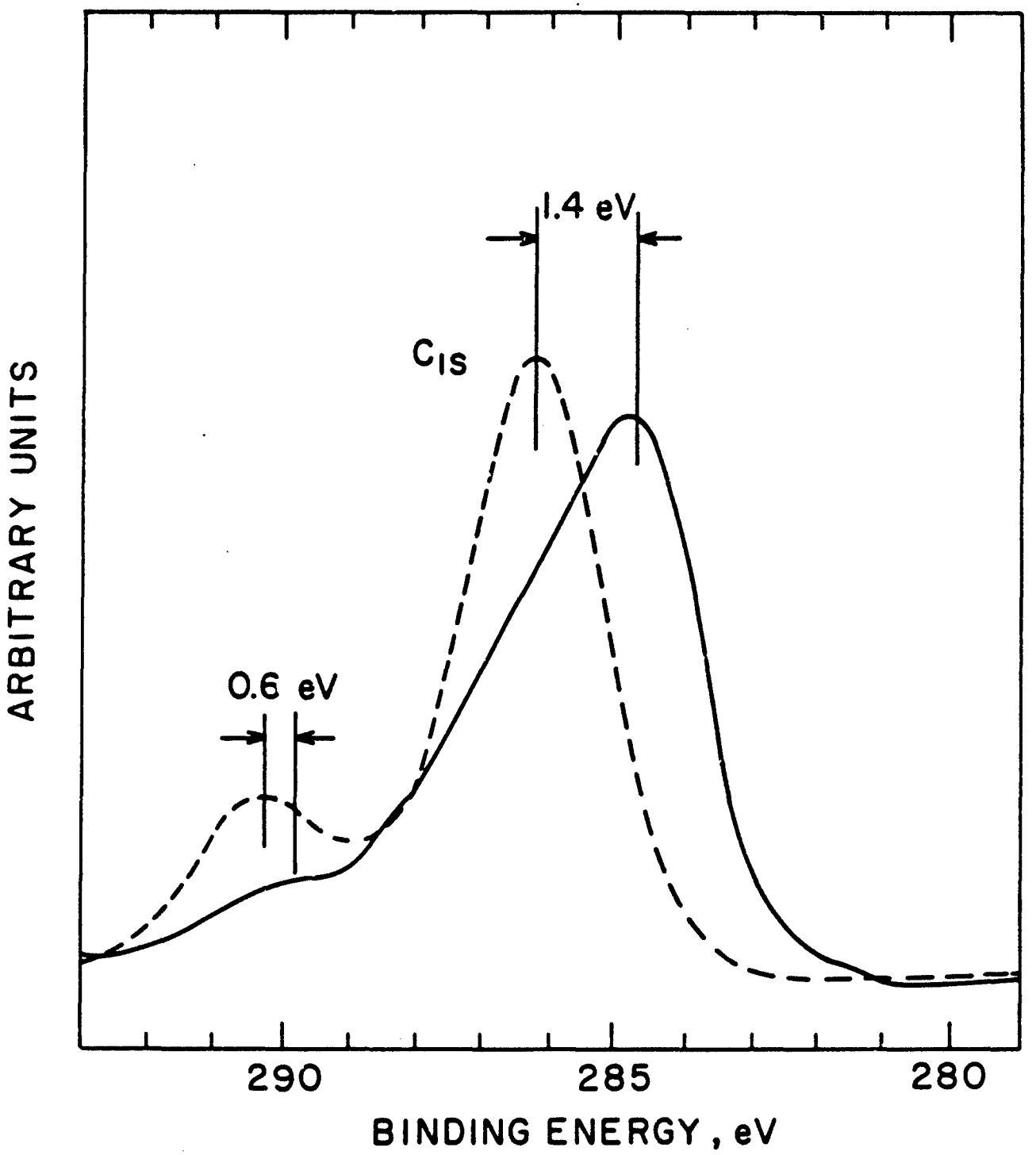

Figure 45. C_{1S} Spectra From (_____) PAA-Coated, and (------) PAA-Modified Zinc Phosphate layers

confirmed from the EDX spectra analysis, the removal of Zn-complexed PAA macromolecules by rinsing with acetone solvent apparently confirmed that the original Zn-O bonding force is much weaker than the COO-Zn bond. The tightly bound oxygen-phosphorus joint in the crystal molecules is likely to be unaffected by COO-Zn complex formations.

The reduction of Zn-O bonding forces caused by increasing PAA concentration was qualitatively interpreted using IR spectrometry. IR measurements were made on PAA-cross-linked Zn·Ph powder samples (size 0.04 mm) removed by scraping the substrate surface. The IR spectra for the samples prepared in the form of KBr discs were recorded in the range 1200 to 1000 cm^{-1}. The resultant IR spectra for all the Zn·Ph samples modified with up to 3.0% PAA were characterized by the presence of two conspicuous absorption bands. Table 4 presents the positions of the two bands obtained in this study. In the 0.5% PAA-Zn·Ph system, the first absorption band at 1110 cm^{-1} would seem to be due to the P=O double bond, and the second band at 1030 cm^{-1} is assigned to the stretching frequencies of $P-O^-$ groups.[47] As shown in Table 4, the positions of these two bands tend to shift to lower frequencies as the PAA content increases. It appears that the band shift is dependent on the PAA concentrations in the Zn·Ph hydrate. Even though the position of the Zn-O frequency is not detectable in the Zn·Ph compounds, it can be interpreted that such a pronounced shift of both the P=O and $P-O^-$ frequencies may be due to the reduction of the bonding energy between nonbridging oxygen ions and zinc ions in the P-O-Zn units. This implies that the extended PAA-Zn bonding force leads to a weaker Zn-O bond. However, the transformation mechanisms and conversion processes for PAA-cross-linked Zn·Ph layers from its solution state to a solid film are not evident from these limited data.

Attempts to identify the crystalline conversion products of the PAA-zinc phosphate systems were made using x-ray powder diffraction (XRD) and differential scanning calorimetry (DSC). Both are reliable methods for detecting the constitution and alteration of deposition surface layers. XRD using Cu Kα radiation at 50 kV and 16 mA and DSC at a heating rate of 10°C/min in N_2 gas were conducted on unmodified and 1.0% PAA-modified Zn·Ph powders.

TABLE 4

Variation in Infrared Absorption Band Positions For Zinc Phosphate Compounds as a Function of PAA Content.

PAA, %	Infrared absorption band positions (cm^{-1})	
	P=O groups	$P-O^-$ groups
0.5	1110	1030
1.0	1100	1025
2.0	1090	1020
3.0	1080	1010

XRD tracings recorded in the diffraction range 4.67 to 2.49 Å for powdered samples are given in Figure 46. For the control samples, the strong lines at 4.51 and 2.83 Å, the medium intensities at 3.44 and 3.36 Å, and the weak diffractions at 3.99, 2.62, and 2.59 Å are near ly identical to the XRD pattern for zinc orthophosphate hydrate [$Zn_3(PO_4)_2 \cdot 4H_2O$]. Although the pattern shows other weaker lines which might represent some unidentified phosphate compounds, the major phase of crystalline conversion products yielded from the conventional zinc phosphating treatment is believed to be hopeite. In contrast, XRD patterns for the 1.0% PAA composite layer revealed quite different spacings, compared with those of the control. This suggests that the PAA leads to the transformation of the hopeite into the Zn·Ph compound phases having different chemical constituents and structures. The pattern in the limited diffraction regions seems to demonstrate that the transformed deposition layers consist of a hybrid phase of the ternary Zn·Ph-based hydration compounds. One of these compounds was identified as tertiary zinc orthophosphate dihydrate, $Zn_3(PO_4)_2 \cdot 2H_2O$, represented by the broad spacings at 3.17 and 2.91 Å and the small diffraction effects at 3.01, 2.61, and 2.50 Å. The presence of other unknown products is evident from the medium lines at 4.18 and 3.91 Å. However, a speculative mechanism for the transformation into the dihydrate-based Zn·Ph layers by the PAA is not clear at present. The role of Zn-complexed PAA macromolecules in transforming the conventional zinc phosphate molecular structures remains a subject for speculation and further research is required.

In support of the XRD data, typical DSC thermograms recorded as a function of temperature during the thermal decomposition of these samples are illustrated in Figure 47. The thermal measurements were performed in the temperature range 50° to 400°C. The thermogram for the control samples shows endothermic peaks at 80°, 175°, 225°, and 235°C. The very slight endothermic peak at 80°C indicates a loss of moisture adsorbed on the sample surfaces. The prominent peak at 225°C, with an onset

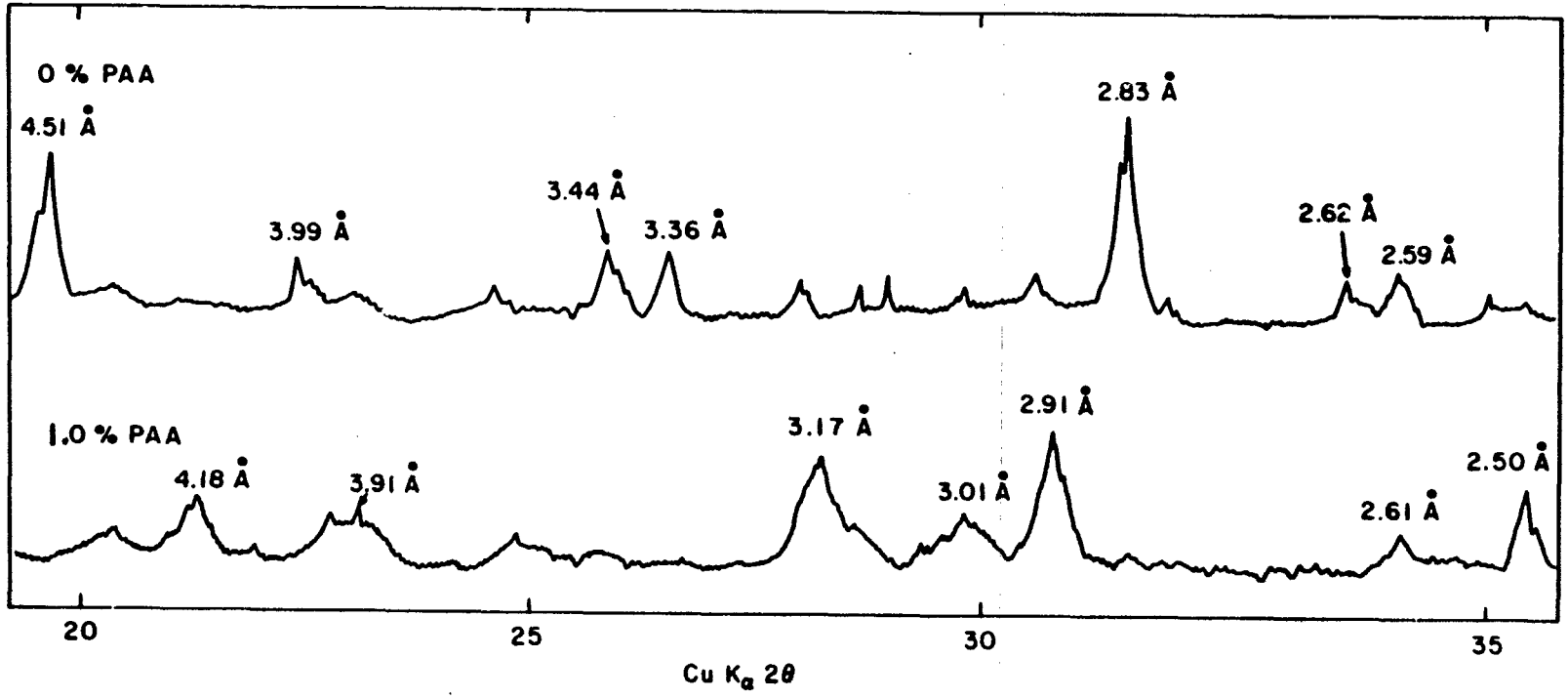

Figure 46. Powder x-ray diffraction patterns of unmodified and 1.0% PAA-modified zinc phosphate crystal layers.

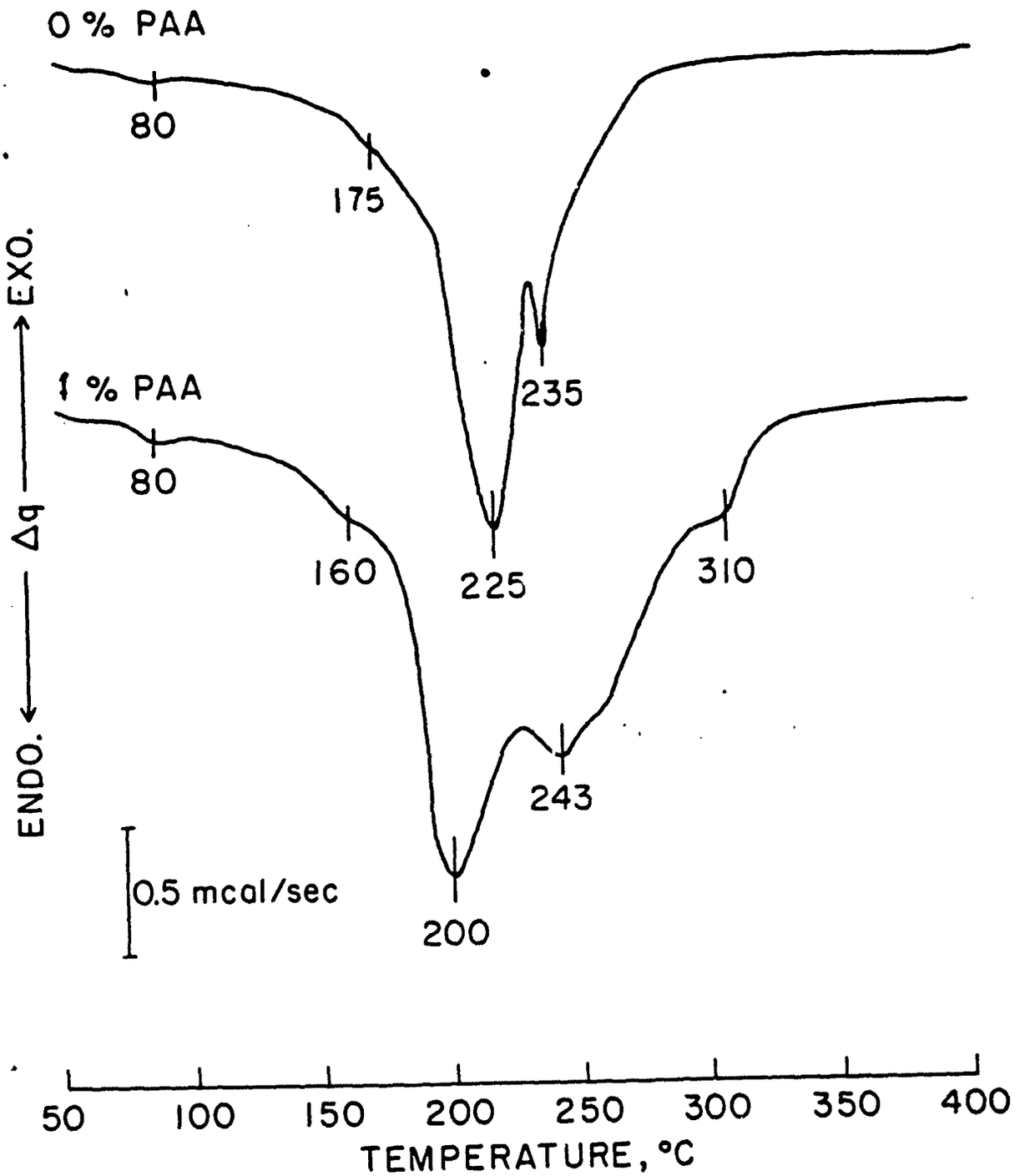

Figure 47. Typical DSC thermograms for the control and 1.0% PAA-modified zinc phosphate hydrate crystals.

temperature of decomposition at ~175°C, is associated with the dehydration of the crystallized and coordinated water removed from the samples. The dehydration can also be recognized from an extreme reduction in the absorption intensity at 1630 cm^{-1} frequency on the IR spectrum for samples heated to 225°C. The peak at 235°C may mean the approach to the end of the transition from the hydrated to the unhydrated zinc orthophosphate. On the other hand, the endothermal curve for PAA-complexed Zn·Ph layers indicates that the major thermal decomposition of the samples begins at ~160°C and the rate of decomposition rises to a maximum. This is followed by increasing decomposition heat which reaches a main peak at 200°C and subsequently leads to the generation of a new endothermal peak at 310°C. The latter may represent the temperature approaching the end of the transition phase. The temperature at this major peak corresponds to a 25°C reduction in the decomposition temperature, compared with that of the control. This shift is likely to be associated with a low degree of crystallinity of the Zn·Ph hydrate formed by the complex reaction with PAA. The conventional zinc layer is highly crystalline which results in a brittle nonflexible material. The lower crystallinity of the PAA-modified films makes them more flexible. This is discussed in the next section. Consequently, the results from the XRD and DSC studies suggest that the addition of PAA to the conventional layers results in the assembly of hybrid Zn·Ph crystalline phases consisting of constituents and a chemical structure different from those of the conventional film. Furthermore, the functional polyacid macromolecular acts to reduce the degree of crystallinity of the Zn·Ph hydrate deposited on the metal substrate surfaces and also leads to the production of finely crystallized coating layers.

F. Elastic Behavior

The ductility and toughness properties of the crystalline conversion film itself are of considerable importance when the physical deformation characteristics of the metal substrates are considered. For instance, increased thickness of the deposition film layers makes the film increasingly brittle, thereby enhancing the potential for failure during flexure or

other deformation. Generally, deformation failures of the layers having a low stiffness characteristic relate directly to the development of micropores and fissures which reduce the effectiveness of corrosion-resistant coatings.

Figure 48 is a typical stress-strain diagram for control and 2% PAA-complexed Zu·Ph layers deposited on metal surfaces. The stress was computed assuming elastic behavior of the flexural member, and the strains were computed from the deflection measurements.

In the figure, the elastic region is the straight-line portion of the stress-strain curve from zero strain to the strain at point A. The elastic behavior implies the absence of any permanent deformation, so that point A is termed the proportional limit of the material. The slope of the line from the origin to A is the elastic modulus E. Physically, E represents the stiffness of the material to an imposed load. The resultant flexural modulus for PAA-complexed layers was computed to be 9.53×10^6 psi (6.57×10^4 MPa), corresponding to a value more than twice that of the control specimens. This suggests that the stiffness of conventional crystal layers can be improved significantly by the incorporation of PAA.

The stress associated with the yield point of a layer is represented by the position of the line ab in Figure 48. The flexural stress at the yield point for the control was increased by a factor of 1.7 by adding a 2% concentration of PAA. In addition, the stress of the complexed layer during yielding increased somewhat with an extended strain, and an ultimate stress of 33.6×10^3 psi (232 MPa) was obtained at 1.08% strain. Further increases in strain resulted in stress reduction. In contrast, the control exhibited no increase in stress after the onset of yielding deformation was noted. The deformation takes place at an essentially constant stress of 19.2×10^3 psi (132 MPa) until the stress reduction occurs around 0.75% strain.

The magnitude of the relative toughness of the materials can be obtained from the stress-strain curves by drawing perpendicular lines from the ends of the curves to the strain coordinates and then measuring the

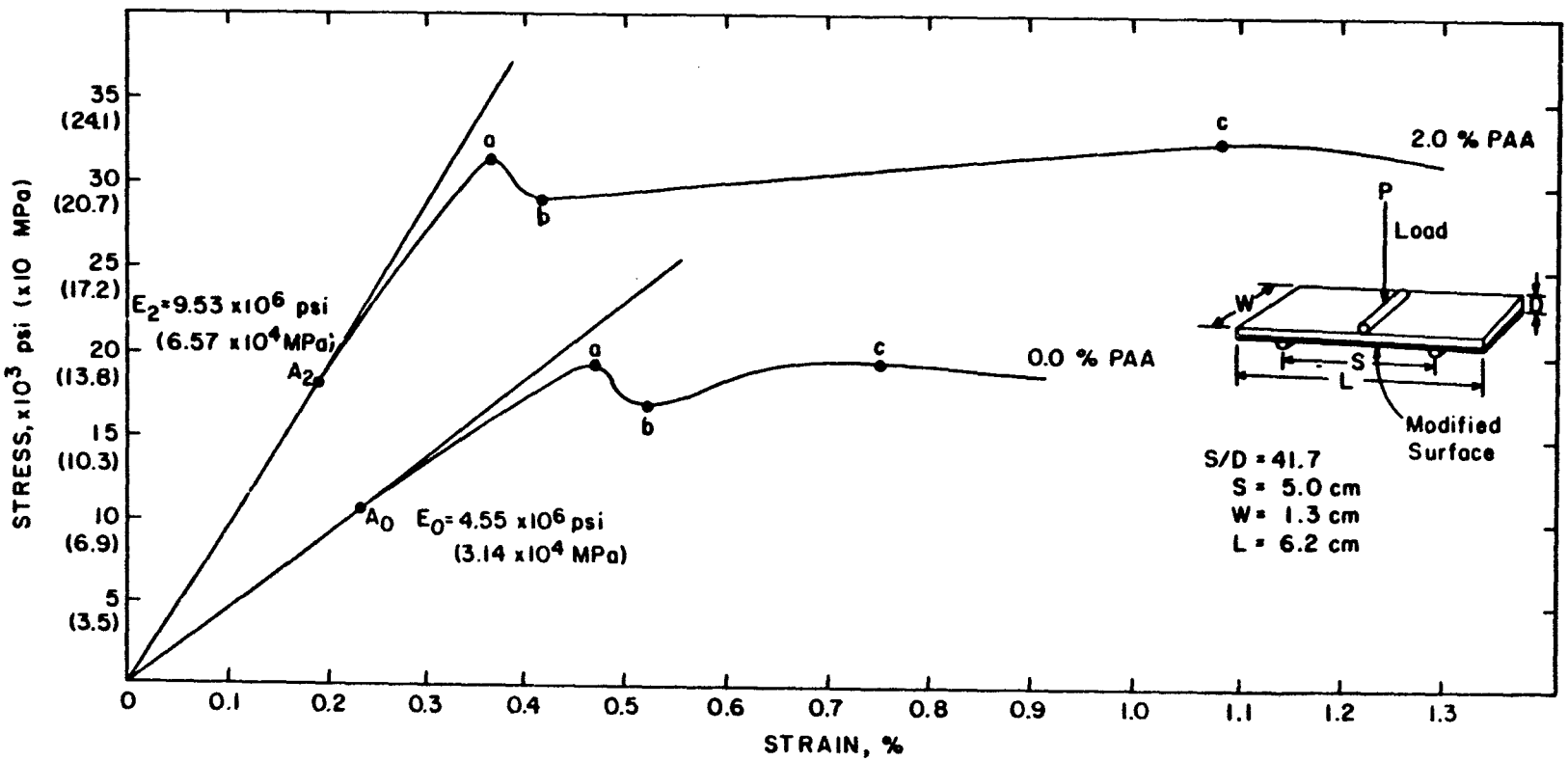

Figure 48. Flexural stress-strain relations for unmodified and 2% PAA-modified zinc phosphate crystal conversion coatings.

total area under the curves. The area for the complex specimens was considerably greater than that for the control specimens. This apparently verifies that the deformation nature of the conventional crystal deposition can be made more ductile by the formation of a complex structure with PAA macromolecules.

Figure 49 shows the flexural modulus plotted against PAA concentration. The curve indicates that in the PAA concentration range from 0.4 to 3.0%, the modulus increases progressively. The maximum flexural modulus of 99.0×10^5 psi (68.2×10^3) was obtained at a 3.0% concentration, which is an improvement of more than a factor of 2 over specimens without PAA. Further PAA additions result in modulus reductions. Similar trends were observed from the results of stress at the yield points of these specimens. A yield stress of 18.1×10^3 psi (125 MPa) for the control specimens was increased by a factor of 1.7 by the modification with 3.0% PAA.

On the other hand, changes in thickness and fineness parameters of the deposited complex crystals appear to have a direct effect on the stiffness and toughness of the crystalline layers. Therefore, changes in these parameters resulting from variations in the PAA concentration over the range of 0 to 4.0% were assessed from SEM images. Factors which appeared to affect the mechanical properties of the crystals were then correlated with flexural modulus values for the coatings.

The variation in flexural modulus as a function of the average thickness of the crystal is given in Table 5. It is apparent that the modulus value increases markedly with a decrease in the crystal thickness, ranging from 120 to 52 μm. Further decreases in thickness are likely to result in reductions in the modulus. The maximum modulus was obtained with an ~50 μm thick layer, which is representative of the most suitable crystal thickness value.

Since the PAA overlayers can be removed with an organic solvent rinse, considerable attention was given to the contrast between the relative crystal fineness of the conversion coatings under the PAA. Metal surfaces used in this test series were treated with 0, 0.5, 2.0, and 4.0%

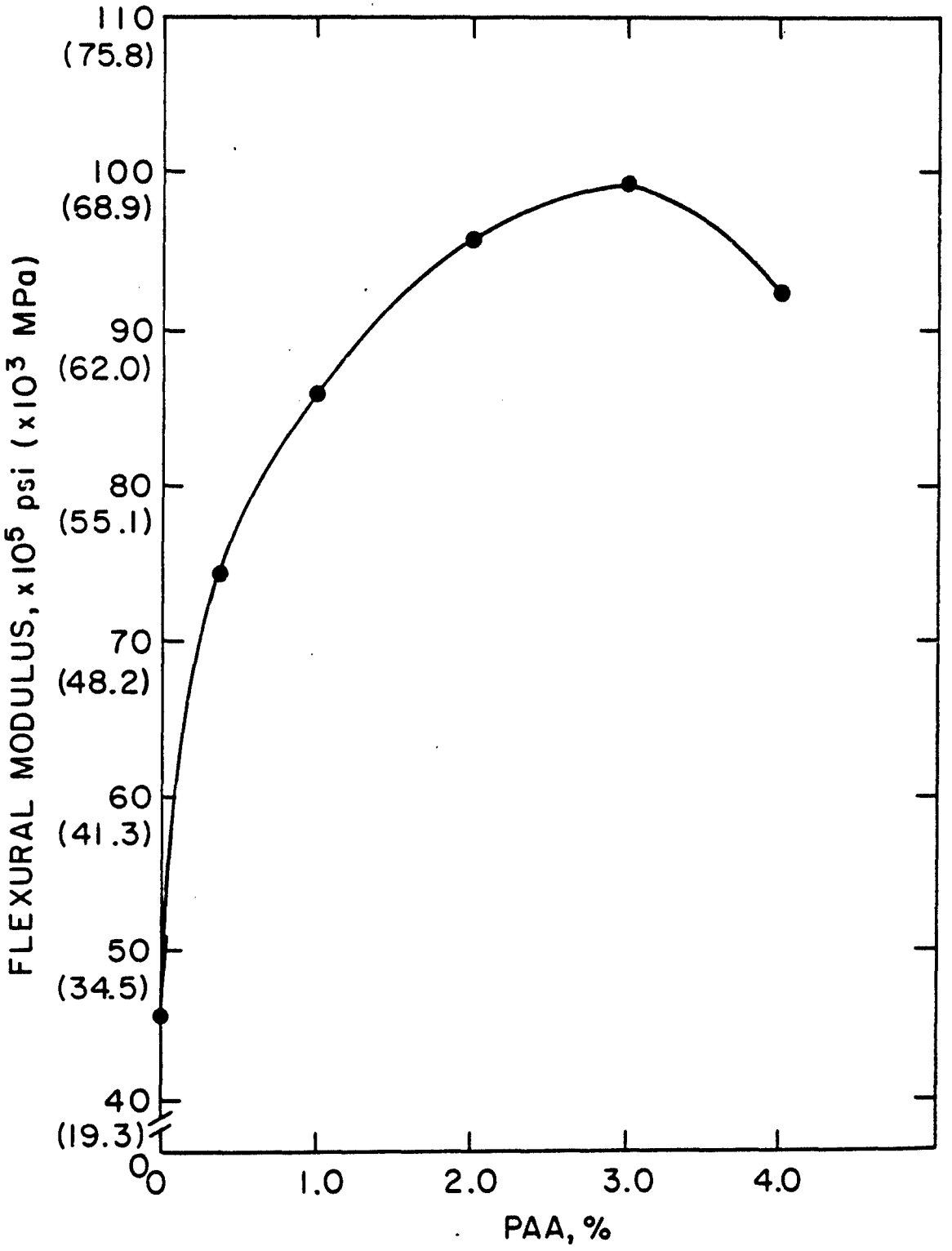

Figure 49. Changes in flexural modulus of conversion layer as a function of PAA concentration.

TABLE 5

Relation Between Crystal Thickness and Flexural Modulus

PAA, ——	Average thickness, μm	Flexural modulus, x 10^5 psi (x 10^3 MPa)
0.0	120	46.2 (31.8)
0.4	82	73.8 (50.9)
1.0	70	86.5 (59.6)
2.0	63	95.3 (65.7)
3.0	52	99.0 (68.2)
4.0	35	92.1 (63.5)

PAA-modified phosphating liquids, and then washed with acetone to remove any PAA polymer. The plates were then rinsed with water and dried in a vacuum oven at 150°C. The changes in crystal size as a function of PAA concentration were observed using SEM. Visual comparison of these micrographs confirms that the dimensions of the deposited crystals decrease as the quantity of PAA in the conventional phosphating liquid is increased. The micrograph for the surface treated conventionally indicated a dense agglomeration of rectangle-like crystals ~420 μm in length. This crystal length was reduced by half by the addition of 2.0% PAA. With 4.0% PAA, the conversion formation consisted of short rectangularly shaped coarse crystals ranging in size from ~180 to ~20 μm.

From the viewpoint of surface topographical features, the SEM images indicated that the uniformly distributed conventional Zn·Ph crystal is converted into randomly distributed fine crystals as the PAA concentration is increased. Thus, the dense arrangement of very fine crystals formed irregularly on the substrate surfaces resulted in a modulus somewhat lower than that for layers having a desirable crystal size. The most effective crystal length to achieve the high modulus was consequently noted to be in the range of ~200 to 60 μm. The optimum crystal formation, therefore, appears to be a highly dense agglomeration of complex crystals ~50 μm thick and ~60 to 200 μm in length.

The increase in the stiffness of the layers is not only due to the thickness, fineness, and density of the plasticized conversion formations, but also is associated with the average molecular weight of the PAA. The effect of the PAA molecular weight (M.W.) on the flexural modulus of the precoat layers was investigated over a M.W. range of 5×10^2 to 2.5×10^5. In these studies, the complex precoats were derived from a mix solution prepared by incorporating a 3% concentration of the various PAA polymers into the conventional zinc phosphating solution. Figure 50 shows the correlation between the flexural modulus and the molecular weight of the PAA. The curve indicates that the modulus related directly to the molecular weight. The use of PAA with a molecular weight of 2.4×10^5 resulted in the formation of crystal layers having a modulus 1.6 times greater

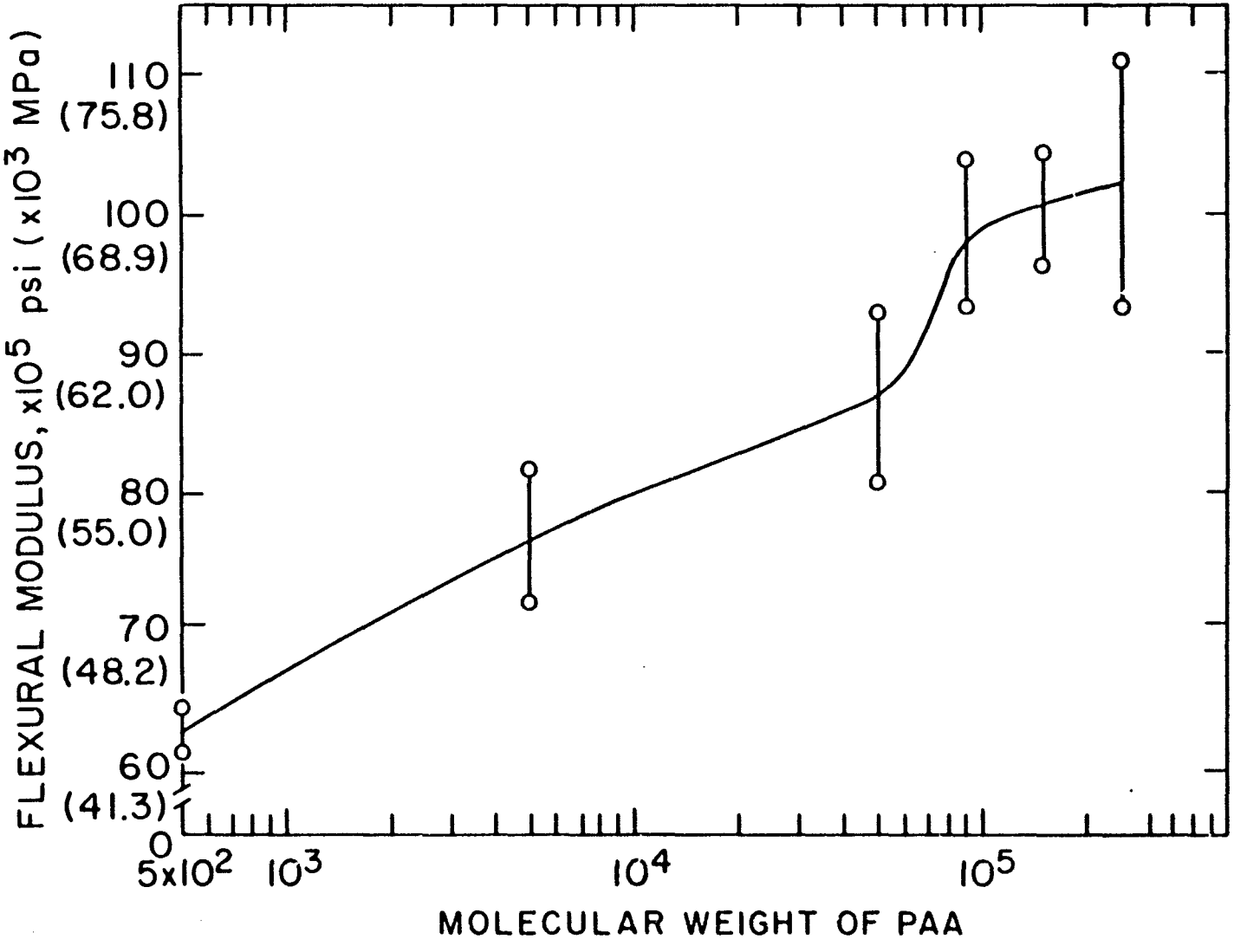

Figure 50. Effect of molecular weight of PAA on the flexural modulus of conversion crystal layers.

than that of the layers produced with PAA of M.W. 5 x 10^2. The layers derived from acrylic acid monomer exhibited a modulus of 58.3 x 10^5 psi (40.2 x 10^3 MPa), ~7% lower than that from M.W. 5 x 10^2. These results suggest that the M.W. of the PAA polymer plays an important role in increasing the stiffness of the complex conversion layers. This increase in stiffness also increases the ductility.

G. Adhesion at Topcoat/Precoat Interface

Necessary properties for the complex conversion films are chemically and physically attractive surfaces which promote adhesion to organic polymer topcoatings, and the ability to form corrosion-resistant protective coatings on metal substrate surfaces. With regard to the former, the presence of the functional PAA polymer on the complex precoating surface results in a film which acts in a manner similar to a primer for conventional polymer topcoats. This primer formation displays an ability to promote bonding forces at the interfaces between the complex precoating and the polymer topcoating materials. The interfacial adhesive mechanism was inferred to be due primarily to polymer - polymer chemical affinity. Hence, it can be expected that the elastic behavior of the precoating sites in the chemically bonded interfacial region depends primarily on the mechanical and adhesive characteristics of the organic materials employed as the topcoating system. These properties include the modulus of elasticity, tensile strength, and elongation for the polymer topcoat materials and the bond strength at the topcoat-precoat interface.

A study was conducted to understand the interplay between the topcoat and precoat in improving the stiffness and ductility of the crystal conversion layers. The two different topcoating systems described in the Materials Section, polyurethane (PU) classified as an elastomeric polymer, and furan (FR), a glossy polymer, were used in the study. Some mechanical properties of these polymers are given in Table 6. As is indicated in the table, the modulus of elasticity for the FR polymer was 2.28 x 10^5 psi (1.57 x 10^3 MPa), greater by an order of magnitude than that of the PU

TABLE 6

Mechanical Properties of Glassy Furan and Elastomeric Polyurethane Polymers Used as Topcoating Systems

Topcoating	Modulus of elasticity, psi (MPa)	Tensile strength, psi (MPa)	Elongation, %
furan	2.28×10^5 (1.57×10^3)	1820 (12.5)	1
polyurethane	1.47×10^4 (1.01×10^2)	3390 (23.4)	1040

polymer. The tensile strength and elongation values for the elastomeric PU are considerably higher than those of the glassy FR polymer. The extremely high elongation of 1040% for the PU is three orders of magnitude greater than that for the FR polymer (1%).

The adhesive characteristics for the elastomeric PU topcoat to the precoat surfaces were evaluated on the basis of 180° - peel strength tests. The test specimens used to determine the bonding force at the PU-precoat interface were prepared by overlaying an initiated PU polymer onto the metal substrate surfaces that had been modified with the zinc phosphating solutions containing up to 4% PAA polymer (M.W. 104,000). Overlaid specimens were then left in a vacuum oven at 80°C for ~10 hr to cure the PU polymer. The 180° - peel strength tests were performed at room temperature and the results presented in Table 7, indicate that over the PAA concentration range of 0 to 3%, the peel strength increases progressively with increasing PAA content. In the absence of PAA, the bond strength was 3.88 lb/in. (0.70 kg/cm). The addition of 3% PAA increased the value by a factor of 2.6. Further increases in concentration up to 4.0% resulted in a strength reduction.

The failure surfaces generated by peeling were microscopically inspected to obtain information regarding the failure mode and failure locus. These observations indicated that although the PU topcoat for the control specimens without PAA delaminated from the rough crystal surfaces, the failure was clearly cohesive since a considerable amount of the PU polymer remained on the precoat surfaces. This was probably due to the strong mechanical interlocking produced by anchoring of the topcoat as a result of PU resin penetration into the open spaces in the interlocked crystal layers. After testing, all of the PU-overlaid complex precoat specimens, except for the one containing 4.0% PAA, exhibited very rough surfaces on both the peeled PU and precoat sides. This led to extensive plastic deformation and fibrillation which represent cohesive failure in the ductile topcoat. This cohesive failure can be interpreted as a well-made joint. It is apparent that the highly stable nature of the interphase region is due to direct chemical bonding between the PU and PAA.

TABLE 7

180°-Peel Strength of Polyurethane Complex Crystal Coating Interfaces and Lap Shear Bond Strength of Complex Substrate-to-Furan Adhesives

PAA, %	Peel strength, lb/in. (kg/cm)	Lap-shear bond strength, psi (MPa)
0	3.88 (0.70)	640 (4.41)
1.0	5.63 (1.01)	920 (6.34)
2.0	9.41 (1.68)	1160 (7.99)
3.0	10.25 (1.84)	1130 (7.79)
4.0	8.41 (1.51)	950 (6.55)

Inspection of the peeled surfaces of the specimens containing 4.0% PAA indicated that they were much smoother than the surfaces of the other specimens and the extent of plastic deformation was much less. This implies that the failure may have been through a mixed mode of cohesive and adhesive failure.

In addition to being affected by the reactive surface nature of the PAA-complexed precoat layer, the peel strength at the interface was also found to be dependent upon the average molecular weight (M.W.) of the PAA polymer used to restrain crystal growth. Figure 51 illustrates the variation in peel strength of PU/precoat interfaces resulting from changes in M.W. up to 5×10^5. A PAA macromolecule concentration of 3% was used to prepare the conversion precoating systems in this test series. The data indicate that the interfacial bonding forces increase notably with increasing M.W. over the range of 1×10^3 to 1.5×10^5. The maximum strength of 10.45 lb/in. (1.87 kg/cm) was attained with a M.W. of 1.5×10^5. Further increases in M.W. up to 5×10^5 seemed to have little effect on the bond strength. Although the results are not shown in the figure, the precoat surfaces derived from PAA monomer yielded a peel strength of only 3.71 lb/in. (0.66 kg/cm). A speculative explanation for the effects of M.W. on peel strength is as follows: when the polyacid macromolecule is introduced into the zinc phosphating liquid system, an appreciable number of divalent Zn ions dissociated from $Zn_3(PO_4)_2 \cdot 2H_2O$ are preferentially taken up by the functional carboxylic acid (COOH) pendent groups in the PAA molecular structure which appear to act as a miniature ion-exchange system. A salt complex formation consisting of COO^-Zn^{2+} coordinated groups could be yielded as a result of the charge-transfer characteristics of the COOH groups and the active nucleophilic Zn^{2+} ions.[49] Thus, the formation of the complex structure, which involves intramolecular pairs of COO^- groups associated with Zn ions, would result in the intermolecular entanglement and coiling of the PAA macromolecules. The extent of the entanglement is commonly associated with an increase in the degree of neutralization. The loss of functional groups at available absorption sites for the highly neutralized PAA polymers leads to a decrease in the magnitude of the dispersion and wettability forces on the complex film

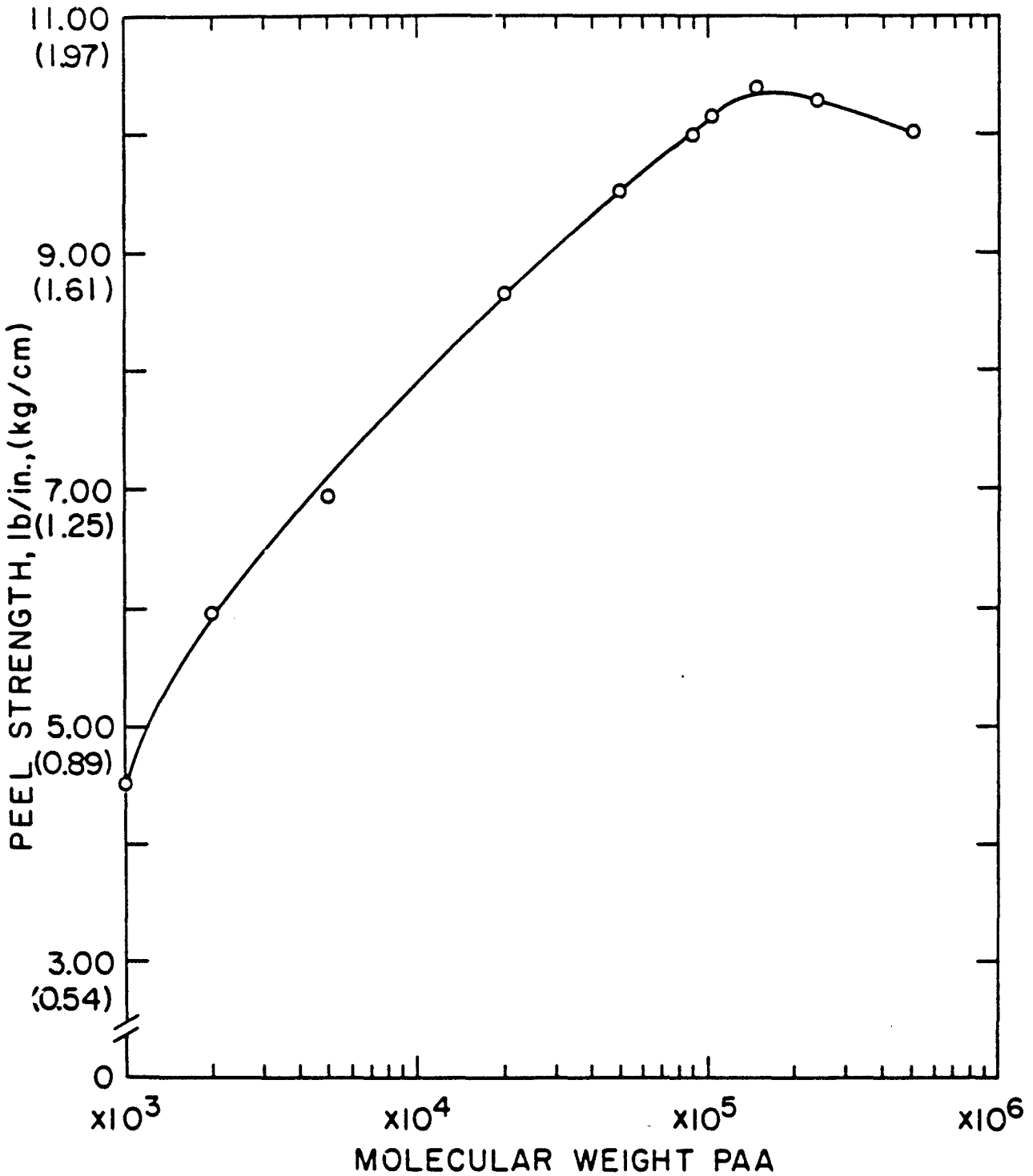

Figure 51. 180°-peel strength of PU-complex precoat joints as a function of PAA molecular weight.

surfaces by PU resin, thereby decreasing the interfacial adhesive bonds. A high M.W. PAA, which is comprised of long chain units, will act to suppress the extent of the coil-up and entanglement of molecules. A lesser alteration of the chain conformation will result in a regularly oriented configuration of PAA polymer containing a plentiful number of functional groups, therefore, resulting in an increase in mobility of PU resin at the interfacial regions.

The theoretical explanation given above was tested experimentally by measurements of the interfacial contact angles at the PU resin-complex precoat boundary. The Zn-complexed PAA salt formations which are yielded at the outermost surface sites of the crystal precoat layers were made by overlaying 3% PAA-modified zinc phosphating solutions. The M.W. of the PAA was varied from 5×10^3 to 2.5×10^5. The overlaid samples were then heated in a vacuum oven at 110°C to solidify the complex salt films. The contact angles were determined within 30 sec after deposition of uninitiated liquid PU resin on the complex film surfaces, and the results are given in Table 8. The data indicated that small decreases in the contact angle occurred as the M.W. was increased. Since a lower angle corresponds to an increase in the magnitude of the wetting forces, the wettability of the complex film surfaces by PU resin appears to be enhanced by incorporating a higher M.W. PAA. The facile resin mobility at the interfacial areas is developed from the nature of primary covalent bond mechanisms. When a topcoating resin is brought into contact with the oriented high-M.W. PAA overlayer, the resin is mobile enough to migrate to the functional group sites on the layer where conditions for the formation of covalent bonds by chemisorption are particularly favorable. This formation of polymer-polymer covalent bonds, which is primarily responsible for the molecular orientation, contributes significantly to the development of the interfacial adhesion forces. The use of a low-M.W. PAA produces a greater amount of coiled-up molecules, which are most likely to result in the formation of a weak boundary layer which gives poor adhesion at the interfaces. Therefore, controlling the extent of entanglement is one of the important factors in promoting mobility of the resins.

TABLE 8

Contact Angle of Various PAA-Modified Complex Film Surfaces by PU Resin

PAA molecular weight	Contact angles, degree
5,000	59.7
50,000	55.8
100,000	53.1
150,000	51.5
250,000	50.7

The adhesion aspects of glassy rigid-type FA polymer topcoats to complex precoat systems were studied by performance of lap shear tensile strength tests. As seen in Table 7, the effect of the PAA concentration on the bond strength of the FR polymer is similar to that on the PU. Namely, the bond strength increases upon the addition of PAA up to a 3% concentration. The strength of 1130 psi (7.79 MPa) at 3% concentration was ~60% higher than that of the control specimens. At a 4% concentration, the strength declines to 950 psi (6.55 MPa).

H. Elastic Behavior of Polymer-Overlaid Precoat Layers

Tests were performed to obtain stress-strain diagrams for the topcoat-precoat composite layers. In this work, ~1.5-mm-thick PU and FR polymer topcoat systems were placed on complex precoat surfaces which were modified with 3% PAA having a M.W. of 1×10^6. Differences between the flexural modulus computed from the stress-strain relation were then used in an attempt to relate the stiffness of the precoat layer with the mechanical behavior of the topcoats. Typical stress-strain diagrams and the computed flexural modulus for these specimens are shown in Figure 52.

These interesting results indicated that the flexural modulus of the PU-topcoated composite layer specimens is 10.31×10^6 psi (7.10×10^4 MPa), corresponding to an improvement of ~20% over that of the specimens without the topcoating. In contrast, the modulus for FR-coated composite specimens was ~12% less than that of the control. Further, the yield stress of the precoat specimens was improved ~10% by overlaying with PU polymer, whereas a stress reduction of ~16% was noted for FR-overlapped layers. The features and mode of the fracture-initiating cracks at the yield stress for the untopcoated and FR- and PU-topcoated composite surfaces were investigated using SEM. These fractographs are given in Figures 53 to 55. For the untopcoated precoat surfaces, it is of considerable interest to determine the mode of fracture and whether cracking occurs through or around the coarse crystal. Arrows on the figures, as seen in Figure 53, signify the direction of crack growth in a bent specimen surface. As expected, it was confirmed from the diverging crack pattern that the microcrack propagation is diverted around a bulky

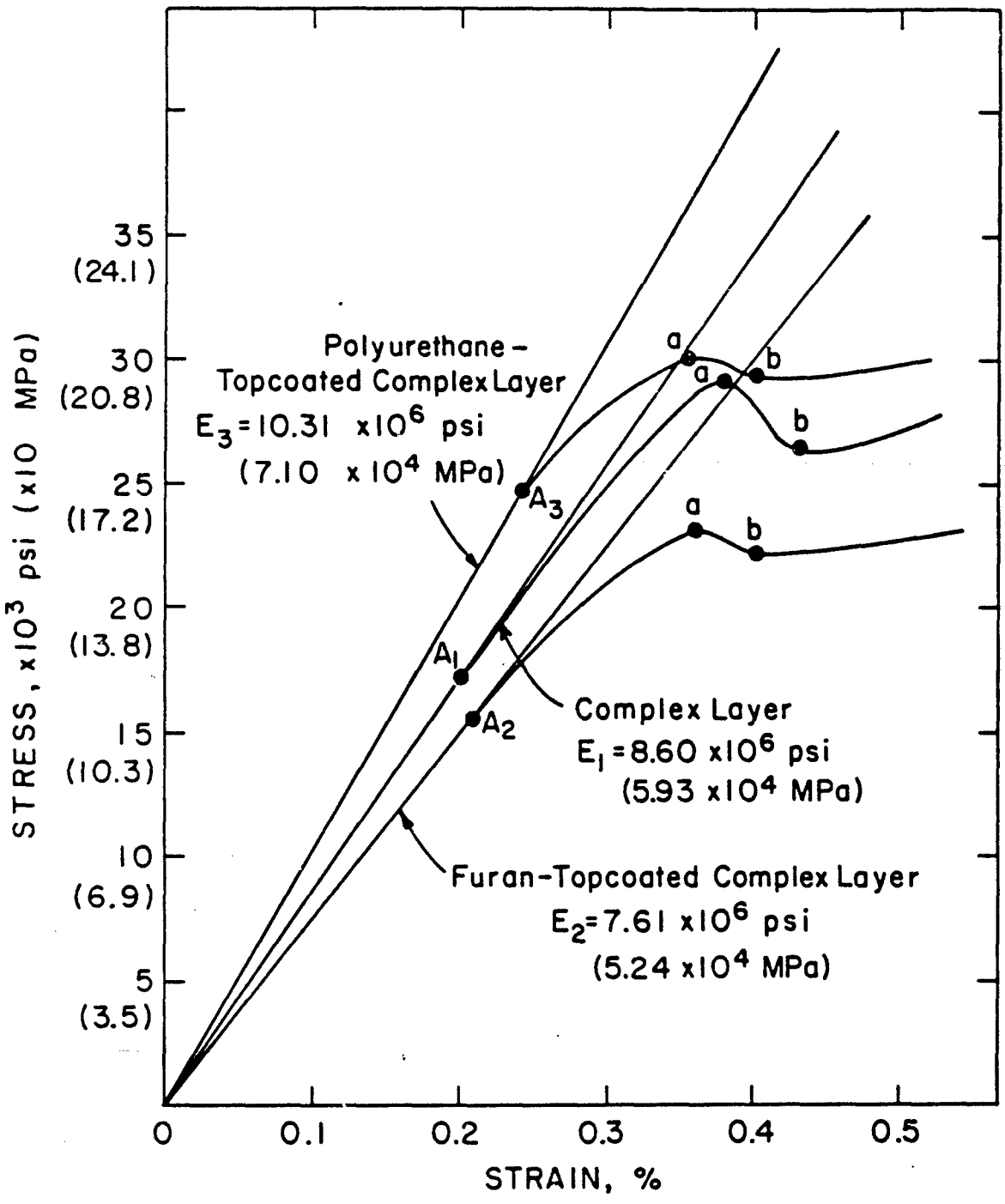

Figure 52. Stress-strain diagrams for uncoated and PU- and FR-topcoated complex layers.

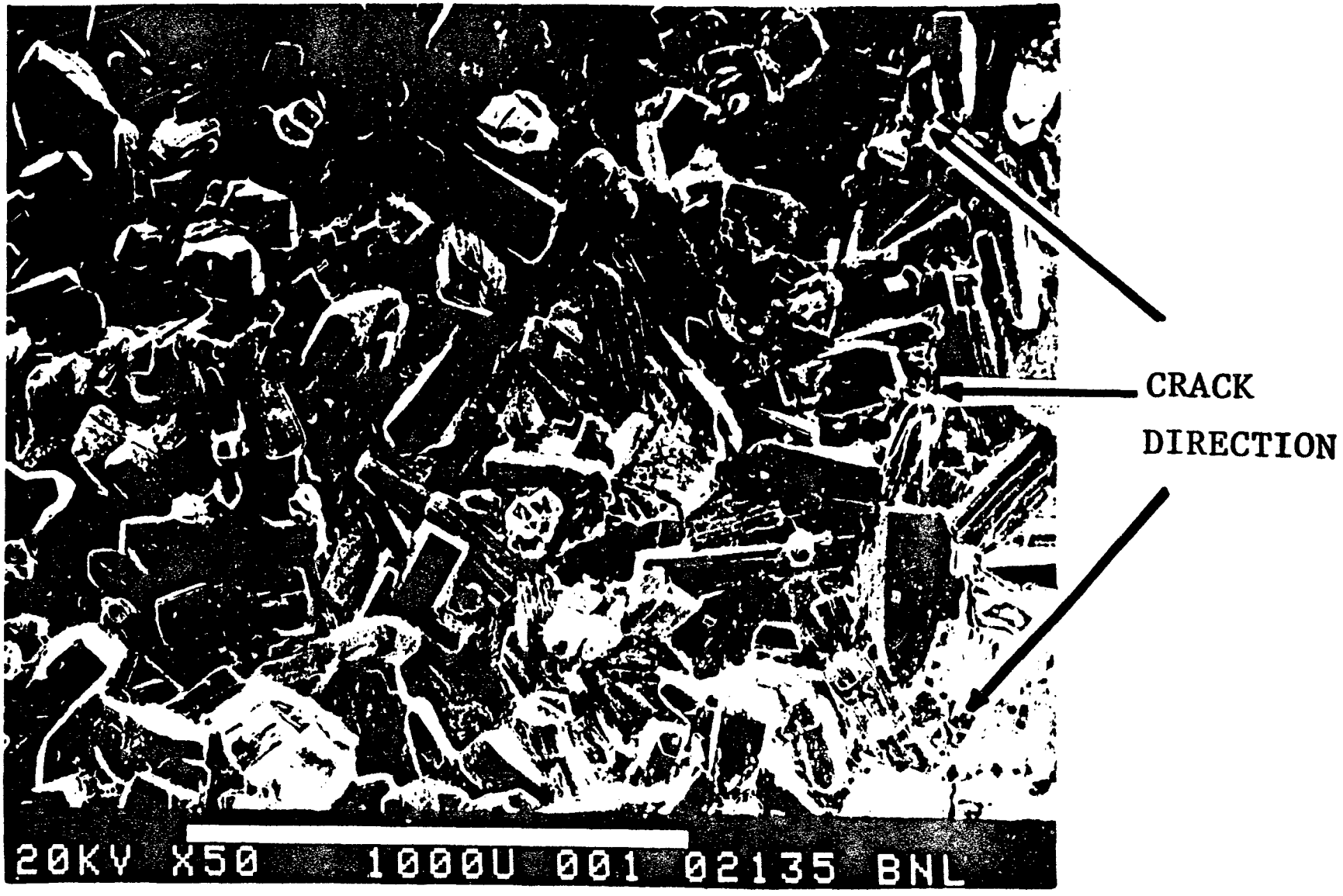

Figure 53. Diverging microcrack pattern of a bent complex conversion precoat.

coarse crystal rather than passing through it. The width of the microcrack, which is very difficult to identify, was ~4 μm. The small size of the flaw produced at the yield stress suggests that the complex precoat layers possess a high degree of flexibility and stiffness.

When compared to the untopcoated specimens, the fracture origin under tension of the FR-topcoated specimens was completely different. This is microscopically discernible in the fractograph shown in Figure 53 and Figure 54(a), respectively. A linear cracking pattern, resulting in failure of the glassy FR polymer, is apparent in the topcoated specimen. Figure 54(b) shows the crack initiation area of the FR polymer overlayer at a higher magnification. As is evident from the micrograph, the failed section exhibits a relatively smooth face. Thus, the fracture of the brittle FR topcoat was probably due to poor plastic deformation in connection with a rapid progression of crack growth. The size of the flaw was determined from the SEM fracture micrographs to be ~30 μm, more than seven times larger than that in the failed precoat layer without the topcoat system.

In contrast, no signs of cracking were detected for the composite layer surface containing the elastomeric PU topcoat (see Figure 55). These results apparently verify that the FR glass topcoat, characterized by its high elastic modulus, extremely low elongation, and good bond strength, acts to promote crack propagation at the interfacial regions. Although some nonlinear stress distribution is observed prior to the deformation failure, the fracture of FR-precoat composition systems occurs almost immediately following the formation of a visible tensile crack. The initial cracking of this composite occurs through the FR polymer-precoat stress, whereby load is transferred from the brittle FR to the ductile crystal layers. For the PU superposition, it was microscopically observed that growth of the interfacially generated initial crack is more likely to be associated with the crystalline precoat sites than with the PU polymer sites. The most significant effect of the use of the high tensile and elongation and low modulus PU topcoat is, therefore, to delay and control of the onset of tensile cracking of the precoat layers. The interfacial bond failure occurs after the precoat layer reaches its yield

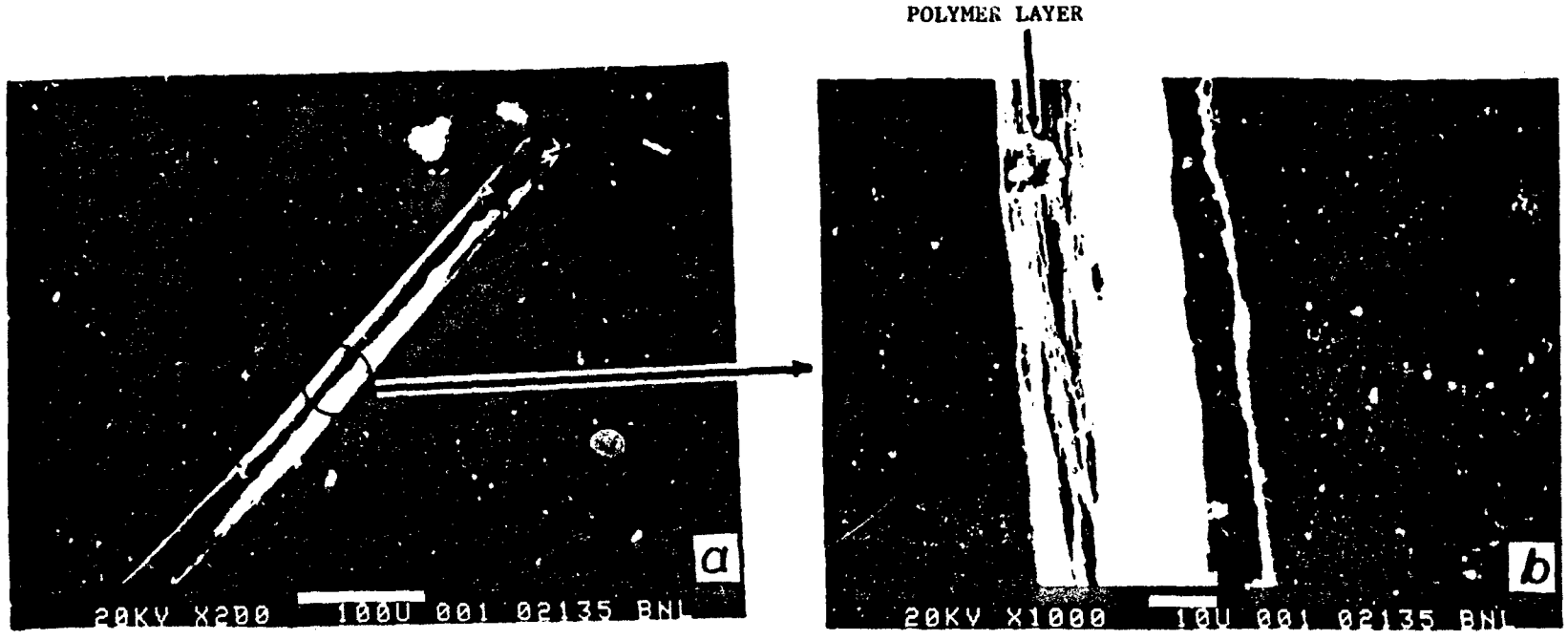

Figure 54. SEM micrographs of glassy FR-topcoated composite layer surface at failure; (a) linear-cracking pattern of failed FR polymer, and (b) enlargement of section shown in (a).

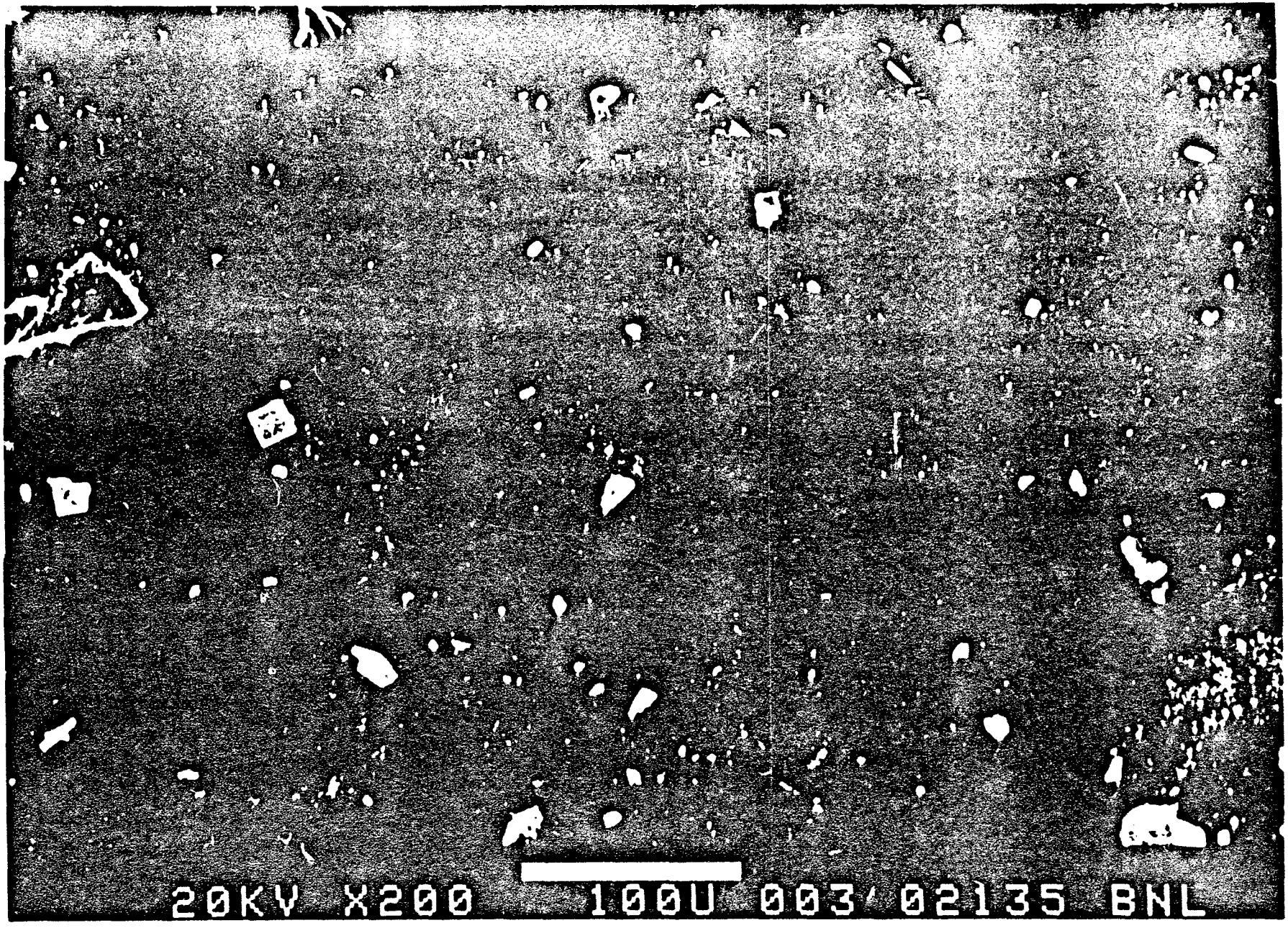
20KV X200 100U 003 02135 BNL

point. Thus, the crack-arresting properties of elastomeric topcoats are found to play the major role in improving the mechanical behavior of the precoat layer during interfacial failure processes.

On the other hand, the effect of the adhesive bonds at the topcoat/precoat interfaces on the elastic behavior of the composite layers cannot be fully ascertained from the experimental data. To gain additional information, precoat surfaces were exposed to a 100% relative humidity (R.H.) atmosphere at 24°C for up to 10 days before application of initiated PU and FR resins. The presence of any moisture on the substrate surfaces would result in a decrease in bonding force with these adhesives. The humidity also reduced the curing rate of the polymeric topcoat in the vicinity of the wetted precoat surfaces. This reduced polymerization rate relates directly to a decrease in elastic modulus of topcoating materials.

Curves showing the flexural modulus for PU- and FR-topcoated composite layers prepared after exposure of the precoat surfaces to 100% R.H. for various periods of time are shown in Figure 56. These data suggest that the presence of a certain amount of moisture on the precoat surfaces may increase the flexural modulus of the composite layers. Surfaces overlaid with PU after 24-hr exposure to 100% R.H. exhibited the maximum modulus of 125 x 10^5 psi (86.13 x 10^3 MPa). This corresponds to an improvement of ~20% over that of the unexposed surfaces. Extending the exposure time for up to 10 days resulted in a modulus reduction, but the value was still higher than that from the dry surface. For the FR-topcoated systems, the data indicate that the modulus increased with exposure times up to ~5 days to an ultimate modulus of ~100 x 10^5 psi (68.90 x 10^3 MPa). Beyond that time, the modulus declined to a value of ~91 x 10^5 psi (62.70 x 10^3 MPa) after 10 days of exposure. From the above findings, it can be concluded that when the resins in the curing propagations are contiguous to moisture, their polymerization rate is suppressed by the humidity existing on the substrate surfaces. This suppression of polymerization acts to produce a rubbery polymer possessing a low elastic modulus and high elongation properties. Thus, even though the interfacial bonding forces are actually reduced by the presence of surface moisture, the decreased modulus of the polymer topcoat at the interface contributes to an increase

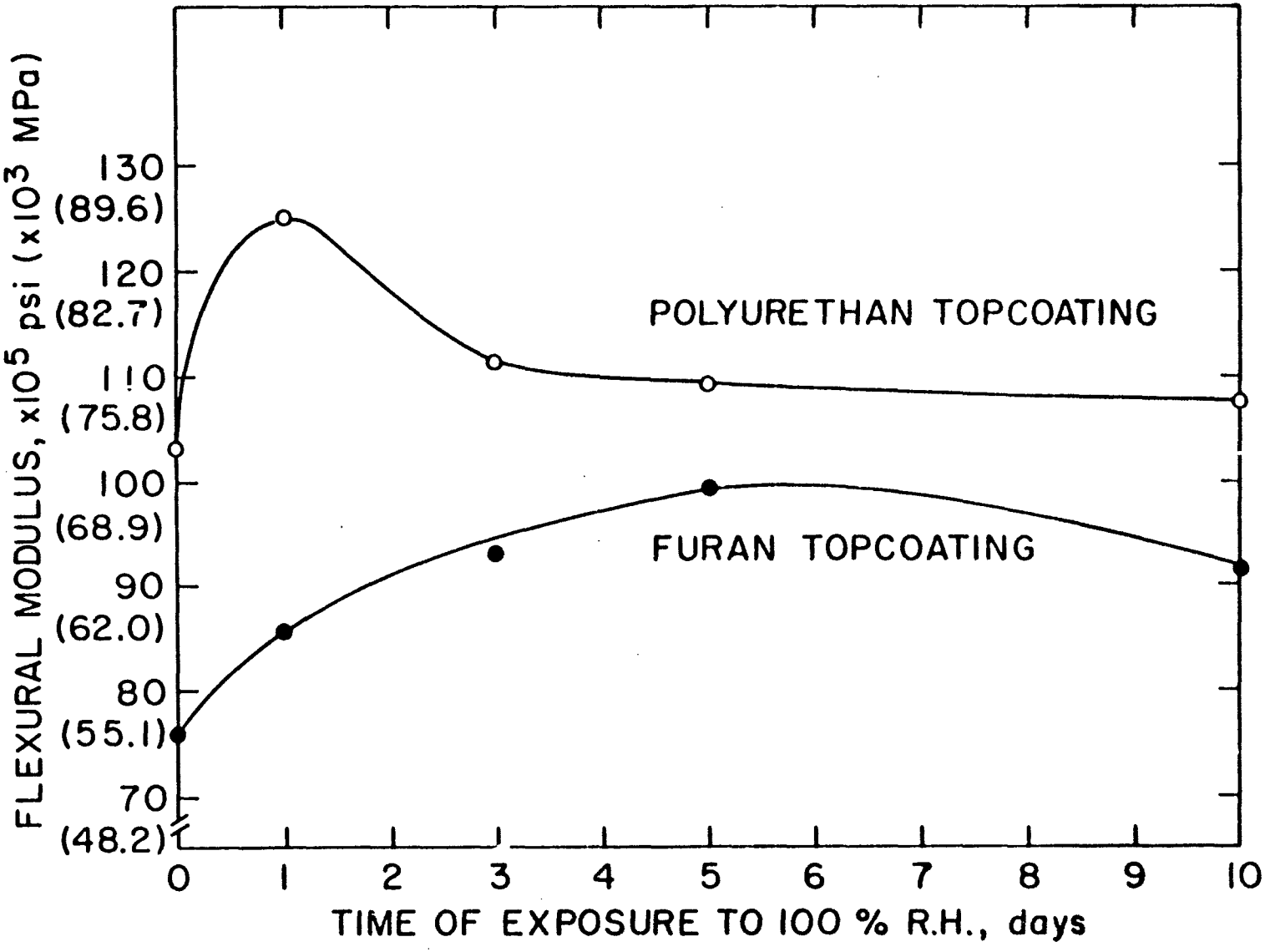

Figure 56. Changes in flexural modulus of PU- and FR-topcoated complex crystal layers as a function of time of exposure to 100% R.H.

in the flexural modulus of the crystalline precoat layers. This enhances the stiffness of the composite layers. The results further suggest that the interfacial stress transfer is of major importance in the topcoat-precoat composite systems. For instance, the enhanced brittleness at the interface, when a glassy FR topcoat is used, tends to result in a more rapid decrease in the interfacial stress transfer because of an increased rate of compaction. The increased flexural modulus of the composite layers containing moisture at the interface is associated with an increase in interfacial stress transfer which is due to the absorption of a certain amount of energy by the rubbery topcoat prior to the initial cracking of the precoat layers. Accordingly, the interfacial adhesive bonds were found to have a lesser effect on the crack-arresting behavior and stiffness characteristics of the composite layers.

1. Conclusions

Crystalline Zn·Ph conversion coatings deposited on carbon steel substrates by immersing the metals in nongassing phosphating solutions are generally thick (~120 μm) and are comprised of relatively coarse crystals. These crystal formations which consist of a pronounced dendritic microstructure result in a high coating weight which is economically undesirable. Although well-crystallized conversion coatings play a role in the development of strong mechanical interlocking bonds with polymeric topcoating systems, the deposition of a thick layer of coarse crystals resulted in the formation of brittle coatings which failed upon flexing.

In particular, the dimensions and coating weight of the conventional conversion crystals decrease dramatically with increasing PAA concentrations. It is speculated that this grain-refining action of PAA is due to the following mechanism. When the polyacid is introduced into the zinc phosphating liquid, the active nucleophilic divalent zinc cations dissociate from the zinc orthophosphate dihydrate in an aqueous solution. These may produce reversible salt complex formations with fuuctional carboxylic acid (COOH) pendent groups in the PAA molecular structure. The complexes appear to act as a miniature ion-exchange system. The formed complex structure may also play a key role in restraining the conversion crystal

growth, thereby resulting in a uniform dense coating of fine crystal size and low coating weight. The microstructure of the PAA-modified Zn·Ph layers was confirmed to be a composite formation consisting of a thin PAA macromolecule overlaying continuously on a uniform array of fine dense crystals.

To study the interfacial interaction mechanisms between the PAA polymer and the Zn·Ph crystal layers, elemental analyses of the composite surfaces and subsurfaces were conducted by means of the highly sensitive analysis techniques such as XPS and EDX. These results suggested that the interaction at the interfaces is most likely chemical. The chemical interaction is initiated by charge transfer reaction mechanisms in which the proton-donating functional COOH groups in PAA are strongly chemisorbed to the Zn atom at the outermost surface sites of the crystal layers. The carboxylic anions converted from the COOH groups are terminatively transformed into unique bridge formations through a cross-linking reaction with Zn. Thus, the chemical effect of Zn atoms in the hypothetical interaction model was presumed to be intermolecular bridging, acting to connect between the PAA and the crystal phases. The deposition products of the PAA-complexed Zn·Ph crystal were identified to be the assemblage structure of hybrid phases consisting of the tertiary zinc orthophosphate dihydrate as the major product and some unidentified phosphate compounds as the minor ones. The assemblage of this fine crystal further suggested that the PAA significantly acts to reduce the degree of crystallinity of the Zn·Ph compounds, resulting in the production of finely crystallized coating layers.

On the other hand, the plasticized complex coating layer plays an essential role in increasing the stiffness and the ductility of the conventional crystal layers. The flexural modulus of 3% PAA-complexed crystal layers was more than two times greater than that of the conventional crystal layer without PAA. The physico-chemical factors governing the mechanical behavior of the conversion complex crystal layers depended

primarily upon the thickness, fineness, and density of the layers, and the average M.W. of the PAA. With a high M.W. of 1×10^5, the most effective complex crystal formations and dimensions for achieving the ultimate flexural modulus were a uniform array of fine dense crystals ~5 μm thick and ~60 to 200 μm in length. The ductile complex crystal layer and surface not only provide a corrosion barrier on the substrates, but also possess the ability to promote adhesive bonds with polymeric topcoat systems because of the thin complex PAA polymer existing at the outermost surface sites of the crystal layers. The increase in adherent forces of the complex PAA overlayers results in a lower magnitude in the degree of coil-up and entanglement of the macromolecules brought about by the complex reaction between the proton-donating PAA polymer and the nucleophilic Zn^{2+} ions released from the $Zn_3(PO_4)\cdot 2H_2O$ in a low pH aqueous medium. The use of high M.W. and an adequate amount of PAA contributes to a reduced alternation of chain conformation and the presence of a large number of functional COOH groups, thereby enhancing the magnitude of wettability of the complex precoat surfaces by the resins.

The mechanical characteristics of the polymeric topcoating in the topcoat-precoat composite layers play a key role in improving the stiffness, the post-cracking ductility, and the flexural crack-arresting properties of the precoat layers. The improvement of these characteristics is more likely to be associated with a low elastic modulus, high tensile strength, and extremely high elongation properties of the topcoats, rather than the interfacial adhesive bonds. In fact, the flexural modulus for the elastomeric polyurethane-superposed composite layers was ~36% higher than that for the glassy furan polymer composite layers. Furthermore, no cracking of the polyurethane surfaces was detected microscopically at the yield stress of bent composite layers. This suggests that the interfacial bond failure occurs after the precoat layer reaches its yield point. In contrast, the initial cracking of the brittle furan polymer composite layers occurred through the polymer-precoat stress, whereby a load was transfered from the brittle polymer to the ductile layers.

V. DISCUSSION AND CONCLUSIONS

Generally, organic polymers containing functional groups such as amines, esters, and acetals, in which any two atoms selected from N, O, and S are joined to the same carbon atom, are very susceptible to hydrolysis, particularly under hydrothermal conditions. When polymers having these functional groups in either their main chains or in pendent sites of macromolecules, were applied as protective coatings on metal surfaces, the hydrothermal disintegration of the polymers lead to disbondment of the coatings from the substrate surfaces. This failure was associated with the following four factors, (1) high segmental mobility of chains, (2) low thermal relaxation, (3) increased hydrophilic groups, and (4) low dynamic mechanical properties. It was found that the degradation of the polymers can be suppressed by the inclusion of calcined reactive fillers. The inclusion of a hydraulic calcium silicate ($CaO \cdot SiO_2$) reactive filler having a CaO/SiO_2 mol ratio of 0.68, resulted in the production of crystalline inorganic macromolecules and dissociation of the divalent metallic ions from the filler surfaces in the hot aqueous media. In $CaO \cdot SiO_2$ additive-filled polymethylmethacrylate (PMMA) composite systems, the hydrothermal interactions at the polymer-filler interfaces can be interpreted as follows: the cation-acceptable functional groups formed by hydrolysis of PMMA electrostatically reacts with the electropositive metallic ions migrated from the $CaO \cdot SiO_2$ surfaces. This reaction leads to the formation of chemically stable ionomer structures. Simultaneously, the mixed inorganic macromolecules of amorphous and crystalline $CaO\text{-}SiO_2\text{-}H_2O$ macromolecular-ionomer complex was identified as being formed in the superficial layers of the PMMA composite during exposure in an autoclave at a temperature up to 200°C. This superficially formed complex acts as a self-healing protective layer which is directly related to the molecular structure that has polymer chains with low segmental mobility, thereby improving the mechanical strength and thermal stability. It was also determined that these complex films have a relatively low surface free energy, low surface roughness, and low water permeability.

When organic polymer materials are applied as a protective coating to steel substrate surfaces, the surface preparation of the substrate prior to application of the polymer coating, is very important in achieving good bonding. In this regard, crystalline Zn·Ph preparations are often used commercially as a means for improving the corrosion resistance and paint adherence properties of ferrous and zinciferrous, (especially galvanized) metal surfaces. With cold-rolled steel plates, this preparation, expressed in terms of a conversion crystal precoating, can be accomplished by immersing steel plates in a BNL-developed zinc phosphating formulation consisting of zinc orthophosphate dihydrate, [$Zn_3(PO_4)\cdot 2H_2O$], phosphoric acid, (H_3PO_4), and water.

For the surface preparation of high carbon-containing steel, the use of conventional ZnO-H_3PO_4-H_2O systems commonly results in the production of a porous zinc phosphate conversion layer.[50,51] In contrast, the use of the BNL-developed $Zn_3(PO_4)_2\cdot 2H_2O$-H_3PO_4-H_2O system on the same steel produces a high quality, insoluble conversion crystal precoat. The topographical features of the well-crystallized precoat surfaces were characterized by the formation of a thick layer of highly dense interlocking rectangular crystals having an open surface structure. This typical crystal structure was found to be a primary factor in the degree of bonding of paint and resin coatings to steel substrates. Increased mechanical anchoring is obtained when the liquid resins can penetrate into the open surface microstructure and microfissures of the deposited precoat layers.

Chemical treatments can be used, not only to increase the roughness of the substrate, but also to modify the chemical composition. The latter is an important factor affecting the degree of chemical affinity for polymeric adhesives. In the study of interaction mechanisms at the functional polymer-zinc phosphate crystal interfaces, it was identified that the crystallized H_2O molecules existing at the outermost surface sites of the conversion precoats, play essential roles in wetting and spreading by the liquid resins which have functional carboxylate and carboxylic acid groups located in either their main chains or the pendent side of macromolecules. The most possible intermolecular reaction was considered to be due to the

formation of hydrogen bonds, $COO---H_2O$, between the carboxylate groups and the water molecules of hydration at the crystal surface sites. Alternative interfacial attraction was rationalized to be associated with the acid-base and charge transfer interaction mechanisms, namely, the proton-donating carboxylic acid groups chemisorbed strongly with the polar OH groups at hydrated crystal surfaces. The carboxylic anions formed by the chemisorption induce strong ionic bonding as a result of these interaction machanisms. A large crystal surface area, corresponding to the presence of a plentiful supply of polar groups on the outermost surface sites, was more strongly chemisorbed by the functional polymers than were those with lesser surface areas. Otherwise, the preferred macromolecule orientations in the polymer layer contribute significantly to the development of the interfacial bond strength, whereas the conformation change caused by the free-ion-complexed molecular structure, resulting in coiled-up macromolecules, is likely to result in a decrease in interfacial bonding forces.

As described above, the intrinsic adhesion nature at the functional polymer/zinc phosphate joints was attributed primarily to mechanical interlocking, and secondarily, to the presence of a weak chemical bond such as hydrogen bond and acid/base interactions. However, the most ideal interaction mechanism to provide a strong adhesion force and a highly stable interphase region corresponds to a primary covalent chemical bond associated with a high dissociation energy of 50-200 kcal/mole. On the other hand, although thick zinc phosphate precoats appear to be suitable as corrosion inhibitors for the substrates, the fragile characteristics of these bulky crystal structures lead to failure during flexure or other deformation of the substrate. Deformation failures of layers, having low stiffness characteristics, appear to be directly related to the development of micropores and fissures which reduce the effectiveness of the corrosion-resistant coatings.

The results from considerable efforts to solve these problems, have shown that the introduction of an appropriate amount of polyelectrolyte macromolecules, used as a controllable admixture for crystal growth,

significantly improves both the interfacial adhesion forces to the polymeric topcoat and the stiffness and ductility of brittle conversion layers. The physico-chemical factors governing the mechanical behavior of the organic macromolecule-treated zinc phosphate complex layers depend primarily upon the thickness, fineness, density of the layers, and the average molecular weight (M.W.) of the macromolecules. In order to modify the crystal layers by the use of polyacrylic acid (PAA) macromolecules from among the various polyelectrolyte species, it was found that the polyelectrolyte with a high M.W. of 1×10^5 results in the most effective PAA-complexed zinc phosphate crystal formation and dimensions for achieving the ultimate flexural modulus. The ductile precoat layer and surface, not only provide a corrosion barrier on the substrates, but also possess the ability to promote adhesive bonds with polymeric topcoat systems. The latter was due to the presence of a thin functional PAA polymer film at the outermost surface sites of the precoat layers. Therefore, it was apparent that the highly stable nature of the interphase region is caused by direct chemical bonding between the polymer topcoat and PAA.

The mechanical characteristics of the polymeric topcoating in the topcoat-precoat composite layers play a key role in improving the stiffness, the post-cracking ductility, and the flexural crack-arresting properties of the precoat layers. The improvement of these characteristics is more likely to be associated with a low elastic modulus, high tensile strength, and extremely high elongation properties of the topcoats, rather than the interfacial adhesive bonds.

Acknowledgements

The authors wish to acknowledge the support and guidance received from Dr. Robert R. Reeber of the U.S. Army Research Office, Research Triangle Park, NC.

References

1. T. Sugama, L.E. Kukacka, and W. Horn, J. Appl. Polym. Sci. 24, 2121 (1979).

2. T. Sugama, L.E. Kukacka, and W. Horn, J. Mater. Sci. 15, 1498 (1980).

3. T. Sugama, L.E. Kukacka, and W. Horn, J. Mater. Sci. 16, 345 (1980).

4. R. Speiser, C. H. Hills and C. R. Eddy, J. Phys. Chem. 49, 328 (1945).

5. J. R. Hulescye, P. F. Grieger and F. T. Wall, J. Am. Chem. Soc. 72, 2636 (1950).

6. F. T. Wall, J. J. Ondrejei and M. Pikramenon, J. Am. Chem. Soc. 73, 2821 (1951).

7. I. Michaeli, J. Polym. Sci. 48, 291 (1960).

8. A. Ikegami, Bipolymers 6, 431 (1968).

9. C. A. J. Heve, J. Polym. Sci. Part C 30, 361 (1970).

10. A. Silbergerg, J. Colloid Interface Sci. 38, 217 (1972).

11. R.B. Kemp, C.W. Lloyd, and G.M. W. Cook, Prog. Surf. Membr. Sci. 7, 271 (1973).

12. B. Vincent, Adv. Colloid Interface Sci. 4, 193 (1974).

13. F. Th. Hesselink, J. Colloid Interface Sci. 60, 448 (1977).

14. D.J. Belton and S.I. Stupp, Adhesion Aspects of Polymeric Coatings, K.L. Mittal, ed., p. 235, Plenum Press, NY, 1983.

15. S.B. Wallon, J.B. Barr, and B. A. Petro, J. Chromatography 54, 33 (1971).

16. R.H. Leitheiser, M. E. Loudrigan, and C.A. Rude. Plastic Mortars, Sealants, and Caulking Compounds, R. B. Seymour, Ed., ACS Symposium Series 113, Washington, D. C., 1979, p. 7.

17. J.B. Barr and S.B. Wallon, Appl. Polym. Sci. 15, 1079 (1971).

References cont.

18. E.R. McCartney and A. E. Alexander, J. Colloid Sci. 13, 383 (1958).

19. J.E. Crawford and B. R. Smith. J. Colloid Interface Sci. 21, 623 (1966).

20. C.H. Nestler, J. Colloid Interface Sci. 26, 10 (1968).

21. Yu.S. Lipatov, Dokl. Akad. Nauk. SSSR 143, 1142 (1962).

22. I. Galperin, J. Appl. Polym. Sci. 11, 1475 (1967).

23. G.J. Howard and R.A. Shanks, J. Appl. Polym. Sci. 26, 3099 (1981).

24. D.H. Droste and A.T. Dibenedetto, J. Appl. Polym. Sci. 13, 2149 (1969).

25. K. Iisaka and K. Shibayama, J. Appl. Polym. Sci. 22, 3135 (1978).

26. L.E. Nielsen, J. Appl. Polym. Sci. 17, 1897 (1979).

27. L.B. Clapp, The Chemistry of the OH Group, Prentice-Hall, Inc., Englewood Cliffs, NJ, p. 24 (1967).

28. A.D. Wilson and S. Crisp, Br. Polym. J. 7, 279 (1975).

29. J.E. Field and L.E. Nielsen, J. Appl. Polym. Sci. 12, 1041 (1963).

30. L.D. Wakeley, B.E. Scheetz, M.W. Grutzeck, and D.M. Roy, Cem. Concr. Res. 11, 131 (1981).

31. F.M. Lea and C.H. Desch, The Chemistry of Cement and Concrete, Edward Arnold Ltd., London, p. 225 (1956).

32. L.H. Lee, J. Appl. Polym. Sci. 12, 719 (1968).

33. T. Young, Phil. Traus. Roy. Soc. (London) 95, 65 (1805).

34. A. Dupre, Theorie Mechanique de la Chaleur, Gouthier-Villars, Paris, p. 369 (1869).

35. W.A. Zieman, Ind. Eng. Chem. 55, 18 (1963).

36. H.W. Fox and W.A. Zisman, J. Colloid Sci. 5, 514 (1950).

37. D.K. Owens and R.C. Wendt, J. Appl. Polym. Sci. 13, 1744 (1969).

References cont.

38. A. Baszkin and L. Ter-Minassian-Saraga, J. Colloid Interface Sci. 43, 190 (1973).

39. F.M. Fowkes, J. Phys. Chem. 66, 1863 (1962).

40. F.M. Fowkes, Chemistry and Physics of Interfaces, American Chemical Society, Washington, DC, Chap. 1, p. 8 (1965).

41. P.F. A. Bijlmer, J. Adhesion. 5, 319 (1973).

42. J.D. Wenables, D. K. McNamara, J. M. Chen, J. S. Sun and R. Hopping, Appl. Surf. Sci. 3, 88 (1979).

43. D.E. Packham, K. Bright, and B.W. Malpass, J. Appl. Polym. Sci. 18, 3237 (1974).

44. J.R. Evans and D.E. Packham, Adhesion I., K.W. Allen, ed., p. 297, Applied Science Publishers, London, 1977.

45. ASTM in Method D-903, Peel or Stripping Strength of Adhesive Bonds.

46. F.T. Wall and J.W. Drenan, J. Poly. Sci. 7, 83 (1951).

47. K. Nakamoto, Infra-red Spectra of Inorganic and Co-ordination Compounds, Wiley, New York, 1963.

48. E.P. Popov, Introduction to Mechanics of Solids, Prentice-Hall, Inc., Englewood Cliffs, New Jersey, 1968, p. 110.

49. R.Y.M. Huang, C.J. Gao, and J.J. Kim, J. Polym. Sci. 3036 (1983).

50. A.I. Robert and H. Leidheiser, Jr., Corrosion 37, 28 (1981).

51. J.A. Kargol, D.L. Jordan, and A.R. Palermo, Corrosion 39, 213 (1983).

APPENDIX

Program Presentations, Publications, and Patent Applications

Papers Presented

T. Sugama and L.E. Kukacka. Hydrothermal Durability of Ca-Complexed MMA-TMPTMA Copolymer Films and Coatings Containing Superficially Formed $CaO-SiO_2-H_2O$ Type Inorganic Macromolecules. Proceedings of the 1983 Scientific Conference on Chemical Defense Research, Aberdeen Proving Ground, Maryland, November 14-18, 1983.

T. Sugama and L.E. Kukacka. Characteristics of Polyacrylic Acid-Complexed Zinc Phosphate Conversion Films Deposited on Metal Surfaces. Proceedings of the 1984 Scientific Conference on Chemical Defense Research, Aberdeen Proving Ground, Maryland, November 12-16, 1984.

Published

T. Sugama, L.E. Kukacka, N. Carciello, and J.B. Warren. Factors Affecting the Durability of Ca-Complexed Methylmethacrylate Copolymer Films Containing $CaO-SiO_2-H_2O$ Macromolecules. J. App. Polym. Sci. 29, 2889-2920 (1984).

T. Sugama, L.E. Kukacka, and N. Carciello. Nature of Interfacial Interaction Mechanisms Between Polyacrylic Acid Macromolecules and Oxide Metal Surfaces. J. Mater. Sci. 19, 4045-4056 (1984).

T. Sugama, L.E. Kukacka, N. Carciello, and J.B. Warren. Adhesion Aspects of Levulinic Acid-Modified Furan Polymers to Crystalline Zinc Phosphate Metal Surfaces. J. Appl. Polym. Sci. 30, 2137-2155 (1985).

In Press

T. Sugama, L.E. Kukacka, N. Carciello, and J.B. Warren. Polyacrylic Acid Macromolecule-Complexed Zinc Phosphate Crystal Conversion Coatings. BNL-35764, October 1984, J. Appl. Polym. Sci.

T. Sugama, L.E. Kukacka, N. Carciello, and J.B. Warren. Factors Affecting Improvement In the Flexural Modulus of Polyacrylic Acid-Modified Crystalline Films. BNL-36592, February 1985, J. Appl. Polym. Sci.

Patent Applications Submitted

T. Sugama, L.E. Kukacka, and N. Carciello. Ductile Polyelectrolyte Macromolecule-Complexed Zinc Phosphate Conversion Crystal Precoatings and Topcoatings Embodying a Laminate. BNL S-62,681, February 1985.